Université de Montréal

Distribution et cinématique des nuages d'hydrogène neutre autour des galaxies naines du Groupe Local

par
Antoine Bouchard
Département de physique
Faculté des arts et des sciences

Mémoire présenté à la Faculté des études supérieures
en vue de l'obtention du grade de
Maître ès sciences (M.Sc.)
en physique

Juillet, 2002

Université de Montréal
Faculté des études supérieures

Ce mémoire intitulé:

Distribution et cinématique des nuages d'hydrogène neutre autour des galaxies naines du Groupe Local

présenté par:

Antoine Bouchard

a été évalué par un jury composé des personnes suivantes:

Anthony Moffat,	président-rapporteur
Claude Carignan,	directeur de recherche
Lister Staveley-Smith,	codirecteur
Gilles Fontaine,	membre du jury

Mémoire accepté le: _____

Sommaire

Les pages suivantes contiennent une analyse détaillée des nuages d'hydrogène neutre que l'on retrouve près des galaxies naines du Groupe Local. Ces nuages sont très souvent décentrés par rapport à la composante optique centrale de la galaxie hôte. Plusieurs scénarios ont été étudiés pour expliquer cette séparation dont les forces de marées et les pressions de contacts.

Une théorie est présentée expliquant comment le flux de radiation ionisante s'échappant d'une galaxie spirale peut ioniser le gaz dans les galaxies satellites les plus proches. Le milieu interstellaire devient alors indédectable. Cette théorie permet également d'expliquer la complexité et la diversité des historiques de formation stellaire des naines.

Une recherche systématique de nuages d'hydrogène neutre a été conduite pour la majorité des naines visibles dans l'hémisphère sud. Du gaz a été détecté dans des configurations qui permettent l'analyse des phénomèmes de dépouillement du gaz. Une autre hypothèse a également été considérée. Les nuages détectés peuvent être des composantes de la Voie Lactée que l'on nomment *High Velocity Clouds*. Il appert que cette hypothèse, quoique non complètement réfutée, demeure bien marginale dans la majorité des cas.

Les données à haute résolution de la naine sphéroïdale Sculptor ont permis une étude plus complète que sur les autres naines. Diverses évidences ont été mises en valeur quant à l'importance relative des méchanismes de dépouillement du gaz par pression de contact, force de marée ou par flux ionisant.

Mots clefs:
Astronomie: extragalactique — groupe local — galaxies: naines — milieu interstellaire: HI

Abstract

This memoire contains a detailed analysis of neutral hydrogen clouds found near dwarf galaxies of the Local Group. These clouds are often found to be off-centered with respect to the central optical core of the dwarf. Several scenarios explaining this separation have been studied. These include tidal stripping and ram pressure.

A theory explaining how the ionizing flux escaping spiral galaxies can ionize the hydrogen present in the core of its closest satellites is presented. This makes the interstellar medium of such galaxies indetectable. The theory can also explain the wide variety and complexity of star formation histories these dwarfs exhibit.

A systematic search for hydrogen clouds near a majority of dwarf galaxies was conducted. Gas was found in configurations that permitted the analysis of the stripping mechanisms. Another hypothesis was also investigated. The clouds could be part of the Milky Way and be the so-called High Velocity Clouds. Although this hypothesis can not be ruled out, it is only a marginal one in many cases.

The Sculptor dwarf sheroidal galaxy received special treatment. High resolution data permitted a much deeper investigation of this galaxy. Many features were exposed, giving the relative importance of each stripping mechanism: ram pressure, tidal forces, and ionising flux in this particular case.

Keywords:
Astronomy: extragalactic — local group — galaxies: dwarfs — interstellar medium: HI

Table des matières

Liste des figures

Liste des tableaux

Abréviations utilisées

Abbréviation	Signification	
AIPS	*Astronomical Image Processing system*	
ATCA	*Australia Telescope Compact Array*	
ATNF	*Australia Telescope National Facility*	
CDM	*Cold Dark Matter*	Matière sombre froide
CMD	*Color Magnitude Diagram*	Diagrame couleur-magnitude
dE	*Dwarf Elliptical Galaxy*	Galaxie naine elliptique
dIrr	*Dwarf Irregular Galaxy*	Galaxie naine irrégulière
dSph	*Dwarf Spheroïdal Galaxy*	Galaxie naine sphéroïdale
GL		Groupe Local
HI		Hydrogène neutre
HIPASS	*HI Parkes All Sky Survey*	
HVC	*High Velocity Cloud*	Nuage à haute vitesse
IGM	*Intergalactic Medium*	Milieu intergalactique
ISM	*Interstellar Medium*	Milieu interstellaire
Jy	*Jansky*	
	$10^{-26} W\ m^{-2}\ Hz^{-1}$	
LGC	*Local Galactic Cloud*	Nuage galactic local
LMC	*Large Magellanic Cloud*	Grand nuage de Magellan
NGC	*New General Catalog*	
SMC	*Small Magellanic Cloud*	Petit nuage de Magellan
UV		Ultra-violet
VL(ou *MW*)	*Milky Way*	Voie-Lactée
ZOA	*Zone of Avoidance*	Zone interdite

À ma mère. À mon père.

Remerciements

Merci à Claude Carignan pour m'avoir enseigné les joies de la recherche,
de m'avoir communiquer la passion des sciences et, surtout,
pour m'avoir abandonné sur les plages d'Australie,
à Lister Staveley-Smith pour ses nombreux conseils,
à David Barnes pour les explications sur les logiciels trop souvent rébarbatifs,
à Erwin deBlok pour m'avoir fait decrocher quelques fois,
à Gilles Fontaine pour son indéfectible support
et, finalement, au groupe OPIOMM pour avoir enduré mes opinions.

Chapitre 1

Introduction

Depuis que Hubble (1925) a clairement identifié pour la première fois un objet n'appartenant pas à la Voie Lactée (VL), des avancements considérables ont été faits dans le domaine de l'astronomie extragalactique. Différentes structures ont été identifiées et ce, à différentes échelles, partant des plus petites étoiles jusqu'aux super-amas de galaxies.

Dans cette hiérarchie céleste, il devint vite évident que les galaxies ne se formaient pas seules mais en groupes, laissant d'immenses vides entre ces derniers. Même ces groupes sont rassemblés et forment des supergroupes.

Toutes ces galaxies réunies vivent et évoluent ensemble, laissant place à différents types d'interactions, de collisions. Comme dans n'importe quel groupe, les plus grosses galaxies dictent le comportement des plus petites, même si ces dernières sont plus nombreuses. Dans un univers où la loi de la gravité est la seule à avoir de l'importance, le sort des plus petits objets est souvent incertain.

Je traiterai ici des galaxies naines, les plus abondantes de l'univers (Marzke & da Costa 1997) et parmi les plus difficiles à observer, à cause de leur petite taille et de leur faible luminosité.

1.1 Le Groupe Local

Les galaxies ont tendance à se condenser en groupes ou amas tel que l'on peut le voir dans la figure 1.1 qui montre plusieurs regroupements. Nous sommes situés au centre du schéma où l'on peut remarquer un amoncellement d'environ 1 Mpc en diamètre appelé le Groupe Local (GL). Marzke & da Costa (1997) prétendent que les galaxies naines sont les plus fréquentes et que, par conséquent, les spirales géantes telle la Voie Lactée sont des cas d'exception. Unavane et al. (1996) prétendent aussi que les membres les plus massifs du GL ne se sont pas formés avec leur taille actuelle mais qu'ils ont aggloméré plusieurs galaxies naines pour atteindre leur état. Les galaxies naines qui survivent à ce phénomène sont celles que nous observons aujourd'hui.

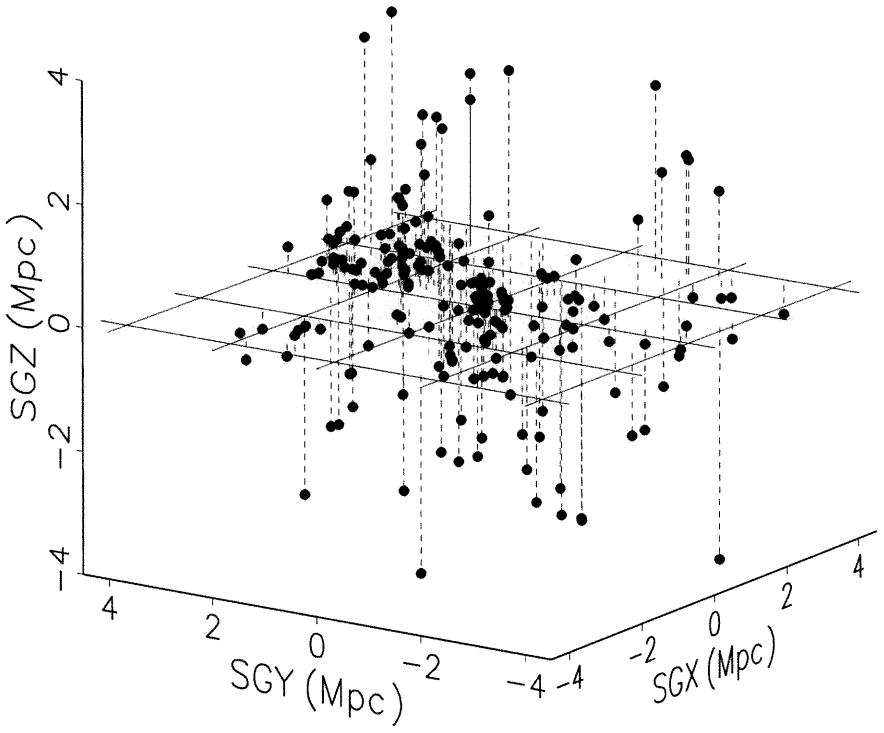

FIGURE 1.1 – Les galaxies proches. Tiré de Carroll & Ostlie (1996)

Près de la VL, se trouvent les groupes de Sculptor (distance de 1,7 à 4,4 Mpc) (Jerjen et al. 1998) et M81 (3,7 Mpc) (Karachentsev et al. 2000). Par contre, à cause des distances importantes, le seul groupe dans lequel nous pouvons espérer trouver un ensemble complet de galaxies est le GL.

Le GL est formé d'une quarantaine de galaxies pour la plupart naines. On peut en lire les détails dans le tableau 1.1 tiré en grande partie de la revue faite par Mateo (1998). On y aperçoit cinq galaxies dites géantes, soit M31, le petit nuage de Magellan (SMC), M33, le grand nuage de Magellan (LMC) et la VL.

Le groupe est subdivisé en quatre sous-groupes soit la Voie Lactée, M31, NGC 3109 et le Nuage Local (LGC pour *Local Galactic Cloud*). Les trois premiers sont définis par la proximité d'une galaxie géante hôte. Le dernier est un nuage étendu contenant principalement des naines irrégulières. Pour GR8, aucune appartenance à un ou l'autre sous-groupe n'a été identifiée. Elle est donc placée dans sa propre catégorie.

TABLE 1.1 – Les galaxies du Groupe Local (Mateo 1998)

Nom	α_{2000}	δ_{2000}	l	b	Type	Sous-groupe
WLM	00 01 58	-15 27.8	75.9	-73.6	IrrIV-V	LGC
NGC55	00 15 08	-39 13.2	332.7	-75.7	IrrIV	LGC
IC 10	00 20 25	+59 17.5	119.0	-3.3	dIrr	M31
Cetus[a]	00 26 11	-11 02.6	101.45451	-72.85447	dSph	VL
NGC147	00 33 12	+48 30.5	119.8	-14.3	dSph/dE5	M31
And III	00 35 17	+36 30.5	119.3	-26.2	dSph	M31
NGC 185	00 38 58	+48 20.2	120.8	-14.5	dSph/dE3p	M31
NGC 205	00 40 22	+41 41.4	120.7	-21.1	E5p/dSph-N	M31
M32	00 42 42	+40 51.9	121.2	-22.0	E2	M31
M31	00 42 44	+41 16.1	121.2	-21.6	SbI-II	M31
And I	00 45 43	+38 00.4	121.7	-24.9	dSph	M31
SMC	00 52 44	-72 49.7	302.8	-44.3	IrrIV-V	VL
Sculptor	01 00 09	-33 42.5	287.5	-83.2	dSph	VL
LGS 3	01 03 53	+21 53.1	126.8	-40.9	dIrr/dSph	M31
IC 1613	01 04 54	+02 08.0	129.8	-60.6	IrrV	M31/LGC
And II	01 16 27	+33 25.7	128.9	-29.2	dSph	M31
M33	01 33 51	+30 39.6	133.6	-31.3	ScII-III	M31
Phoenix	01 51 06	-44 26.7	272.2	-68.9	dIrr/dSph	VL/LGC
Fornax	02 39 59	-34 27.0	237.1	-65.7	dSph	VL
EGB0427+63	04 32 01	+63 36.4	144.7	+10.5	dIrr	M31
LMC	05 23 34	-69 45.4	280.5	-32.9	IrrIII-IV	VL
Carina	06 41 37	-50 58.0	260.1	-22.2	dSph	VL
Leo A	09 59 24	+30 44.7	196.9	+52.4	dIrr	VL/N3109
Sextans B	10 00 00	+05 19.7	233.2	+43.8	dIrr	N3109
NGC 3109	10 03 07	-26 09.5	262.1	+23.1	IrrIV-V	N3109
Antlia	10 04 04	-27 19.8	263.1	+22.3	dIrr/dSph	N3109
Leo I	10 08 27	+12 18.5	226.0	+49.1	dSph	VL
Sextans A	10 11 06	-04 42.5	246.2	+39.9	dIrr	N3109
Sextans	10 13 03	-01 36.9	243.5	+42.3	dSph	VL
Leo II	11 12 29	+22 09.2	220.2	+67.2	dSph	VL
GR 8	12 58 40	+14 13.0	310.7	+77.0	dIrr	GR8
Ursa Minor	15 09 11	+67 12.9	105.0	+44.8	dSph	VL
Draco	17 20 19	+57 54.8	86.4	+34.7	dSph	VL
Voie Lactée	17 45 40	-20 00.5	0.0	0.0	Sbc	VL
Sagittarius	18 55 03	-30 28.7	5.6	-14.1	dSph-N	VL
Sag DIG	19 29 59	-17 40.7	21.1	-16.3	dIrr	LGC
NGC 6822	19 44 56	-14 48.1	25.3	-18.4	IrrIV-V	LGC
Aquarius[b]	20 46 46	-12 51.0	34.0	-31.3	dIrr/dSph	LGC
IC 5152	22 02 42	-51 17.7	343.9	-50.2	dIrr	LGC
Tucana	22 41 50	-64 25.2	322.9	-47.4	dSph	LGC
UKS2323-326	23 26 27	-32 23.3	11.9	-70.9	dIrr	LGC
Pegasus	23 28 34	+14 44.8	94.8	-43.5	dIrr/dSph	LGC

[a]Tiré de Whiting et al. (1999)
[b]Généralement appelé DDO210

1.1.1 Appartenance au Groupe Local

L'appartenance au GL n'est pas simple à démontrer. Il faut posséder des informations sur la distance de chacun des objets pour déterminer s'ils sont réellement à l'intérieur du groupe ou non. De plus, des informations sur la vitesse (radiale et tangentielle) de chaque élément peuvent être nécessaires quand on cherche à savoir si chaque objet est lié gravitationellement au groupe. Certains de ces objets pourraient ne pas être liés au groupe et le traverser sans être retenus par son potentiel gravitationnel.

Aspects cinématiques

La grande luminosité des galaxies géantes permet facilement les études spectroscopiques nécessaires pour connaître leur champ de vitesse radiale. Mais la faible luminosité des naines rend cette mesure plus ardue (Gallart et al. 2001). Aussi, une panoplie de problèmes et de questions sont soulevés lorsqu'une telle étude est accomplie. Armandroff & Da Costa (1986) citent quelques-unes de ces interrogations et se questionnent sur la validité des résultats qui sont obtenus. Le problème majeur est la dispersion des vitesses mesurées. La seule façon d'expliquer les résultats est de supposer que les naines sont les systèmes les plus riches en matière sombre jamais détectés, avec une densité qui pourrait atteindre 1 $M_{\odot}$ pc^{-3} (Moore 1996).

Il est également théoriquement possible d'utiliser des données radio pour déterminer ces vitesses, comme l'ont fait St-Germain et al. (1999) dans le cas de la naine irrégulière/sphéroïdale Phoenix. Ces données ont récemment été confirmées par la spectroscopie optique (Gallart et al. 2001). Cet aspect sera traité plus en détail ultérieurement dans ce mémoire.

Pour ce qui est des vitesses tangentielles, l'étude est encore plus difficile. Les distances impliquées dans le GL empêchent généralement de distinguer un mouvement propre pour ces objets. Jusqu'à ce jour, seules les dSph Sculptor (Schweitzer et al. 1995), Ursa Minor (Schweitzer & Cudworth 1996) et Ursa Major (Schweitzer et al. 1997) possèdent un mouvement propre qui nous est connu.

Mais le mouvement réel d'une galaxie n'est pas suffisant pour déterminer si cette galaxie est liée ou non au groupe. Ce que nous voulons savoir, en définitive, c'est si elle peut s'échapper du groupe. Il faut donc connaître la masse du GL pour en déduire la vitesse d'échappement. Elle serait déterminée en traçant les orbites des corps les plus externes du groupe puis, avec l'aide des lois de Kepler, nous pourrions reconstruire la masse du corps central (Wilkinson & Evans 1999). Une autre technique, expérimentale cette fois, servant à déterminer les paramètres orbitaux des galaxies en interactions a été développée par Wahde (1998).

Tous ces facteurs font que les études sur l'appartenance d'une galaxie au GL sont souvent assez limitées. Par contre, ces problèmes disparaissent dès que nous sortons de notre environnement immédiat. Il devient alors plus facile d'associer spatialement une galaxie à un groupe puisque, grâce aux plus grandes distances en jeu, le dit groupe sous-tend un angle

solide beaucoup plus petit que celui sous-tendu par le GL (soit 4π stéradians). Il est donc plus facile de le voir au complet et le besoin de connaître les orbites exactes disparaît.

Problèmes de détection

D'un autre côté, à cause de leur faible luminosité, les galaxies naines sont parfois difficiles à détecter. La galaxie Cetus (Whiting et al. 1999) fut la dernière à être découverte dans le GL. Sa distance (775 ± 50 kpc, $(m - M)_0 = 24{,}45 \pm 0{,}15$) est probablement le facteur le plus important qui a retardé sa découverte. Cette distance pousse sa magnitude apparente intégrée sur la surface de la galaxie jusqu'à une valeur de $m_v = 14.4$. Ce ne sont cependant pas là les seuls problèmes de détection que l'on retrouve.

Il est à noter que la très grande majorité des galaxies connues résident loin du plan de la Voie Lactée. La poussière interstellaire et la densité d'objets près du plan galactique nuisent fortement aux moyens de détection standards.

C'est ainsi qu'a été définie la zone interdite (ZOA pour *Zone of Avoidance*). Il s'agit d'une mince bande qui traverse le ciel et qui correspond au plan de la Voie Lactée. La poussière interstellaire, concentrée dans le plan (Krautter 1980), empêche littéralement toute détection extragalactique dans cette zone à l'aide de longueurs d'ondes optiques. Nous devons donc travailler à des fréquences qui ne seront pas affectées par la poussière.

Il existe entre autres deux choix pour pallier à cette situation. Les longueurs d'ondes de 21 cm et infrarouges permettent justement d'observer au travers du disque galactique. Pour le 21 cm (ou HI pour hydrogène neutre), de grands sondages, comme ceux des équipes ZOA (Henning et al. 1999) et HIPASS (Staveley-Smith & et al. 2000) à Parkes en Australie, ont déjà démontré leurs capacités de découvrir de nouvelles galaxies, invisibles optiquement (Kilborn et al. 2000). Pour l'infrarouge, la mise en service de nouveaux télescopes tels que les Gémini permettra ce genre d'observations (Jacobson et al. 1998). Nous pourrons donc nous débarrasser tranquillement de la ZOA en trouvant les objets qui s'y situent et ainsi nous débarrasser d'un important effet de sélection dans la distribution des galaxies.

1.1.2 Formation galactique

La formation de la VL (et du GL) fait encore l'objet de plusieurs théories. Parmi celles-ci, certaines impliquent que les amas globulaires et les galaxies naines sont des restants de la formation de la VL (Carroll & Ostlie 1996).

Des fluctuations de densité, peu après le Big Bang, auraient engendré la formation de petits objets qui se seraient ensuite assemblés pour former la VL. Cette théorie a l'avantage de tenir compte de la présence des amas globulaires et des étoiles, dans le halo galactique, qui suivent parfois un mouvement rétrograde par rapport à la rotation de la galaxie (van den Bergh 1993).

Ces systèmes nains montrent souvent des traces de collisions et d'interactions avec d'autres

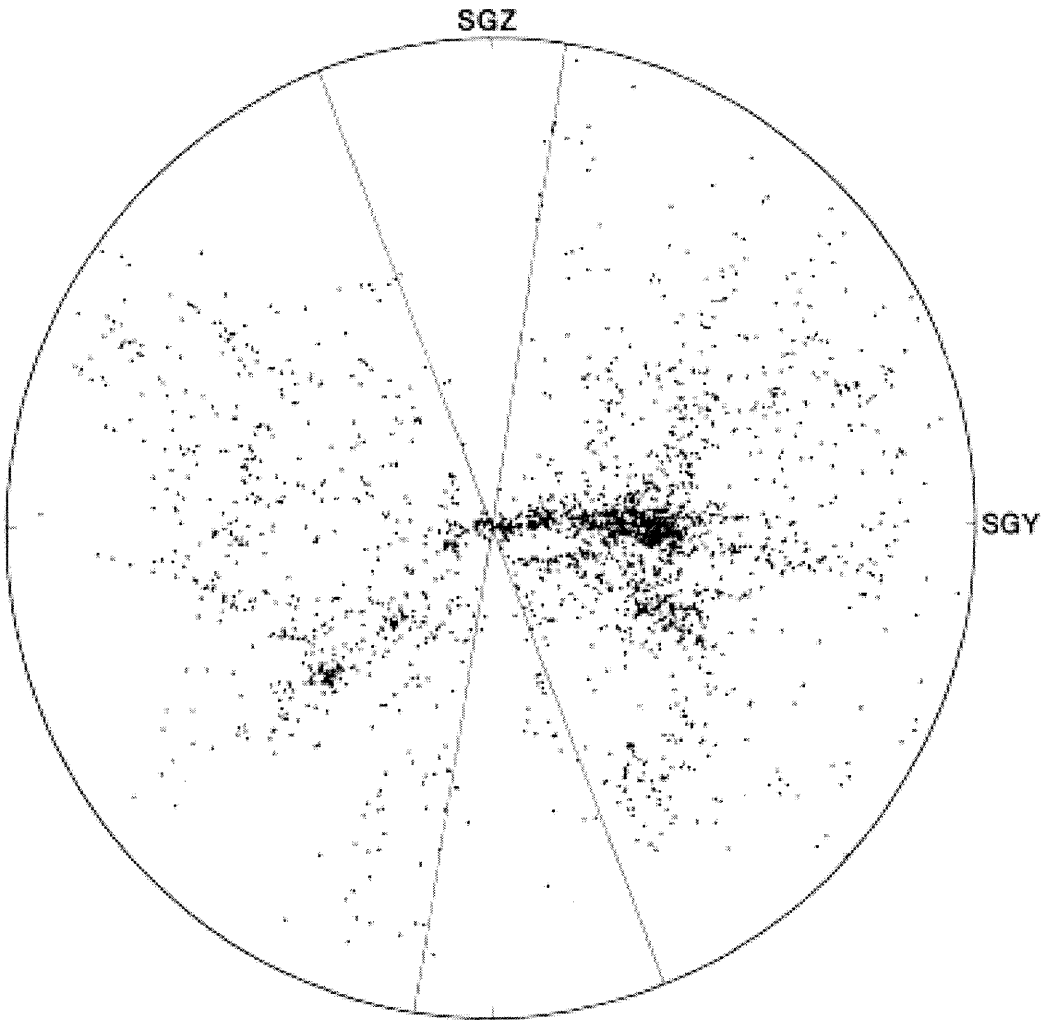

FIGURE 1.2 – Tully (1982) démontre bien les problèmes engendrés par le plan galactique. On voit 2175 galaxies brillantes connues à l'époque presque toutes à l'extérieur des deux droites qui définissent la ZOA. Les axes (SGY et SGZ) sont les coordonnées cartésiennes supergalactiques.

galaxies plus massives telles que la VL et la galaxie d'Andromède (M31). C'est le cas de la naine Sagittarius (Ibata et al. 1994) qui est littéralement engloutie dans la VL. C'est ainsi, par agglomération de galaxies naines et d'amas globulaires, que les galaxies géantes se seraient formées (Bullock et al. 2001). Les galaxies qui survivent à ce phénomène sont celles que nous observons aujourd'hui.

Mais ces traces de collisions pourraient être le signe d'un autre type de formation. Braine et al. (2000) parlent des collisions galactiques comme une des causes possibles de formation des naines. Même si le scénario exact de formation de ces galaxies est encore inconnu, une chose est certaine: les collisions jouent un rôle important dans l'évolution de celles-ci (Arribas et al. 2000).

Collisions de galaxies

Les collisions galactiques sont des phénomènes fréquents dans n'importe quel groupe. Spitzer & Baade (1951) avaient déjà émis l'idée qu'une galaxie pourrait entrer en interaction proche avec une vingtaine d'autres galaxies durant une période d'environ 10^9 années, dans les amas les plus denses.

Ces effets peuvent prendre plusieurs formes. Les plus fréquentes sont les effets de marées. Puisque la force gravitationnelle décroît en $1/r^2$, il est facile d'imaginer un système où le corps qui attire produit un champ de gravité assez grand près de lui et qui décroît rapidement avec la distance, ce qui induit une force gravitationnelle différentielle dans la galaxie. Les effets peuvent être très importants et détruire la structure classique des galaxies, comme le démontre la figure 1.3.

Il arrive très souvent que les interactions gravitationnelles entre les galaxies ne soient apparentes qu'en regardant la matière interstellaire qui compose cette galaxie (de Blok & Walter 2000). En effet, le gaz qui se retrouve dans le halo est plus sensible à ce genre d'interaction puisqu'il est en général beaucoup plus étendu que la composante stellaire du système. Cela constitue donc un marqueur potentiel pour trouver la distance d'une galaxie, pourvu que nous connaissions la distance d'un compagnon proche. L'interaction gravitationnelle sert ici à démontrer que les deux galaxies sont effectivement proches l'une de l'autre.

Le phénomène devient nettement plus intéressant dans le cas des dSph dans un amas plus ou moins dense. Dans ces systèmes, les forces de marées appliquées à la galaxie peuvent dépasser en intensité ses forces internes de cohésion (Oh et al. 1995). Dans ce cas la galaxie pourrait être complètement détruite par le processus, comme dans le cas de Sagittarius où des débris ont été détectés à 60° du centre de la naine (Dohm-Palmer et al. 2001). Carignan (1999) et Blitz & Robishaw (2000) s'entendent à dire que certaines de ces galaxies contiennent du gaz et plusieurs nuages ont été détectés loin du centre optique des galaxies, donnant plus de poids aux théories dites de *tidal stripping*.

Depuis la découverte du mouvement propre de Sculptor par Schweitzer et al. (1995), une

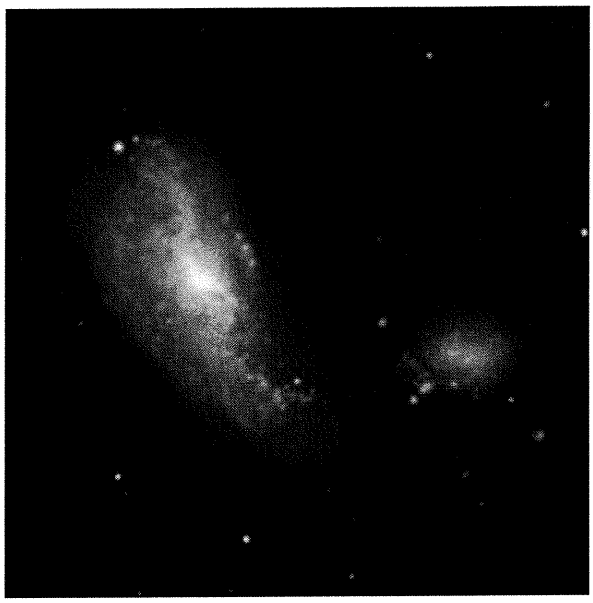

FIGURE 1.3 – Le couple de galaxies ARP269 est un exemple parfait de collision. La plus grosse des deux galaxies a été déchirée par les forces de marées appliquées par la plus petite mais montre encore des résidus de bras spiraux. L'image est tirée du répertoire OPIOMM (`http://www.astro.umontreal.ca/~opiomm`).

autre théorie a fait surface. C'est celle du *Ram pressure stripping*. Le milieu intergalactique, quoique très peu dense, agit sur le milieu interstellaire d'une galaxie. Lorsque celle-ci se déplace à l'intérieur d'un amas, son propre gaz ou milieu interstellaire entre en choc avec le milieu de l'amas. Puisque le gaz est beaucoup plus léger que les étoiles de la galaxie, il est plus affecté par ce choc et est, par conséquent, ralenti comparativement à la course des étoiles. En pratique, on verra le gaz décentré par rapport à la contrepartie optique de la galaxie.

1.1.3 Galaxies naines

Comme le montre la table 1.1, il y a plusieurs types de galaxies proches de nous. Les plus faciles à étudier sont invariablement les plus brillantes. Mais ce ne sont pas les plus abondantes. Les galaxies naines sont les plus nombreuses de l'univers (Marzke & da Costa 1997). Elles constituent un élément important dans la compréhension de la dynamique interne des amas car, à cause de leur grand nombre, elles sont d'excellent traceurs des sous-structures (Karachentsev 1996). C'est pourquoi il est important de connaître leur sort pour pouvoir déterminer par quel processus les amas se forment (Pearce et al. 1999; van Dokkum et al. 1999).

À cette fin, le GL est le laboratoire idéal pour étudier les interactions entre les galaxies puisqu'il est possible d'y observer les objets les plus faibles, même si certains membres n'ont été découverts que très récemment (Whiting et al. 1999, la naine sphéroïdale Cetus).

Ces galaxies peuvent être subdivisées en plusieurs classes que l'on croit interreliées (Ferguson & Binggeli 1994; Puche & Westpfahl 1994). Ces classes sont les naines irrégulières (dIrr), les naines elliptiques (dE) et les naines sphéroïdales (dSph). Il existe également d'autres types de naines telles que les *Blue Compact Dwarfs* ou BCD qui ne seront toutefois pas discutées dans ce mémoire (voir Audouze et al. 1980, pour une description complète).

En général, nous pouvons dire que le lien majeur qui relie les galaxies sous l'emblème «naine» est leur faible luminosité absolue $M_B \lesssim -15$. Cette caractéristique provient principalement de leur faible masse. Ce sont des systèmes stellaires de formes plus ou moins sphéroïdales dont la structure est maintenue par la dispersion de la vitesse des étoiles dans la galaxie et non par la rotation de celles-ci, comme dans le cas des spirales.

Le problème de définir une nomenclature uniforme et universelle pour les galaxies naines n'est pas trivial et plusieurs auteurs (Binggeli 1994, entre autres) se sont déjà penchés sur le problème. Voici ce qui en résulte.

Les naines irrégulières

Les dIrr sont des systèmes riches en gaz qui supportent la formation d'étoiles plus ou moins intense mais continue. En effet, elles ont généralement une bonne quantité d'étoiles de population I (donc des étoiles jeunes) (Grebel 1998). Elles possèdent également de grandes quantités de HI (Mateo 1998).

Les naines elliptiques

Les naines elliptiques (dE) sont des galaxies avec une luminosité de surface extrêmement faible et sont généralement dénudées de gaz. Elles sont principalement peuplées d'étoiles de population II (Grebel 1998). Il s'agit du terme général pour désigner ce type de galaxies. Plusieurs auteurs incluent les galaxies naines sphéroïdales dans cette catégorie même s'il existe encore certaines distinctions à faire entre les deux.

Les naines sphéroïdales

Il n'est pas évident de différencier les naines sphéroïdales (dSph) des naines elliptiques. La différence morphologique majeure est l'absence d'un noyau central brillant comme celui des elliptiques.

Plusieurs auteurs classent en fait les dE et les dSph dans la même catégorie, affirmant qu'il n'y a pas de définition stricte des termes employés et que les appellations sphéroïdale et elliptique réfèrent aux mêmes objets. Par tradition historique, celles qui font partie du GL ont acquis le nom de sphéroïdales alors que les autres (par exemple celles des groupes tels que Fornax ou Virgo) portent le nom d'elliptiques.

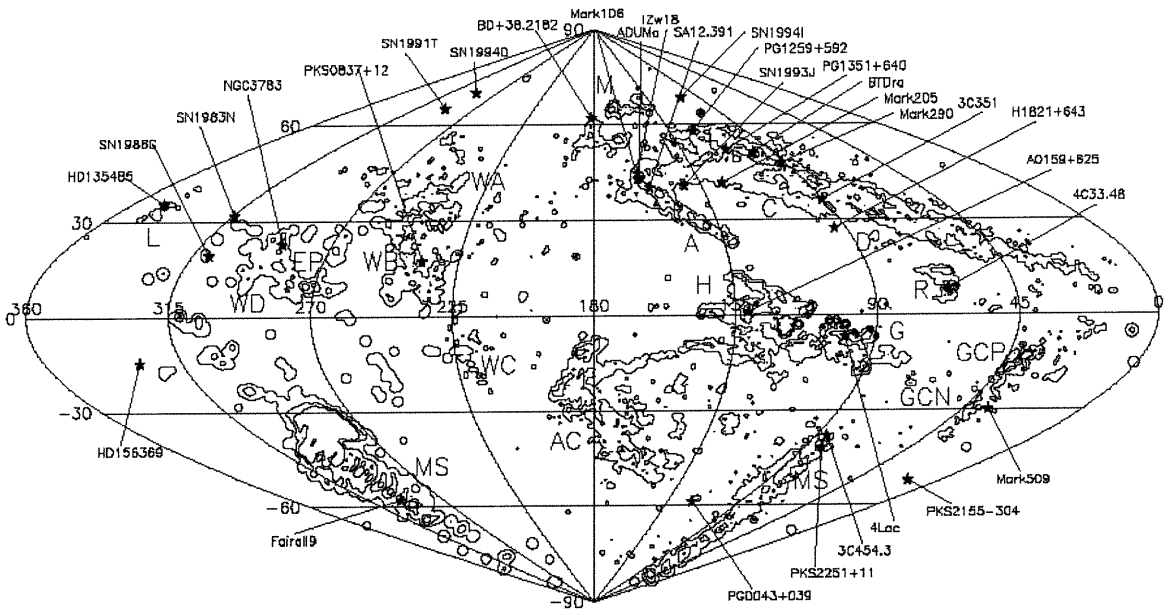

FIGURE 1.4 – La distribution spatiale des HVC. On peut voir qu'ils couvrent la majorité du ciel. Plusieurs de ces nuages ont été rassemblés en complexes qui sont probablement d'origines différentes. La figure est tirée de l'article de Wakker & van Woerden (1997).

1.1.4 *High Velocity Clouds*

On ne peut conclure un aperçu, aussi bref soit-il, du GL sans parler de ces objets omniprésents et pourtant extrêmement mystérieux que sont les HVC (pour *High Velocity Clouds*).

Selon Wakker & van Woerden (1997), ce sont des nuages d'hydrogène neutre (HI) incompatibles avec un modèle de rotation différentielle de la galaxie. En pratique, tous les nuages correspondant à une vitesse radiale par rapport à la référence de repos local (LSR pour *Local Standard of Rest*) $V_{LSR} \gtrsim 90$ km/s sont généralement classés comme HVC. La figure 1.4 montre la distribution des HVC de la VL.

Le problème majeur en ce qui a trait à ce type de nuage est qu'il n'existe presque aucune information sur leur distance. Mais certaines techniques existent pour la découvrir. La plus prometteuse est celle qui consiste à prendre le spectre d'étoiles dans la même ligne de visée qu'un HVC et d'essayer de détecter la présence dudit HVC dans le spectre de l'étoile (Schwarz et al. 1995). Si des traces d'absorption par un nuage d'hydrogène sont visibles dans le spectre et que le décalage spectral de ces traces correspond à la vitesse du HVC, celui-ci doit être situé entre l'étoile et l'observateur pour influencer la lumière analysée.

Donc, si l'on détecte des raies d'absorption venant du HVC et que l'on connaît la distance de l'objet, on peut placer une limite supérieure à la distance du nuage. De la même façon, si les raies d'absorption ne sont pas présentes dans le spectre, le nuage est alors situé derrière

l'étoile et on obtient ainsi une limite inférieure à la distance. Une description plus complète de la mesure de distance des HVC peut être trouvée dans l'article de van Woerden et al. (1999a).

Il reste que les distances qui ont été mesurées jusqu'à maintenant sont de l'ordre de 5 à 10 kpc (van Woerden et al. 1999a), ce qui les place à l'intérieur du halo de la VL (le halo de matière sombre s'étend jusqu'à un maximum de 50 kpc selon Little & Tremaine (1987)). Les HVC pourraient très bien être des résidus de collisions galactiques ou des débris arrachés à d'autres galaxies par des forces de marées, bien que van Woerden et al. (1999b) préfèrent penser aux fontaines galactiques comme sources pour ces nuages. Si nous prenons l'exemple de la dSph Sculptor qui se trouve à environ 79 kpc du Soleil, donc à la limite extérieure du halo galactique sombre, de la matière éjectée de cette galaxie pourrait très bien se retrouver classée parmi les HVC (Blitz & Robishaw 2000).

Alors que la majorité des auteurs semblent croire que les HVC ont des origines galactiques plutôt qu'extragalactiques, il reste encore certains auteurs, dont Braun & Burton (1999), qui croient que ces objets n'ont eu que très peu d'interactions avec les galaxies massives et, par conséquent, seraient des objets placés beaucoup plus loin que le halo local bien que membres du GL.

La réalité pourrait cependant ne pas être aussi simple. Après une étude détaillée de l'hémisphère austral utilisant le relevé HIPASS (Staveley-Smith & et al. 2000), Putman & Gibson (1999) démontrent qu'il est pratiquement impossible que tous les HVC soient de la même origine. Il existe donc plusieurs types de HVC et ceux-ci sont souvent rassemblés en complexes, définis selon leurs provenances supposées, comme ceux provenant du Grand Nuage de Magellan (Putman et al. 1998). Mais il y a aussi les nuages qui ne font pas partie de ce type d'association et qui pourraient originer de fontaines galactiques (de Avillez 2000).

Finalement, il est intéressant de noter que le phénomène des HVC n'est pas exclusif à la VL puisque van der Hulst & Sancisi (1988) ont découvert dans M101 des structures qui leur ressemblent beaucoup.

1.2 Contenu stellaire

Une des façons les plus efficaces pour étudier les galaxies est de se pencher sur leur contenu stellaire. Les étoiles nous donnent beaucoup d'informations sur le passé d'une galaxie, entre autres, grâce à l'étude des diagrammes couleur-magnitude (CMD).

Les CMD de Grebel (1998) prouvent que ces astres ont parfois eu plus d'une étape de formation stellaire, plusieurs milliards d'années auparavant et que certaines sont même assez récentes (quelques centaines de milliers d'années). Ells ne sont donc pas des systèmes aussi simples que ce que l'on croyait il y a 20 ou 30 ans.

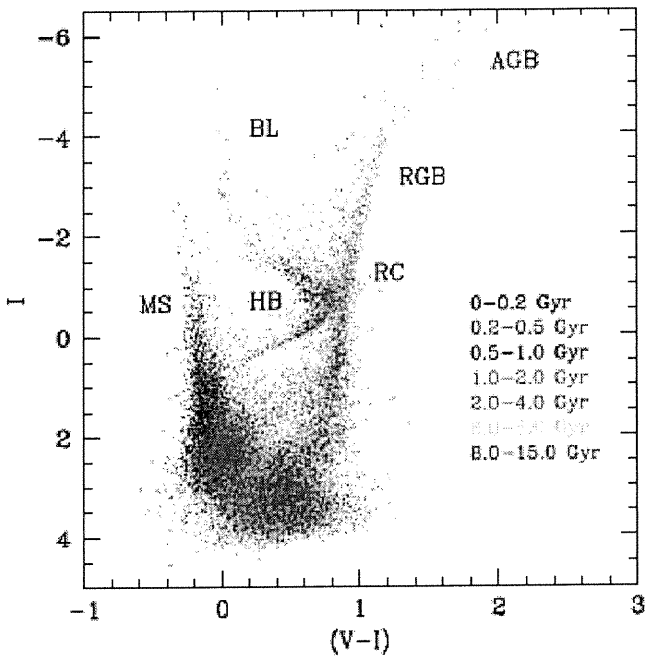

FIGURE 1.5 – Le diagramme couleur-magnitude est un outil essentiel à l'étude des populations stellaires. Celui-ci est tiré de la thèse de David Martìnez-Delgado. Il s'agit d'un diagramme théorique d'une galaxie ayant un taux de formation stellaire constant depuis 15 milliards d'années.

1.2.1 Formation stellaire

Jusqu'à tout récemment, il était admis que les dSph et les dE étaient des systèmes morts qui n'avaient que des populations stellaires vieilles (Baade & Gaposchkin 1963). Il s'est avéré que cette description quelque peu simpliste ne collait pas tout à fait à la réalité. Récemment, Hurley-Keller et al. (1999) ont en effet montré que la galaxie de Sculptor avait subi une période de formation stellaire plus étendue que ce que l'on croyait. Et ce n'est pas le seul exemple. Les CMD sont l'outil de prédilection de toutes personnes intéressées à la formation stellaire. Comme le montre la figure 1.5, les différents types d'étoiles occupent différentes positions dans le diagramme.

Ainsi, nous pouvons facilement voir que la présence d'une branche horizontale (HB) est un signe infaillible d'une population stellaire vieille (~15 Gyr), alors que la présence d'étoiles dans l'anneau bleu (BL pour Blue Loop), qui sont des étoiles de masses intermédiaires brûlant de l'hélium, est une indication de formation stellaire récente (~1 Gyr).

La séquence principale (MS) est l'endroit où les étoiles passent la plus grande partie de leur vie. Il s'agit également d'un indicateur (pas particulièrement efficace mais un indicateur quand même) de l'âge d'un amas. La présence d'étoiles massives sur la MS implique un amas jeune. Une concentration rouge (RC pour Red Clump) est le signe d'une population intermédiaire

plus ou moins importante (de 1 à 2 Gyr).

Un exemple frappant est probablement celui de Leo I (Gallart et al. 1999) où les étoiles les plus vieilles manquent à l'appel. Comme le montre bien la figure 1.6, les étoiles semblent toutes avoir été formées depuis 7 milliards d'années avec une coupure abrupte il y a 1 milliard d'années. Ce qui attire l'attention dans cet exemple, c'est que dans le cas de la majorité des dSph, le sursaut initial de formation stellaire est le plus important de l'histoire de cette galaxie, alors que dans le cas de Leo I, les étoiles ont commencé à se former il y a 12 milliards d'années et la véritable formation a commencé 5 milliards d'années plus tard.

1.2.2 Évolution stellaire

Selon Lamers & Cassinelli (1999), la majorité des étoiles perdent une partie importante de leur masse à cause des phénomènes de vents stellaires. Souvent, un noyau d'environ une $M_\odot$ reste à la fin de la vie de l'étoile en général sous forme de naine blanche. Les vents stellaires varient grandement d'une étoile à l'autre et d'un âge à l'autre.

Les étoiles massives (principalement les Wolf-Rayet) dégagent un vent qui interagit fortement avec la matière qui les entoure (Gervais & St-Louis 1999). Avec des vitesses terminales de l'ordre de 1000 km s^{-1} (Prinja et al. 1990) et des taux de perte de masses autour de 10^{-5} $M_\odot$/année (Abbott & Conti 1987), leur influence sur le milieu interstellaire d'une galaxie naine est considérable.

Mais les étoiles massives ne sont pas les seules intéressantes dans le cas des galaxies naines sphéroïdales pour la simple raison qu'en général la phase de formation stellaire la plus intense s'est terminée il y a plus d'un milliard d'années (Grebel 1998). Ainsi, leurs stades évolutifs intéressants, à savoir les stades super-géantes rouges et Wolf-Rayet, sont tous terminés depuis longtemps et les vents stellaires se sont éteints.

Pour les étoiles de masses intermédiaires (entre 1 et 8 $M_\odot$), la plus grande partie de la perte de masse s'opère quand l'étoile est sur la branche asymptotique des géantes (voir la figure 1.5). Ce stade évolutif apparaît après 8 à 15 milliards d'années. Le vent de ce type d'étoiles produit des pertes de masses de l'ordre de 10^{-4} à 10^{-7} $M_\odot$/année. Le vent qui en résulte se dilate à environ 30 km/s, ce qui est considéré comme très petit. Toujours selon Lamers & Cassinelli (1999), une étoile de 8 $M_\odot$ peut renvoyer jusqu'à 90% de sa masse dans l'ISM au cours de son existence.

Donc une dSph qui a typiquement 10^6 $M_\odot$ ou 10^7 $M_\odot$ (principalement sous forme d'étoiles peu massives), pourrait voir sa matière interstellaire augmenter de 1 $M_\odot$/année. Ainsi, à la suite d'une période de 10^6 ans, la quantité de HI présente dans la galaxie, uniquement due à l'évolution stellaire normale, aurait atteint des niveaux détectables avec les grands sondages radio à une distance d'un Mpc (Staveley-Smith & et al. 2000, HIPASS).

De plus, comme décrit précédemment, les étoiles continuent à se former dans certaines de ces galaxies, ce qui implique qu'une quantité assez grande de gaz doit être présente. Mais, sauf

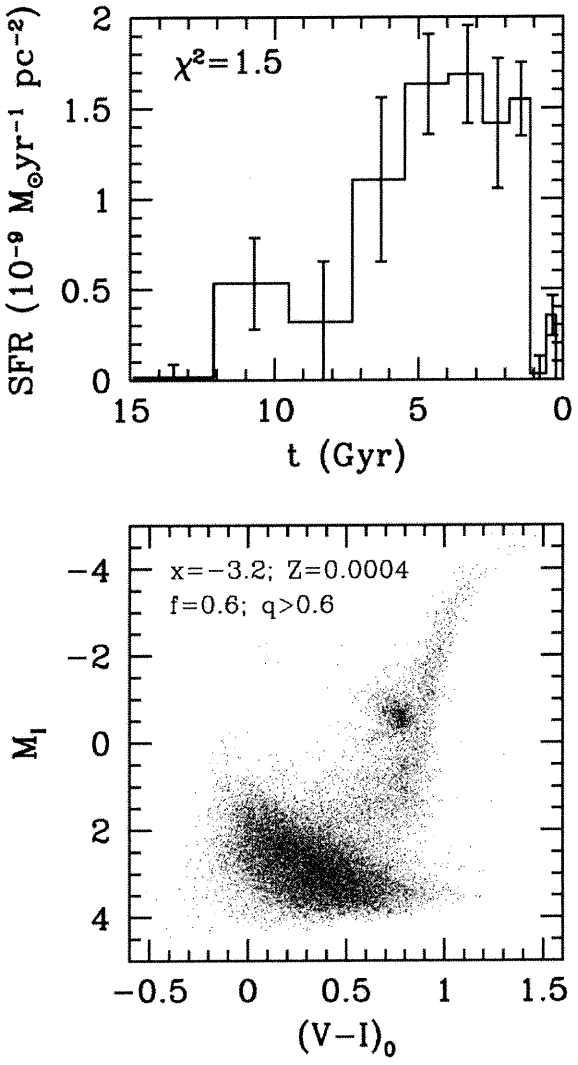

FIGURE 1.6 – La dSph Leo I déroge clairement de la règle et montre une formation stellaire atypique, qui ne colle pas avec les vieilles descriptions. La figure est tirée de l'article de Gallart et al. (1999).

pour quelques exceptions (St-Germain et al. 1999; Carignan et al. 1998, Phoenix et Sculptor respectivement), aucune observation ne permet de conclure à la présence d'une quantité suffisante de gaz pour comprendre l'histoire de la formation stellaire. Les étoiles ont besoin d'hydrogène pour se former et cet hydrogène reste introuvable dans ces systèmes.

1.3 Matière interstellaire

Historiquement, la première composante des galaxies que nous avons découverte fut la composante stellaire optique. Puis, lorsque les astronomes ont commencé à faire des observations à d'autres longueurs d'ondes, ils ont découvert d'autres formes de matière présentes dans ces galaxies. Il s'agit principalement d'hydrogène mais aussi de nuages de poussière et autres molécules. L'hydrogène étant l'élément le plus abondant de l'univers, on peut donc l'utiliser comme traceur pour connaître grossièrement la distribution de la matière interstellaire dans ce type de galaxies.

1.3.1 Pourquoi chercher de l'hydrogène?

Plusieurs études sur le contenu gazeux des naines sphéroïdales ont été éffectuées, ne révélant aucune source de HI (Knapp et al. 1978; Thuan & Martin 1979; Mould et al. 1990; Koribalski et al. 1994). À l'époque, le résultat n'était pas trop surprenant car il était admis que leur historique de formation stellaire était relativement simple (Baade & Gaposchkin 1963). Ce sont des études comme celles de Hurley-Keller et al. (1999) qui ont jeté le doute sur ces non-détections.

1.3.2 Sort probable de la matière interstellaire

Les galaxies naines, et encore plus les naines sphéroïdales, ont de très faibles puits gravitationnels (Mateo 1998) pour garder leur matière interstellaire. Ainsi, dans un environnement rapproché, où les collisions sont fréquentes, la composante gazeuse est souvent la plus affectée (Hogg et al. 1998).

On peut penser facilement à deux phénomènes pour retirer le gaz d'une galaxie. Ces phénomènes sont la pression de contact (Ram Pressure) et les forces de marées (combinées aux vents galactiques). Il n'est pas encore clair lequel des deux domine dans le GL mais nous pouvons facilement concevoir qu'ils sont tous deux présents.

Vents galactiques

Les vents galactiques, causés par l'addition des vents stellaires, sont souvent observables dans les galaxies naines sous la forme d'immenses coquilles de gaz en expansion (de Blok & Walter 2000). Ces coquilles sont souvent centrées sur une région de formation stellaire active (Gervais & St-Louis 1999).

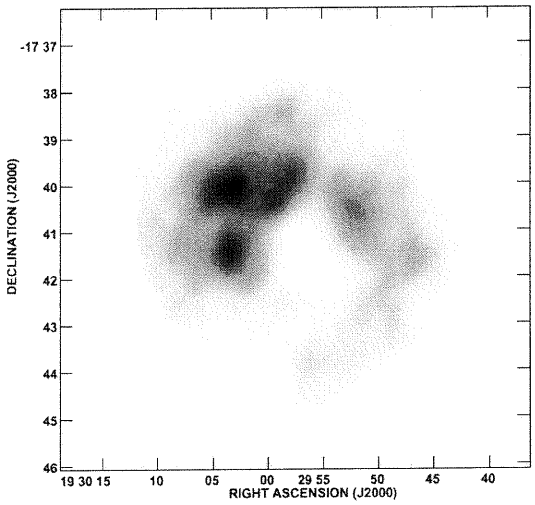

FIGURE 1.7 – Un anneau de gaz entoure complètement Sag DIG. Cette figure est tirée de l'article de Young & Lo (1997b).

Dans d'autres cas, ce sont des galaxies complètes qui ont été trouvées au centre de ces bulles. C'est le cas de la dIrr dans la constellation du Sagittaire Sag DIG (voir table 1.1) tel que le montre la figure 1.7. Donc, ce phénomène existe et il est un élément important en ce qui concerne le sort de la matière interstellaire dans les galaxies naines (Martin 1998).

Mais les simulations numériques de D'Ercole & Brighenti (1999) montrent que le gaz peut être très résistant à ce type de vent et qu'une quantité non négligeable de gaz peut rester à l'intérieur de la naine. La matière interstellaire n'est donc pas automatiquement perdue quand l'énergie du vent dépasse celle du potentiel gravitationel de la galaxie.

Pression de contact

Lorsqu'une galaxie se déplace dans le milieu intergalactique, elle se déplace dans un milieu qui est rempli d'un gaz très peu dense mais quand même capable de freiner le déplacement de cette galaxie. C'est surtout le gaz qui est affecté par cette pression et il est arraché par le vent de particules qu'il rencontre (Carroll & Ostlie 1996). Ce phénomène est très important et ce, même pour les spirales capables de retenir leur propre gaz (Vollmer et al. 2000, NGC4522).

De plus, les courbes de rotation des galaxies spirales montrent clairement que la matière visible qui les compose n'est pas la seule à entrer dans la composition de cette galaxie (Blais-Ouellette et al. 2001). Ces courbes sont formées de trois composantes majeures soit les étoiles, le gaz interstellaire et le halo de matière sombre. Le gaz interstellaire, principalement le HI , est un excellent traceur de la courbe de rotation des galaxies à grande distance du centre, où la composante de matière sombre devient dominante (Carignan & Purton 1998).

Puisqu'aucune théorie jusqu'à aujourd'hui ne peut dire sans l'ombre d'un doute de quoi est composée la matière sombre, il n'est pas encore possible de préciser quel rôle elle joue au

niveau des pressions de contact.

Forces de marées

Lorsque deux galaxies passent très près l'une de l'autre, les forces de marées deviennent très importantes et peuvent déformer de façon significative les galaxies qui interagissent. En effet, lorsqu'une galaxie se déplace dans un champ de gravitation non uniforme, elle s'étire sous l'effet de ce champ. Les régions les plus proches de la galaxie hôte se placent sur des orbites plus raprochées et donc atteignent des vitesses différentes à leurs périgées que celles sur des orbites plus éloignées.

Cet effet est majeur quand le champ de gravité de la galaxie est faible par rapport au champ externe. Comme le montre la figure 1.3, la galaxie a du mal à survivre à la collision. Il s'agit d'un phénomène très efficace pour retirer le gaz de la galaxie, puisqu'il est en général plus étendu que la composante stellaire et, par conséquent, plus affecté par les forces de marées.

Une galaxie naine en collision pour la première fois avec une géante comme la VL se verra donc arracher son gaz qui, en principe, pourrait retomber sur la naine une fois le passage terminé, par les effets de sa propre gravité. Ainsi, l'historique de formation stellaire montrerait alors un sursaut correspondant à l'effondrement du gaz sur la galaxie.

Les nuages qui se détachent ainsi de leur galaxie hôte peuvent alors être pris dans le champ de gravité de l'autre galaxie et rester plus rattachés à la galaxie massive qu'à l'originale.

Mais, à la lumière des chapitres précédents, nous pouvons croire que ce phénomène ne se produit pas seul. Il est en général présent en même temps que les pressions de contact et vents galactiques, à des niveaux plus où moins importants.

1.4 HIPASS comme outil

Le HI Parkes All Sky Survey (HIPASS) fut un des outils les plus importants de la présente étude. Puisque la majorité des objets étudiés n'ont jamais été détectés en HI auparavant et si l'on considère les phénomènes décrits au chapitre précédent, il est important de pouvoir regarder un champ assez large autour de ces objets si l'on veut trouver la matière interstellaire qui s'y rattache. Puche & Westpfahl (1994) avaient déjà suggéré de chercher le gaz à l'extérieur du disque optique des naines sphéroïdales.

1.4.1 HI (*21cm*)

L'hydrogène étant l'élément le plus abondant de l'univers, dans certaines conditions (entre autres lorsqu'il est à l'état neutre) il est la composante la plus facile à détecter dans la matière interstellaire. Sa structure, lorsqu'il est à l'état neutre, lui permet d'émettre un rayonnement électromagnétique d'une longueur d'onde de 21,1049 cm (1420.40575168460 MHz) (Scheffler et al. 1987), dit HI .

Il s'agit de la raie d'émission de la structure hyperfine de l'hydrogène. Lorsque laissé froid (~100 K) assez longtemps (~1000 ans), l'électron dans l'atome d'hydrogène, s'il est au niveau fondamental et si son spin est parallèle à celui du proton, change spontanément de spin pour que celui-ci soit aligné de façon anti-parallèle à celui du noyau. Selon la théorie de la structure hyperfine de l'hydrogène, cet état possède légèrement moins d'énergie que le précédent. Donc un photon est émis, libérant cette énergie. Cette source de rayonnement est un excellent traceur de la quantité d'hydrogène neutre dans l'univers.

1.4.2 Le *HI Parkes All Sky Survey*

HIPASS (Staveley-Smith & et al. 2000) fut un immense projet utilisant le télescope de Parkes en Australie, qui visait à observer tout le ciel de l'hémisphère sud pour y rechercher de l'émission HI et la cartographier. C'est ce sondage qui a posé les bases sur lesquelles s'articule ce mémoire. Il a été utile à plusieurs points de vue.

Plusieurs observations avait déjà été effectuées avec des interféromètres comme ceux du *Very Large Array* au Nouveau-Mexique ou du *Australia Telescope Compact Array* dans le *New South Wales* en Australie qui sont capables d'atteindre des résolutions spatiales inégalées mais au prix de la sensibilité du télescope aux rayonnements électromagnétiques. En effet, ces télescopes sont parfois insensibles à des structures qui dépassent certaines dimensions angulaires comme dans le cas de Sculptor (Carignan et al. 1998).

De plus, la dimension du télescope de Parkes (64 m) lui permet d'atteindre des niveaux de signal sur bruit qui dépassent ceux des interféromètres pour les sources de plus en plus faibles. Et, puisqu'il s'agit d'un sondage de tout le ciel, il n'y a aucun problème de champ de vision (Puche & Westpfahl 1994). Le gaz ne peut que très difficilement se situer à l'extérieur de la zone observée.

Les paramètres d'observation donnés à la table 1.2 montrent les détails du projet HIPASS dont la partie initiale a été officiellement complétée au mois de mars 2000; l'extension nordique a été complètée le 14 mai 2002.

Cubes de données

Les données HIPASS sont sous forme de cubes. Les cubes de données sont formés de plusieurs images à différentes tranches spectrales. En pratique, chacun des canaux correspond à un petit intervalle de fréquences (donc à une vitesse précise) et ceux-ci sont empilés les uns sur les autres pour former le cube. Ainsi, à chaque pixel spatial correspond un spectre de la région qu'il couvre.

La figure 1.8 montre en fait le cube de données de la région de Sculptor, dans lequel on retrouve également la galaxie NGC 300. Il s'agit du même cube qui sera utilisé dans l'article traitant de la galaxie Sculptor, inclus ci-après. Cette dernière n'apparaît pas dans le cube car les niveaux de gris ont été sélectionnés de façon à faire ressortir deux structures

TABLE 1.2 – Projet HIPASS

Paramètres d'observation (Staveley-Smith & et al. 2000)	
Couverture du ciel[a]	$\delta \leq +22°$
Temps d'intégration par points	460s
Température moyenne du système	20 K
Efficacité du faisceau central	63 %
FWHM du beam central	$14.4'$ ($15.5'$[b])
Couverture de vitesse	-1200 à 12700 km/s
Largeur des canaux	13.2 km/s
Résolution en vitesse[c]	18 km/s
Précision de pointage (3σ)	$3.0'$
Limite de détection (3σ)	40 mJy/beam
Limite de masse HI (3σ)[d]	$10^6 d^2_{Mpc} M_\odot$

[a]Avec l'extension nordique
[b]Voir Barnes et al. (2001)
[c]Après application d'un lissage Tukey 25%
[d]Pour une dispersion de vitesse $\Delta V = 100$ km/s

plus intéressantes à cette étape, soit le HI local (à 0 km s^{-1}) et la galaxie spirale NGC 300. Cette dernière montre une signature assez particulière à l'intérieur du cube mais qui est bien typique de ce type de galaxie. En fait, même si le phénomène n'apparaît pas très bien dans cette figure, une galaxie qui soutient une rotation montrera une signature sous forme de «S». Ce phénomène est souvent mis en évidence grâce aux diagrammes Position-Vitesse tel que celui présenté à la figure 2 de l'article de de Blok & Walter (2000).

1.5 Autres observations

Il n'y a pas que HIPASS qui ait été utile. Deux autres séries d'observations seront présentées dans ce mémoire. Elles ont été utiles pour combler deux défauts majeurs de HIPASS. Le premier étant que, pour avoir une meilleure couverture spectrale du ciel, le sondage s'est vu accorder une petite résolution spectrale (13,6 km/s). Puisque le gaz recherché a une dispersion de vitesse d'environ 15 km/s, il est important d'avoir un meilleur échantillonnage de cette dispersion.

Le deuxième défaut du relevé HI est sa résolution spatiale. Puisque les observations ont été effectuées avec un télescope à une seule antenne, la limite de résolution est donc fixée par le diamètre de celle-ci et, pour le télescope de Parkes, cette limite est de $14{,}4'$. À cause de l'utilisation d'un algorithme de lissage de données qui permet de réduire le bruit dans les données HIPASS, la résolution effective est passée à environ $15{,}5'$ (Barnes et al. 2001).

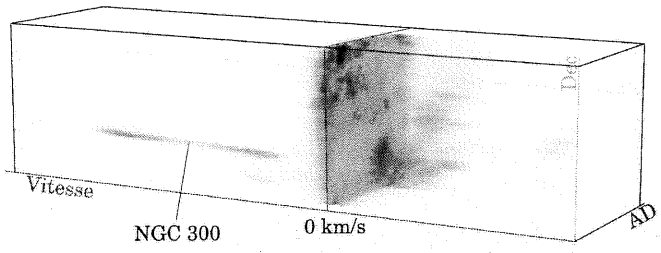

FIGURE 1.8 – Un concept révolutionaire! La représentation tridimensionnelle d'un cube. Les trois axes du cube sont en fait deux axes spatiaux (le bleu est l'ascension droite et le jaune correspond à la déclinaison) alors que le troisième est un axe spectral (le rouge). Ce cube couvre une région de $3° \times 3°$ dans laquelle se trouve la galaxie NGC 300 à une vitesse radiale héliocentrique de 144 km s^{-1}.

1.5.1 Parkes

Le télescope de Parkes dans l'état du New South Wales en Australie est celui qui a été utilisé pour le sondage HIPASS. Son corrélateur en mode HIPASS nous permet d'utiliser 13 faisceaux en même temps ce qui diminue de façon substantielle le temps requis pour imager une région déterminée du ciel. Mais, dans ce mode, la bande passante totale du télescope est de 64 Mhz divisée en 1024 canaux.

En mode à largeur de bande étroite, le corrélateur permet seulement l'usage de sept faisceaux. La bande passante totale est réduite à 8 MHz que le corrélateur divise en 2048 canaux. Ces réglages permettent d'atteindre une résolution spectrale beaucoup plus grande et atteint 0,82 km s^{-1}. Il s'agit d'une valeur beaucoup plus intéressante pour le type d'observation dont nous avions besoin.

Quant à la résolution spatiale, elle reste inchangée car elle dépend de la taille de l'antenne réceptrice. Malgré que le ATCA (discuté à la prochaine section) permet d'obtenir une plus

grande résolution spatiale pour sensiblement la même résolution spectrale, Parkes reste l'un des télescopes les plus performants pour détecter des objets de faible luminosité. Puisqu'il s'agit d'une seule antenne ou *Single Dish*, il n'est pas affecté par les problèmes spécifiques aux télescopes à ouverture de synthèse.

1.5.2 ATCA

Le Australia Telescope Compact Array (ATCA) est un télescope à ouverture de synthèse. Il s'agit en fait d'un interféromètre composé de six antennes et qui reconstruit l'image de la source étudiée à partir des franges d'interférences enregistrées. Il est alors possible de reconstruire un faisceau, l'équivalent du faisceau d'une seule antenne, qui n'est alors plus nécessairement de forme simple (surtout si plus d'une configuration d'antennes ont été utilisées lors des observations).

L'avantage d'un tel appareil est que sa résolution n'est plus fonction de la largeur des antennes qui le composent mais de la distance entre ces dernières. C'est ce qui rend le ATCA intéressant car chaque antenne est montée sur un rail et elle peut se déplacer pour s'adapter à la source qui est observée. Le corrélateur peut également fournir une résolution spectrale de 0,82 km s^{-1}.

Chapitre 2

L'impact de la radiation UV sur l'évolution des galaxies naines

Dans ce chapitre est présenté un article soumis à l'Astrophysical Journal et dont Sergey Mashchenko est le premier auteur. Cette recherche m'a été d'un très grand support dans l'élaboration et la rédaction des chapitres suivants. Il s'agit d'une théorie qui explique pourquoi le gaz d'hydrogène neutre n'a pas encore été détecté dans la majorité des galaxies naines sphéroïdales du Groupe Local et ce à cause de la radiation UV qui s'échappe de la Voie Lactée et ionise le gaz des galaxies satellites.

J'ai fourni quelques-unes des données observationnelles qui sont présentée à la fin du texte. Également, au fil des nombreuses discussions que Sergey et moi avons eu ensemble, nous avons pu établir les mécanismes principaux par lesquels la photoionisation affectait le contenu gazeux des naines qui sont le sujet principal de ce mémoire.

Impact of UV Radiation from Giant Spirals on the Evolution of Dwarf Galaxies

Sergey Mashchenko
Département de physique and Observatoire du mont Mégantic, Université de Montréal, C.P. 6128, Succ. centre ville, H3C 3J7 Montréal, Qué., Canada
e–mail:[redacted]
Claude Carignan
Département de physique and Observatoire du mont Mégantic, Université de Montréal, C.P. 6128, Succ. centre ville, H3C 3J7 Montréal, Qué., Canada
e–mail:[redacted]
and
Antoine Bouchard
Département de physique and Observatoire du mont Mégantic, Université de Montréal, C.P. 6128, Succ. centre ville, H3C 3J7 Montréal, Qué., Canada; and
Australia Telescope National Facility, PO Box 76, Epping, NSW 1710, Australia
e–mail:[redacted]

Submitted to Astrophysical Journal, March 19 2002

We show that ultraviolet radiation, with wavelengths shorter than 2000 Å, escaping from the disks of giant spirals could be one of the principal factors affecting the evolution of low mass satellite galaxies. We demonstrate, using a semi-qualitative model, that the Lyman continuum part of the radiation field can lead to ionization of the ISM of the dwarf galaxies through the process of photoevaporation, making the ISM virtually unobservable. The FUV part ($912 < \lambda < 2000$ Å) is shown to dominate over the internal sources of radiation for most of the Galactic dwarf spheroidals. The proposed environmental factor could be at least partially responsible for the bifurcation of the low mass proto-galaxies into two sequences — dwarf irregulars and dwarf spheroidals. We discuss many peculiarities of the Local Group early-type dwarfs which can be accounted for by the impact of the UV radiation from the host spiral galaxy (Milky Way or M31).

2.1 Introduction

The diverse group of low luminosity ($M_V > -12\overset{m}{.}5$) Local Group dwarf galaxies is loosely divided (based on their recent star formation history, SFH, and neutral gas content) into three categories: dwarf irregulars (dIrr), intermediate type dwarfs (dIrr/dSph), and dwarf spheroidals (dSph). Despite some obvious differences, these galaxies do share a few important properties: (a) they are pressure supported (rotation is dynamically unimportant); (b) for a given luminosity, they have comparable spatial extent (especially when considering the distribution of the old stars); (c) they have comparable low metallicity [Fe/H] ~ -2; (d) in most cases, they have very aspheric shapes with ellipticity $e \sim 0.2 - 0.4$; (e) the available

kinematic data suggest that they are dark matter (DM) dominated.

Local Group dSph galaxies are known to have a wide range of SFHs — from being consistent with a single burst scenario (e.g. Ursa Minor) to the very complex multiple bursts case of Carina (Grebel 1997; Mateo 1998). Low mass dSphs have not formed stars for at least a Gyr. Intermediate type (dIrr/dSph) Local Group dwarfs (LGS 3, Antlia, and Phoenix) had their most recent star bursts $\sim$ 100 Myr ago (Miller et al. 2001; Piersimoni et al. 1999; Martínez-Delgado, Gallart, & Aparicio 1999). Intrinsically faint dIrr galaxies are all forming stars at the present time but with low efficiency ($dm/dt < 0.001$ $M_\odot$ yr^{-1}, Mateo 1998).

A few scenarios have been proposed to explain the complex SFH of dSph galaxies, including episodic accretion of intergalactic gas (Silk, Wyse, & Shields 1987), ISM heating by SN Ia leading to prolonged periods of time with no star formation (Burkert & Ruiz-Lapuente 1997), and bar induced star bursts in the tidally stirred dwarfs scenario of Mayer et al. (2001). The shortcomings of these models will be discussed in Section 2.2.1.

Aside from the differences in the present day star formation rate (SFR), low luminosity galaxies from the sequence dIrr – dIrr/dSph – dSph differ in their neutral gas content. Local Group dIrrs are gas rich: the ratio of the HI mass to the V-band luminosity $M_{\rm HI}/L_V$ ranges from $\sim$ 1.4 for GR 8 to $\sim$ 2.8 for DDO 210 (Mateo 1998). Intermediate type dwarfs have smaller HI content: from $M_{\rm HI}/L_V \sim 0.14$ for Phoenix (St-Germain et al. 1999; Gallart et al. 2001) to $M_{\rm HI}/{\rm L_V} \sim 0.4$ for LGS 3 (Mateo 1998) and Antlia (Barnes & de Blok 2001). Dwarf spheroidals have no or little H I. Two possible detections with the HI emission located within the optical extent of the dSph and the radial velocity of the gas being within 15 km s^{-1} from the optical velocity of the dwarf are those of Sextans ($M_{\rm HI}/L_V \sim 0.06$, Blitz & Robishaw 2000) and Sculptor ($M_{\rm HI}/L_V \sim 0.09$, A. Bouchard, C. Carignan, & S. Mashchenko, in preparation, hereafter BCM).

The location of the intrinsically faint Local Group dwarfs on the dSph – dIrr/dSph – dIrr sequence appears to correlate with their proximity to large spirals (e.g. van den Bergh 1999): dSphs are concentrated in the vicinity of the Milky Way and M31, low mass dIrrs are isolated systems, and the intermediate type dwarfs are somewhere in between. Environment appears to bear a significant impact on the dwarf evolution.

We propose a novel mechanism which can explain the differences in SFHs and neutral gas content between dSphs and dIrrs. Our hypothesis is that the electromagnetic radiation (especially Lyman continuum, LyC, and far ultraviolet, FUV) escaping from the host spiral galaxy can play a decisive role in the evolution of dSphs. Significant amounts of gas can be ionized and heated by the host galaxy LyC when dSphs are on the relatively high galactic latitude parts of their orbits. FUV can also play a role by preventing the formation of the cold neutral medium phase of the ISM, the presence of which is believed to be required for star formation. Moving along their orbits around the host galaxy, dSphs spend relatively short periods of time near the plane of the host, where the fluxes of the LyC and FUV radiation drop to much lower metagalactic levels. For some of the dwarfs, the time spent in the shadow

produced by the HI disk of the host spiral is enough for their ISM to recombine, cool down and form stars in a short burst. The timescale for the repeated star bursts in this scenario is equal to half of the orbital period, or $\sim 1 - 5$ Gyr, which is in agreement with the observed SFHs. dSph galaxies with total masses $< 10^8$ $M_\odot$ gradually lose their ISM when the gas is ionized and heated to $\sim 10^4$ K by the LyC radiation from the host galaxy, leading to the globally declining SFR. This should affect more the dwarfs on almost polar orbits, because their ISM is being kept ionized for the largest fraction of their lifetimes.

For the above mechanism to work, many dSphs should have masses $\gtrsim 10^8$ $M_\odot$ to keep their fully photoionized ISM gravitationally bound for prolonged periods of time. In the best studied case of the Draco dSph, the absence of tidal features down to the ~ 0.001 level of the central surface brightness(Odenkirchen et al. 2001), the observed large spatial extent of the galaxy (Piatek et al. 2001; Aparicio, Carrera, & Martínez-Delgado 2001; Odenkirchen et al. 2001), and modeling of the radial velocities for 159 giant stars out to large projected radii (Kleyna et al. 2001) suggest that in low luminosity dSphs the DM halos are significantly more extended than the stellar bodies, which invalidates the conventional mass estimates of dSphs using the mass-follows-light King models. Thus, the available data cannot exclude the case of dSphs being as massive as $\sim 10^8$ $M_\odot$.

This paper is organized as follows. Section 2.2 presents our semi-qualitative model of the photoionization of the ISM of dSphs by the LyC radiation from the host spiral galaxy, and demonstrates that the external FUV radiation flux at the locations of the most of the Galactic dSphs dominates over the internal FUV flux. Section 2.3 gives the observational evidence for the impact of the electromagnetic radiation from giant spirals on the evolution of the dwarf satellite galaxies. Section 2.4 discusses the implications of our results and gives our conclusions.

2.2 Model

2.2.1 Previous dSph Models

A few scenarios have been proposed in attempt to explain the SFHs of dSph galaxies.

Silk et al. (1987) argued that dwarfs (both dIrrs and dSphs) formed their stars in a few vigorous bursts of star formation from the accreted intergalactic gas. This is in apparent contradiction with the recent results of van Zee (2001), who showed that the observed optical colors of a large sample of isolated dIrr galaxies are best fitted by composite stellar populations that have had approximately constant SFR for at least 10 Gyr. One of the important motivations for the Silk et al. (1987) gas infall model was the argument that dwarfs could not have sustained their observed SFR for more than a short fraction of a Hubble time without producing excessive chemical enrichment, despite apparently having composite stellar populations. Numerical models of Mac Low & Ferrara (1999) seriously undermined the importance of this motivation by showing that low mass dwarfs can retain most of their ISM while losing

virtually all of their metals in SN ejecta.

The importance of SNe Ia for the evolution of dSphs was emphasized by Burkert & Ruiz-Lapuente (1997). In their model, the ISM of dSphs can settle into a hot, hydrostatic equilibrium state, where the rate of energy loss through cooling is balanced by the energy input through SNe Ia. These periods of "dormancy" could last a few Gyr. The essential requirement of the model is the ability of dSphs to keep the hot gas with $T \sim 10^4$ K gravitationally bound, which translates to a lower limit for the DM mass of $\sim 10^8$ $M_\odot$. Unfortunately the model does not explain the observed segregation of the low luminosity ($M_V \gtrsim -15^m$) dwarfs in the Local Group, with all the dwarfs close ($\lesssim 250$ kpc away) to large spirals being dSphs, and all the dIrr galaxies being isolated systems. Neither does it explain the diversity of the SFHs of the comparable luminosity dSphs.

In the scenario of Mayer et al. (2001), the low surface brightness dIrr galaxies moving on bound orbits in the very massive ($\sim 4 \times 10^{12}$ $M_\odot$) DM halo of the Milky Way, were transformed into dSphs by the strong Galactic tidal field. In this model, multiple bursts of star formation in dSphs are explained by the gas funneling to the center of the dwarf because of the tidally induced bar. One of the shortcomings of the model is the inability to predict the large DM content of dSph galaxies: when expressed in the same (B) spectral band, their most DM dominated "GR 8" model with $(M/L)_B \sim 70$ fails to explain the large values of $(M/L)_B \sim 200 - 260$ observed in Draco and Ursa Minor (Mateo 1998) by a large margin.

2.2.2 New Environmental Factor for dSphs

In this paper we advocate a novel environmental factor for the low luminosity dwarf galaxies: ultraviolet radiation escaping from nearby giant spirals. The LyC part of the radiation ($\lambda < 912$ Å) can lead to the photoionization of the ISM of dwarfs, making the ISM unobservable (at least in HI spectral line; the possibility of a tenuous ionized gas detection will be discussed in Section 2.4) and quenching the star formation. The FUV part ($912 < \lambda < 2000$ Å) can prevent star formation by keeping the neutral ISM warm through the photoelectric heating from the interstellar dust. Both components of the radiation field are distributed anisotropically around giant spiral galaxies, with the largest flux being along the polar axis, and the much lower flux in the plane of the spiral. This anisotropy, along with the variety of possible orbits around the host spiral galaxy, can lead to very diverse SFHs for the dSph galaxies.

LyC Radiation

Sculptor is the unusual case of a low mass dSph galaxy apparently possessing a neutral ISM (Carignan et al. 1998; BCM). In other respects, it appears to be a typical dSph, with luminosity $L_V = 2.15 \times 10^6$ $L_\odot$ and distance from the host galaxy ~ 80 kpc being close to the average ones (Mateo 1998). As seen in many other dSphs, Sculptor shows an extended SFH, with stars formed as recently as 5 Gyrs ago. In this section we will use the Sculptor dwarf to

TABLE 2.1 – Parameters for the photoevaporation model

Parameter	Initial "0" State (Neutral ISM)	Final "1" State (Fully Ionized ISM)
Proton number density n, cm^{-3}	0.02	0.005
Temperature T, K	5,000	10,000
Pressure P/k, K cm^{-3}	100	
Cloud radius R, pc	750	1191
Mass $M_{\rm HI}$, M$_\odot$	8.7×10^5	
Proton column density N, cm^{-2}	9.3×10^{19}	3.7×10^{19}

assess the importance of the external LyC radiation for the ISM of dSph galaxies.

We consider the following idealized model for the ISM of Sculptor: a pure HI sphere with initial radius $R_0 = 750$ pc, constant temperature T_0 =5,000 K, and constant number density $n_0 = 0.02$ cm^{-3} (Table 2.1). The radius chosen is well within the optical extent of Sculptor, which has a tidal radius $r_t \simeq 1.5$ kpc (Mateo 1998). The gas pressure, $P_0/k = n_0 T_0 = 100$ K cm^{-3}, is within the range of thermal pressures required to explain the two-phase (CNM/WNM, which stands for cold/warm neutral medium) ISM structure observed in isolated dIrr galaxies (Young & Lo 1996, 1997b). The temperature of 5,000 K is close to the temperature of WNM predicted for the ISM with thermal pressure of 100 K cm^{-3} under low metallicity and low FUV flux conditions (Young & Lo 1997b, their Figure 16).

The total mass of HI gas in our model is $M_{\rm HI} = 8.7 \times 10^5$ M$_\odot$ (Table 2.1). In the case of Sculptor this corresponds to $M_{\rm HI}/L_V \sim 0.4$, which would be typical for a dIrr/dSph galaxy. The largest initial HI column density is $N_0 = 9.3 \times 10^{19}$ cm^{-2}.

To estimate the minimum LyC one-sided flux F_0, required to fully ionize our model ISM in the static case (when the gas does not move), we assume a detailed ionization balance inside the HII region, degree of ionization close to 100% within the photoionized gas, and neglect collisional ionization and three-body recombination. The value of F_0 under the above conditions for a slab of hydrogen gas with proton density n and thickness l is approximately equal to the total rate of recombination along the line of sight, or

$$F_0 \simeq n^2 \, l \, \alpha_0^{(2)}. \tag{2.1}$$

Here $\alpha_0^{(2)} \simeq 2.6 \times 10^{-13}$ cm^3 s^{-1} (for $T = 10^4$ K) is the coefficient of recombination to all but the ground level of the hydrogen atom. Using equation (2.1), we can estimate for our model:

$$F_0 \simeq 4.8 \times 10^5 \text{ cm}^{-2} \text{ s}^{-1}. \tag{2.2}$$

Whether or not a noticeable fraction of the LyC photons escapes from the disks of spiral galaxies is a matter of an ongoing debate (see discussion in Bland-Hawthorn & Putman 2001). The Galactic LyC flux at the present location of Sculptor, predicted by the model of Bland-

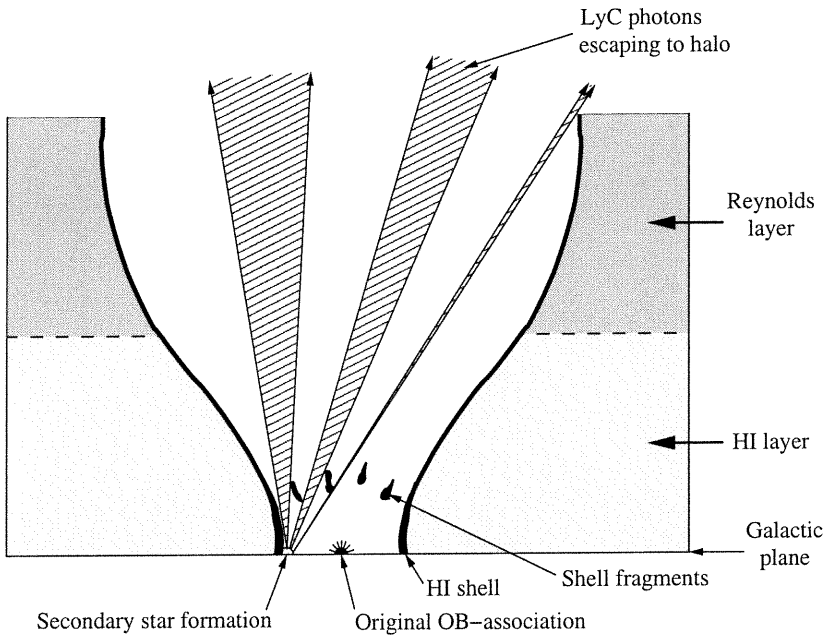

FIGURE 2.1 – Old supershell with a site of secondary star formation. (Only the upper half is shown.) Ionizing photons from the newly born O-stars can escape to the Galactic halo in the directions not obscured by the supershell walls and shell fragments.

Hawthorn & Maloney (2001), is $\sim 4 \times 10^4$ cm^{-2} s^{-1}. The model assumes that LyC photons, produced by massive stars, escape from the Galactic disk through the Reynolds layer with constant optical depth $\tau = 2.8$ in the orthogonal to the disk direction. This low model value of the Galactic LyC flux at the location of Sculptor is at odds with the flux

$$F_{obs} = (4.9 \pm 0.5) \times 10^5 \text{ cm}^{-2} \text{ s}^{-1}, \tag{2.3}$$

derived from the H_α flux 220 ± 23 mR observed in the direction of the Sculptor northeast HI cloud at $\alpha_{2000} = 0^h58^m22^s$, $\delta_{2000} = -34°00'$ (assuming that the cloud is located at the distance of the dwarf) (Weiner, Vogel, & Williams 2001; B. J. Weiner 2001, private communication). This interpretation of the H_α flux assumes that the cloud surface is flat. In the more realistic case of an irregularly shaped cloud, the expected ionizing flux can be lower. The fact that the H_α flux observed in the other parts of the northeast cloud and in the southwest cloud is lower or non-detected (B. J. Weiner 2001, private communication), and the similar situation with the Magellanic Stream where the observed H_α flux varies spatially by a factor of $30 - 40$ (Weiner et al. 2001) could be an indication that the Galactic LyC flux is very patchy on small angular scales.

We speculate that the major contributor to the Galactic ionizing flux could be supershells powered by the combined action of strong stellar winds and SNe explosions in large

OB-associations. Galactic supershells can have the half-size in the perpendicular to the disk direction as large as 2.5 kpc (Mashchenko & Silich 1994; Silich et al. 1996), and can consequently break through the LyC absorbing Reynolds layer which has a scale height of ~ 1 kpc (Reynolds 1991). Hot ($T \sim 10^6$ K) and very rarefied gas filling the superbubble is virtually transparent to the LyC photons emitted by the O-stars from the OB-association. Large supershells have an hourglass shape, with the densest gas located in the most narrow part near the galactic plane (Figure 2.1). In this dense HI ring the conditions for the formation of molecular hydrogen can be met (Mashchenko & Silich 1994), which could lead to a secondary star formation episode inside the superbubble $15 - 50$ Myr after the original star burst. The 600-pc-long arc of young stars and clusters observed inside the LMC4 superbubble powered by a ~ 30 Myr old OB-association (Efremov & Elmegreen 1998) is consistent with this picture of self-propagating star formation. Further support comes from the recent CO observations in the LMC with NANTEN (Yamaguchi et al. 2001), where $\sim 35\%$ of all molecular clouds were suggested to have formed under the dynamical effects of expanding supershells (such as the accumulation of interstellar medium).

If secondary massive star formation does take place inside an old supershell which has already broken through the Reynolds layer, almost 100% of the ionizing photons from the newly born O-stars can escape into the Galactic halo within a cone with an opening angle of $\sim 30^\circ - 120^\circ$, and are fully absorbed by the supershell walls in other directions (Figure 2.1). In this, our scenario differs substantially from the model of Dove, Shull, & Ferrara (2000), who considered the escape of LyC photons only from the original OB-association. The importance of the triggered star formation inside evolving supershells for elevating the fraction of the LyC photons escaping from galactic disks can also be inferred from the results of Tenorio-Tagle et al. (1999). In their simulations, only the case of the continuous star formation (their model C2) resulted in large values of the LyC photons escape fraction. These results are not directly applicable to the problem in question, because Tenorio-Tagle et al. (1999) considered a spiral galaxy with a powerful nuclear star-burst, with the mechanical luminosity of 1.4×10^{42} ergs s^{-1} and the ionizing photon flux of 4×10^{54} s^{-1}. The star bursts in the Milky Way and M31 are of much smaller scale.

The inferred high variability of the Galactic LyC flux on small angular scales can be explained in this picture by the presence inside the superbubble of slowly evaporating shell fragments (Figure 2.1). These dense neutral clouds are remnants of the original shell fragmented due to Rayleigh-Taylor instability and left behind during the blow-out phase of the supershell evolution (e.g Mac Low, McCray, & Norman 1989).

In this scenario of the escape of the Galactic LyC photons, the expected fluxes for different polar angles can differ dramatically from the predictions of the opaque disk models of Weiner et al. (2001) and Bland-Hawthorn & Maloney (2001). Thus we believe that the most reliable information on the LyC flux at the location of Sculptor is the upper limit derived from the H_α flux observed in the direction of the Sculptor northeast HI cloud (eq. [2.3]).

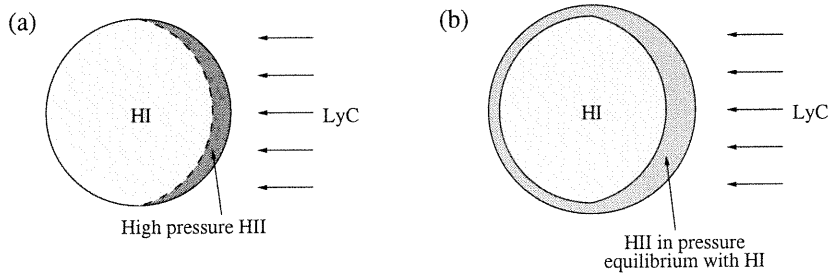

FIGURE 2.2 – Photoevaporation of the ISM of a dSph galaxy exposed to the LyC photons escaping from the disk of the host galaxy: (a) on the side facing the source of the ionizing radiation a thin layer of the high pressure photoionized hydrogen is formed; (b) trying to reach a pressure equilibrium with the neutral gas, the HII gas expands and fills the outer regions of the galaxy, allowing a fresh layer of HI to be ionized. The process repeats itself until the HI gas is fully ionized, or until the ionized gas on the irradiated side of the cloud becomes optically thick to the LyC photons.

The above arguments lead to the conclusion that though poorly constrained, the expected Galactic LyC flux at the location of Sculptor, $F_{Scl} \lesssim 5 \times 10^5$ cm^{-2} s^{-1} (eq. [2.3]), is probably not strong enough to fully ionize our model ISM in the static case: $F_{Scl} \lesssim F_0$.

For a neutral cloud in anisotropic ionizing radiation field, the dynamical effects can be very important. A process called photoevaporation can take place, when the photoionization of the neutral gas heats the cloud's surface and causes the gas to flow away, thereby exposing more neutral gas (Bertoldi & McKee 1990). This mechanism can reduce dramatically the minimum LyC flux required to fully ionize the cloud from the static photoionization value. Bertoldi (1989) and Bertoldi & McKee (1990) developed an analytical theory describing the photoevaporation of an interstellar cloud which is exposed to the ionizing radiation of a newly formed star. This theory is not directly applicable to the case of the ISM of a dSph galaxy because of the invalidity of the following assumptions adopted by the authors: 1) the temperature of the neutral gas is much lower than the temperature of the ionized gas $T_{\rm HII} \simeq 10^4$ K; 2) initially the cloud is in pressure equilibrium with the intercloud medium; 3) the ionized gas is not gravitationally bound to the cloud, and can freely flow away.

Nevertheless, we argue that the process of photoevaporation can also take place in the ISM of a dwarf galaxy. Even in the case of the highest possible WNM temperature $T_{\rm HI} \simeq 10^4$ K, the pressure of the photoionized gas is ~ 2 times higher than the original pressure of HI (because during the photoionization of hydrogen the number of particles doubles, and the temperature is maintained at the $T_{\rm HII} \simeq 10^4$ K level when the heating by the LyC photons is balanced by radiative cooling). Higher pressure causes the HII gas to expand, filling the outer regions of the galaxy, allowing a fresh layer of HI to be ionized (Figure 2.2). The speed with which the ionization front propagates inside the cloud is determined by how fast the photoionized gas can flow away and be redistributed in the outer parts of the dwarf galaxy, and is expected to

be less than the isothermal sound speed in the HII region ~ 10 km s^{-1}.

Instead of deriving a time-dependent solution for this process, for simplicity we consider only the final state of the fully ionized ISM. We assume that, during the photoionization, the HII gas always reaches a state of pressure equilibrium with the HI gas, so that the final pressure P_1 is equal to the initial pressure P_0. We wish to derive the minimum LyC flux F_1 required to keep the ISM fully ionized.

The condition $P_1 = P_0$ leads to the equation $n_0 T_0 = 2 n_1 T_1$, where n_1 and T_1 are proton number density and temperature in the final (fully ionized) state. Introducing the parameter $\chi \equiv 2\,T_1/T_0$, we can write the equations for the final proton number density, $n_1 = \chi^{-1}\,n_0$, radius of the cloud, $R_1 = \chi^{1/3}\,R_0$, and the central proton column density, $N_1 = \chi^{-2/3}\,N_0$. Using equation (2.1), we obtain the minimum LyC flux required to keep the cloud fully ionized:

$$F_1 = \chi^{-5/3}\,F_0. \tag{2.4}$$

For our model ISM with T_0 =5,000 K and T_1 =10,000 K (corresponding to $\chi = 4$) we obtain the following parameters for the final fully ionized state: $n_1 = 0.005$ cm^{-3}, $R_1 \simeq 1.2$ kpc, and $N_1 \simeq 3.7 \times 10^{19}$ cm^{-2} (Table 2.1). The minimum required ionizing flux F_1 is $\chi^{5/3} \simeq 10$ times lower than in the static picture, and is equal to $F_1 \simeq 4.8 \times 10^4$ cm^{-2} s^{-1}. This value is much lower than the observationally derived upper limit on the Galactic LyC flux at the location of Sculptor (eq. [2.3]). The maximum H_α flux from this fully ionized ISM is given by $F_{H_\alpha} \simeq n_1\,N_1\,\alpha_{32}$, where $\alpha_{32} = 1.17 \times 10^{-13}$ cm^3 s^{-1} (for $T = 10^4$ K) is the corresponding photon production coefficient (Spitzer 1978, p. 89). In our case, $F_{H_\alpha} = 20$ mR, which is close to the detection limit of the modern observational techniques (e.g. Weiner et al. 2001).

We can also estimate the appropriate timescales for our model. Assuming that the photoevaporation is efficient, the speed of the ionization front is ~ 10 km s^{-1}, leading to the full ionization time $t_{ion} \sim 150$ Myr. If the ionizing flux drops to zero, the HII gas will recombine within $t_{rec} = [n_1\,\alpha_0^{(2)}]^{-1} \simeq 24$ Myr, and cool down to the CNM temperature of ~ 25 K (Young & Lo 1997b, their Figure 16) within ~ 0.5 Myr (using the cooling function of Chiosi et al. 1998). In the absence of the turbulent, rotational, and magnetic support, the cold gas will collapse toward the center of the dwarf on timescales of the order of the free-fall time (~ 100 Myr). All these timescales are significantly shorter than the orbital periods of dSphs $t_{orb} \sim 2 - 10$ Gyr.

The density of the fully ionized gas in our example, $n_1 = 0.005$ cm^{-3}, is small enough to raise concerns about the possibility that such tenuous ISM could be completely stripped away by the ram pressure of the diffuse gas in the Galactic halo. The density of the Galactic gas n_h at the distances of the dSph satellites is a poorly known quantity (see discussion in Quilis & Moore 2001). One of the strictest available upper limits, $n_h < 10^{-5}$ cm^{-3} at the distance 50 kpc, is imposed by requiring the survival of the Magellanic Stream cloud MS IV for 500 Myr (Murali 2000). For a King model, the condition for a complete ram pressure stripping of the

ISM with density n is $n_h V^2 \gtrsim 3.5\, n\, \sigma^2$, where V and σ are the orbital velocity and the one-dimensional stellar velocity dispersion of the dwarf (Takeda, Nulsen, & Fabian 1984). Adopting $V = 220$ km s^{-1} and a typical for dSphs value of $\sigma = 7$ km s^{-1} (Mateo 1998), we derive for our ionized ISM the following condition for the total ISM removal: $n_h \gtrsim 1.8 \times 10^{-5}$ cm^{-3}. Taking into account the fact that most of the Galactic dSphs are located at distances $\gtrsim 80$ kpc, where the halo gas is expected to have even lower density than at a distance of 50 kpc, the upper limit of Murali (2000) suggests that ram pressure stripping is not large enough to significantly affect our results.

The conclusion we draw from the above simplified analysis is that the flux of the LyC photons escaping from the Milky Way is probably strong enough at the distances of dSphs to keep significant amounts of gas fully ionized, thus suppressing star formation and making the ISM virtually unobservable for most of the lifetime of the galaxy. Only during relatively short periods of time when a dSph moving along its orbit crosses the Galactic plane, does the ionizing flux drop to the low metagalactic background level $F_{bg} \sim (2.5 - 15) \times 10^3$ cm^{-2} s^{-1} (Maloney 1993; Shull et al. 1999; Tumlinson et al. 1999; Madsen et al. 2001; Weymann et al. 2001), allowing the ionized gas to recombine and potentially form stars.

Another way to assess the importance of the LyC radiation from the host spiral galaxies for the evolution of dSph satellites is to compare the amounts of energy transferred to the ISM of the dwarfs from the external ionizing radiation field to the more conventional mechanism of gas heating by supernovae type Ia considered e.g. by Burkert & Ruiz-Lapuente (1997).

In a photoionized hydrogen cloud exposed to the LyC radiation with photon energies $h\nu > 13.6$ eV $+ kT$, a constant thermal flow occurs from the radiation to the gas (Kaplan & Pikelner 1970, p. 87). (Here T is the temperature of the gas.) For the ionizing radiation with the spectrum of an O-star, each LyC photon absorbed by the gas increases the thermal energy of the gas by $\bar{\varepsilon} \simeq 4.5 \times 10^{-12}$ ergs on average (Kaplan & Pikelner 1970, p. 88). The number of the absorbed ionizing photons is determined by the detailed balance of the photoionization and recombination rates. The corresponding heating rate is given by $\dot{e}_{LyC} = \bar{\varepsilon} n_1^2 \alpha_0^{(2)}$, where n_1 is the proton number density of the gas, and $\alpha_0^{(2)}$ is the coefficient of recombination to all levels $n > 1$ of the hydrogen atom. For the Sculptor model $\dot{e}_{LyC} \simeq 29 \times 10^{-30}$ ergs cm^{-3} s^{-1} (for the fully ionized state "1"; see Table 2.1).

To estimate the heating of the model ISM by supernovae type Ia, we adopt the SN Ia rate of 0.18 SNu appropriate for early type galaxies from the paper by Cappellaro, Evans, & Turatto (1999). For the case of Sculptor, with blue luminosity $L_B = 1.13 \times 10^6$ L$_\odot$ (Mateo 1998), we derive the supernovae Ia rate of $r_{SN} \sim 0.2$ Myr^{-1}. Each SN Ia is assumed to transfer $E_{SN} \sim 10^{50}$ ergs of energy into the ISM (Thornton et al. 1998). The volume averaged rate of the heating by the supernovae is $\dot{e}_{SN} = E_{SN}\, r_{SN}/\Omega$, where Ω is the volume of the ISM. For Sculptor we derive $\dot{e}_{SN} \simeq 12 \times 10^{-30}$ ergs cm^{-3} s^{-1} (neutral state "0", with the cloud radius 750 pc), and $\dot{e}_{SN} \simeq 3 \times 10^{-30}$ ergs cm^{-3} s^{-1} (ionized state "1"; the radius of the cloud is 1191 pc).

From this particular example, heating of the ISM of dSphs by the ionizing radiation escaping from the disk of the host spiral galaxy appears to dominate over the internal SN Ia heating: $\dot{e}_{LyC} \gg \dot{e}_{SN}$.

FUV Radiation

FUV radiation between 912 and 2000 Å, absorbed by interstellar dust, is the most important source of heating for the Galactic neutral ISM (Wolfire et al. 1995). The UV heating is proportional to the density of the gas. The denser CNM phase of the ISM is thus more sensitive to changes in the level of the FUV radiation than the WNM phase, and for sufficiently large FUV fluxes can be completely evaporated (CNM→WNM phase transition). The presence of CNM is believed to be essential for molecular hydrogen cloud formation, and hence for star formation.

Even the smallest isolated dIrr galaxies are known to possess two-phase ISM (Young & Lo 1996, 1997b). Theoretical models predict that a very low level radiation field, 0.001–0.01 of the local Galactic value, produced by stars in a low mass dIrr can maintain its ISM in a two-phase state at pressures $\sim 10 - 200$ K cm^{-3} (Young & Lo 1997b, their Figure 16). If such a dwarf is exposed to external FUV radiation (e.g. from a nearby spiral galaxy) with flux larger than the internal one, the balance between CNM/WNM phases of the ISM will be shifted toward the WNM phase, reducing the SFR. For large enough external FUV flux the star formation will be quenched. Thus it appears that the FUV radiation from giant spirals could be another important environmental factor for intrinsically faint satellite galaxies.

The FUV radiation field inside early-type dwarfs has two main components: internal (from the Population II stars), and external (from the host spiral galaxy).

From Table 4 of Welch, Mitchell, & Yi (1996) we derive the following estimate of the intensity of the FUV interstellar radiation from the old population stars averaged over the wavelength interval $900 - 1100$ Å at the center of the dwarf elliptical galaxy NGC 185: ~ 2000 cm^{-2} s^{-1} Å^{-1}. We assume that the FUV flux at the center of a dwarf scales as in a homogeneous stellar sphere as $I_0^{2/3} L_V^{1/3}$, where I_0 is the central V-band luminosity density and L_V is the V-band luminosity of the galaxy. For NGC 185, Mateo (1998) gives the following values: $I_0 = 1.76$ L$_\odot$ pc^{-3} and $L_V = 1.25 \times 10^8$ L$_\odot$. We obtain the following estimate of the FUV flux at the center of early-type dwarfs, expressed in units of the standard local FUV background with the flux $F_{loc} = 1.0 \times 10^5$ cm^{-2} s^{-1} Å^{-1} at $\lambda = 1000$ Å (Draine 1978, their eq. [11]):

$$f_{int} \simeq 2.7 \times 10^{-5} I_0^{2/3} L_V^{1/3}, \tag{2.5}$$

where I_0 is in L$_\odot$ pc^{-3}, and L_V is in L$_\odot$.

The FUV luminosity of the Local Group giant spirals (Milky Way and M31) is not well known. We assume that, for face-on giant spiral galaxies, the FUV flux is proportional to the

H_α flux (because most of both types of radiation can be traced back to the same source — young massive stars). Two nearby face-on spiral galaxies, similar to M31 and the Milky Way in their Hubble type and luminosity, have been observed with the Ultraviolet Imaging Telescope (UIT, Stecher et al. 1997) aboard the space shuttles: NGC 628 (M74) and NGC 5457 (M101). Bell & Kennicutt (2001) presented for these galaxies both FUV flux at $\lambda = 1521$ Å (UIT filter B1), and H_α flux. In accord with our expectations, the ratio of the H_α flux to the FUV flux is comparable for the two spirals: $f_{H_\alpha}/f_{1521} = 14$ Å for NGC 628, and 10 Å for NGC 5457 (the units for f_{H_α} are ergs cm^{-2} s^{-1}, and for f_{1521} are ergs cm^{-2} s^{-1} Å $^{-1}$ — hence the units of Å for the ratio of the fluxes). The average value of the ratio is

$$\frac{f_{H_\alpha}}{f_{1521}} \simeq 12\,\text{Å}. \tag{2.6}$$

The observed H_α flux from M31 is $f_{H_\alpha} \simeq 5.1 \times 10^{-10}$ ergs cm^{-2} s^{-1} (Devereux et al. 1994). M31 is a highly inclined spiral with $i = 77.^\circ5$ (Ma, Peng, & Gu 1997). Adopting the average H_α optical depth value $\tau_{H_\alpha} = 1.23$ of Walterbos & Braun (1994) and assuming that the absorbing layer is thin, the deprojected face-on H_α flux from M31 is $\exp[\tau_{H_\alpha}(1 - \cos i)] \simeq 2.6$ times larger than the observed flux, or $f'_{H_\alpha} \simeq 1.3 \times 10^{-9}$ ergs cm^{-2} s^{-1}. Using the empirical conversion factor (eq. [2.6]), we estimate the M31 face-on flux in B1 filter as $f'_{1521} \simeq 1.1 \times 10^{-10}$ ergs cm^{-2} s^{-1} Å $^{-1}$. We adopt the distance to M31 of 780 kpc (see discussion in Section 2.3.2). The FUV flux from M31 along its polar axis at the distance $R_{\rm kpc}$ expressed in units of the standard local FUV background with the flux $F_{loc} = 2.0 \times 10^5$ cm^{-2} s^{-1} Å $^{-1}$ at $\lambda = 1521$ Å (Draine 1978) is then:

$$f_{ext} \simeq 25\, R_{\rm kpc}^{-2}. \tag{2.7}$$

Finally, dividing equation (2.5) by equation (2.7), we obtain a rough estimate of the ratio of the internal FUV flux to the flux from the host galaxy at the center of the early-type dwarf satellites of M31 and the Milky Way (assuming, that the Milky Way FUV luminosity is comparable to that of M31):

$$\frac{f_{int}}{f_{ext}} \simeq 1.1 \times 10^{-6}\, I_0^{2/3} L_V^{1/3} R_{\rm kpc}^2. \tag{2.8}$$

This equation is applicable to dwarfs located far from the plane of the host galaxy, where the dust attenuation becomes insignificant.

Using equation (2.8) and the data on dSphs from the review of Mateo (1998), we can estimate the relative importance of the external FUV radiation for the Milky Way satellites. For all but one dSphs (Sextans, Ursa Minor, Draco, Carina, Sculptor, Fornax, and Leo II) the internal FUV flux is found to be much smaller than the external flux even at the center of the dwarf, with the f_{int}/f_{ext} values ranging from ~ 0.01 (Sextans and Ursa Minor) to ~ 0.4 (Fornax and Leo II). Leo I appears to be the only Galactic dSph for which the internal FUV

flux at the center of the dwarf dominates over the external flux: $f_{int}/f_{ext} \sim 2$.

It is interesting to note that for the dIrr/dSph type galaxy LGS 3, the f_{int}/f_{ext} ratio is estimated to be less than 1 (more accurately, $f_{int}/f_{ext} \simeq 0.56$), despite its relatively large distance from M31 (270 kpc). This is in accord with the results of Young & Lo (1997b), who were not able to detect the CNM phase of the ISM in this dwarf, and could be an indication that the FUV radiation from large spirals is responsible for the phenomena of intermediate type dwarfs.

In an M31-like spiral, with low star formation activity and relativey small bulge, most of the FUV radiation comes from the sources in the plane of the galaxy, closely associated with the spiral arms. The FUV flux from a normal spiral galaxy is then expected to be anisotropic, with the most of the radiation near the plane of the galaxy being absorbed by the dust. In Figure 2.3, we use two nearby spirals similar to M31 and the Milky Way, face-on NGC 5457 and edge-on NGC 891, to illustrate this anisotropy. A typical dSph galaxy on orbit around a giant spiral would spend most of its lifetime in the regime $f_{int}/f_{ext} \ll 1$, with relatively short periods of time of $f_{int}/f_{ext} \gtrsim 1$ when the dwarf crosses the plane of the host spiral galaxy every $1 - 5$ Gyr (half of the orbital period).

The above arguments appear to make a reasonably strong case for the external FUV radiation as being an important evolutionary factor for low mass dwarfs on orbits around large spirals.

There are two important caveats to the above analysis. First one is related to the poorly known contribution to the FUV radiation field inside dwarf galaxies from the metagalactic background. The observed FUV background radiation is known to be strongly dominated by the local (Galactic) sources, making it almost impossible to put an accurate upper limit on its flux (see discussion in Sasseen et al. 1995). Upper limits for the extragalactic background derived by different authors differ by more than an order of magnitude, and are as low as 380 cm^{-2} s^{-1} Å $^{-1}$ in 4π solid angle at $\lambda = 912 - 1100$ Å (Murthy et al. 1999), or ~ 0.004 in the local background units. Calculations of the propagation of FUV radiation from QSOs and AGNs through the intergalactic space (Haardt & Madau 1996, their Figure 5a) give an estimate of the lower limit for the background flux, 28 cm^{-2} s^{-1} Å $^{-1}$ at $\lambda = 1000$ Å (2.7×10^{-4} in the local units). From equation (2.7), this range of the possible background values corresponds to the radius $83 < R < 310$ kpc of the sphere around M31 where its FUV radiation dominates over the background (except for the narrow zone near the plane of the galaxy).

The second caveat is that the heating by soft X-ray radiation, which is inferior to the FUV heating for the Galactic neutral ISM, could be the dominant heating mechanism under the low metallicity, low radiation field conditions in dwarf galaxies (Wolfire et al. 1995). We estimate the M31 deprojected face-on X-ray luminosity in the band $0.1 - 2$ keV to be $\sim (0.5 - 1) \times 10^{40}$ ergs s^{-1}. (For this we used the observed M31 soft X-ray luminosity value of 0.43×10^{40} ergs s^{-1} from Supper et al. 2001, recalculated for the distance to M31 of 780 kpc, and

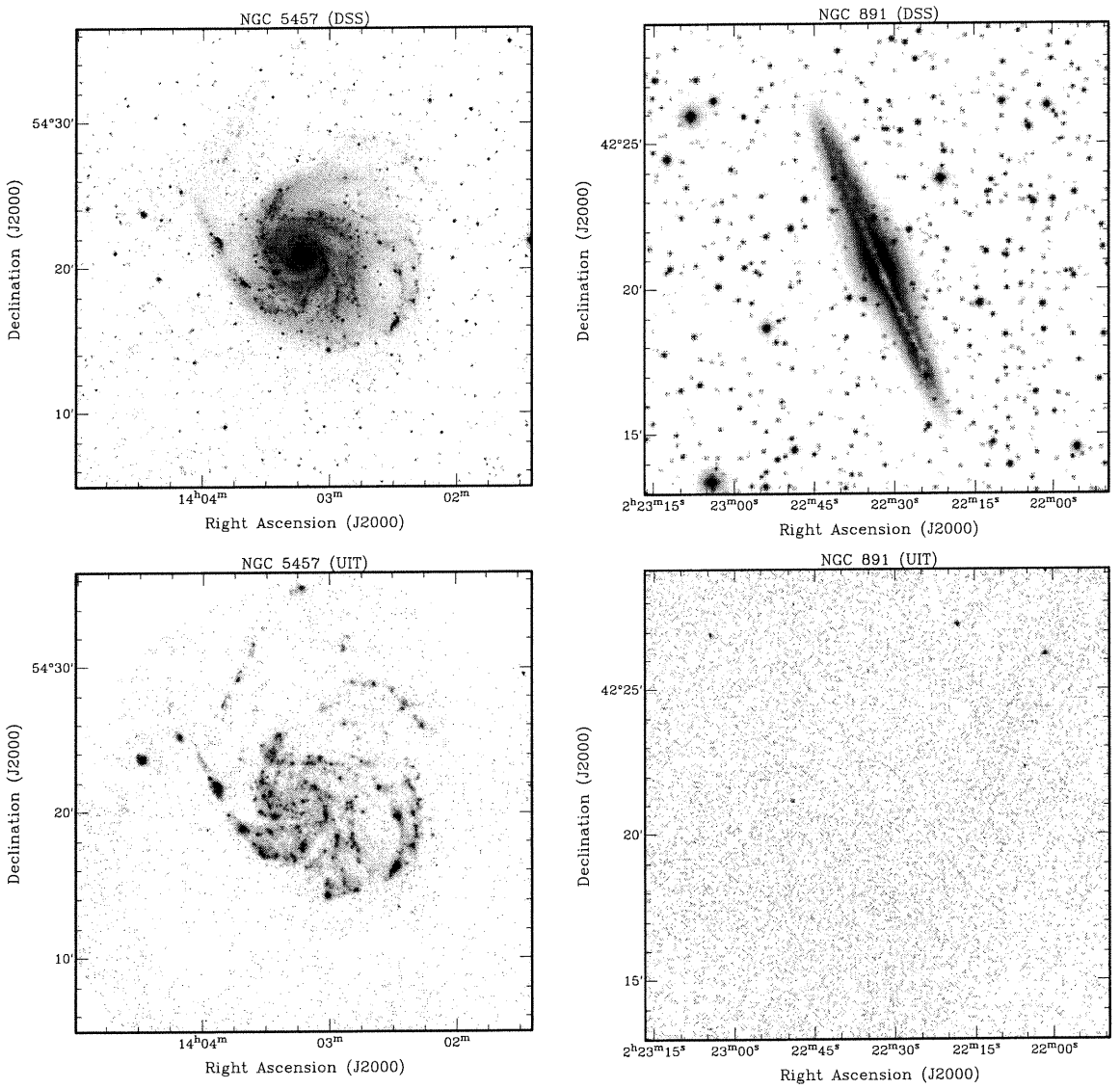

FIGURE 2.3 – Optical DSS (top) and FUV UIT (bottom) images for two M31-like galaxies — face-on NGC 5457 (left panels), and edge-on NGC 891 (right panels). UIT images were obtained with B1 and B5 filters ($\lambda \simeq 1500$ Å), and have comparable sensitivity (within a factor of 2). Weak features in both optical and FUV images were emphasized by using the square-root intensity scale. The fact that NGC 891 is not detected in FUV (bottom right image) points to strong anisotropy of the FUV radiation field around normal spiral galaxies.

the X-ray luminosity of the face-on spiral NGC 5457 1.0×10^{40} ergs s^{-1} from Read & Ponman 2001, recalculated for the distance of 7.0 Mpc from Stetson et al. 1998.) The extragalactic soft X-ray background flux is believed to be known relatively accurately. Chen, Fabian, & Gendreau (1997) give the following estimate of the background spectral density within the $0.1 - 7$ keV band: $10.5\,E^{-1.46}$ keV cm^{-2} s^{-1} sr^{-1} keV^{-1}, where E is the photon energy in keV units. Integrated over the $0.1 - 2$ keV interval of photon energies, this gives the following value of the metagalactic soft X-ray background flux (in 2π solid angle): 5.0×10^{-7} ergs cm^{-2} s^{-1}. Combined with the derived above face-on X-ray luminosity of M31, the radius of the soft X-ray "dominance sphere" for M31 is found to be very small: $\sim 9 - 13$ kpc. Thus the ISM heating by soft X-ray radiation from normal spiral galaxies cannot be an important environmental factor for dwarf galaxies.

This leads to the conclusion that FUV radiation escaping from spiral galaxies can be an important environmental factor for dwarf satellite galaxies only if the resultant ISM heating rate is larger than the heating rate from the metagalactic soft X-ray background. This issue can be addressed only through solving numerically the equations of thermal and ionization equilibrium with inclusion of all relevant physical processes (similarly to Wolfire et al. 1995), which is beyond the scope of this paper.

2.3 Observational Evidence

The previous section gives support to the idea that the electromagnetic radiation escaping from the host spiral galaxy can be an important evolutionary factor for dwarf galaxies. This mechanism can explain in general the principal differences (in SFHs and neutral gas content) between two classes of dwarfs — dSphs and dIrrs. In this section we will present the observational evidence for the impact of the UV radiation from the Milky Way and M31 spirals on their dwarf satellites, which gives further support to the above idea.

2.3.1 Sculptor DSph: Evidence for the ISM Photoevaporation

Two HI clouds observed within the optical extent of the Sculptor dSph are most probably physically associated with the dwarf (Carignan et al. 1998; BCM). Assuming that they are located at the distance of Sculptor, their total mass is $\sim 2 \times 10^5$ $M_\odot$. The fact that most of the other dSph galaxies do not possess a detectable neutral ISM is suggestive of Sculptor being in a transient state.

We argue that the two HI clouds in the vicinity of Sculptor are part of the ISM of the dwarf, and are being photoevaporated by the Galactic LyC radiation. The most direct evidence confirming this scenario comes from the comparison of the radial velocity of the H_α emitting gas in the northeast cloud (Weiner et al. 2001; B. J. Weiner 2001, private communication) with the velocity of the HI gas integrated over the same area. BCM obtained that the ionized

gas is blue-shifted by 12 ± 8 km s^{-1} relative to the neutral gas. This is consistent with the prediction of the photoevaporation model (Section 2.2.2), where the HII gas is expected to be blue-shifted relative to the HI gas by ~ 10 km s^{-1} (sound speed in a 10^4 K plasma).

2.3.2 The Puzzle of the "Twin" Galaxies NGC 147 and NGC 185

The two dwarf elliptical satellites of M31, NGC 147 and NGC 185, appear to be almost identical in many respects (Young & Lo 1997a): they have comparable blue luminosities, Holmberg diameters, $B - V$ colors, average surface brightness, light profile shapes, mean stellar dispersions, and projected distances from M31. Both galaxies show evidence for an intermediate-age stellar component (Young & Lo 1997a).

Despite all these similarities, NGC 147 and NGC 185 are strikingly different in their recent SFHs, and in their present day neutral gas content. NGC 185 formed stars as recently as 20 Myr ago (Lee, Freedman, & Madore 1993a), and contains substantial amounts of HI (1.1×10^5 M$_\odot$) and H_2 (4.1×10^4 M$_\odot$) (Young 2001). Conversely, NGC 147 has not formed stars for at least a Gyr (Han et al. 1997), and appears to be devoid of neutral ISM (Young & Lo 1997a; Sage, Welch, & Mitchell 1998).

We argue that the present-day differences between NGC 147 and NGC 185 can be explained by different fluxes of the LyC and FUV radiation escaping from M31 at the present locations of the dwarfs.

To quantify this effect, we need to know the accurate distances to the dwarfs and to M31. To avoid large systematic errors, we use the distance measurements obtained with the same technique — the tip of the red giant branch (TRGB) method, which was shown to work very well for low-metallicity Population II stars (Lee, Freedman, & Madore 1993b). Two available TRGB distance measurements for NGC 185 (Lee et al. 1993b and Martínez-Delgado & Aparicio 1998) give virtually the same values of the true distance modulus: $(m - M)_0 = 23.95 \pm 0.1$. The situation with NGC 147 is different — Lee et al. (1993b) gave the value $(m - M)_0 = 24.13 \pm 0.1$, whereas Han et al. (1997) obtained $(m - M)_0 = 24.37 \pm 0.06$. We choose to use the latter value, because it was derived from the high quality WFCP2 data for $\sim 117,000$ stars in two different fields, both producing identical true distance modulus estimates. In contrast, the distance value of Lee et al. (1993b) was based on the photometry of only ~ 500 stars from the paper of Mould, Kristian, & Da Costa (1983). Two relevant distance measurements for the M31 galaxy agree very well: Durrell, Harris, & Pritchet (2001) obtained TRGB true distance modulus $(m - M)_0 = 24.47 \pm 0.12$ based on a wide-field photometry of the field in outer halo of M31, and Holland (1998) derived $(m - M)_0 = 24.47 \pm 0.07$ by fitting theoretical isochrones to the observed red giant branches of 14 globular clusters in M31. (It is interesting to note that the identical value was obtained by Stanek & Garnavich (1998) from comparing the red clump stars with parallaxes known to better than 10% in the Hipparcos catalog with the red clump stars observed in three fields in M31 using the Hubble

Space Telescope: $(m-M)_0 = 24.47 \pm 0.08$.) Finally, we adopt the following values of the true distance modulus for NGC 185, NGC 147, and M31: 23.95 ± 0.1, 24.37 ± 0.06, and 24.47 ± 0.07, respectively.

We derive the following distances from M31: 100^{+13}_{-4} kpc for NGC 147, and 186^{+34}_{-33} kpc for NGC 185. If the FUV and ionizing radiation from M31 were isotropic, NGC 147 would receive $2.8^{+0.9}_{-0.8}$ times larger flux than NGC 185. This difference is probably not large enough to explain the observed differences in the neutral gas content and recent SFH of the dwarfs.

It is expected though that the LyC and FUV fluxes from a giant spiral galaxy are strongly anisotropic, being at maximum along the polar axis (local galactic latitude $b_{loc} = \pm 90°$), and dropping virtually to zero in the plane of the galaxy ($b_{loc} = 0°$). To estimate b_{loc} values for NGC 147 and NGC 185, we adopt the inclination angle of the M31 disk $i = 77.^{\circ}5$ from Ma et al. (1997), and the position angle of the galactic line of nodes PA $= 37.^{\circ}7$ from de Vaucouleurs (1958). The uncertainty in both angles is assumed to be 1°. We use the fact that the NW side of M31 is the near side (e.g. Walterbos & Kennicutt 1988), and arbitrarily choose the local northern pole to be on the opposite side of the M31 disk.

Taking into account all the uncertainties, we derive $b_{loc} = (3^{+4}_{-3})$ dgr. for NGC 185, and $b_{loc} = (37^{+11}_{-8})$ dgr. for NGC 147. It appears that NGC 185 is located almost in the plane of the M31 disk, and is therefore shielded from the FUV and LyC electromagnetic radiation by the HI disk of M31. In contrast, from the location of NGC 147 the M31 spiral is seen half-open, resulting in significant fluxes of the ionizing and FUV radiation, which can ionize and heat the ISM of the dwarf thus preventing star formation.

The present location of NGC 147 is consistent with the observed age ~ 1 Gyr (Han et al. 1997) of its most recent star burst: if we assume that the dwarf is on a polar circular orbit around M31 with orbital velocity $V_c = 220$ km s^{-1} and has already passed the galactic pole, then the most recent passage of the plane of M31 was $1.03^{+0.27}_{-0.04}$ Gyr ago.

2.3.3 Disturbed ISM of NGC 205

The neutral ISM of the NGC 205 dwarf elliptical satellite of M31 consists of 4.3×10^5 $M_\odot$ of HI and $\sim 1 \times 10^5$ $M_\odot$ of H_2 (Young 2000). The morphology and kinematics of the neutral gas is very unusual: the central and northern parts of the ISM look relatively unperturbed with the radial velocity being close to that of the stellar body, whereas the southern part appears to be compressed from the SE direction and red-shifted by $\sim 20 - 30$ km s^{-1} relative to the stars (Young & Lo 1997a, their Figures 2 and 4).

We note that the line drawn along the compressed gas in the southern part of the galaxy is perpendicular to the direction toward the center of M31, which is located to the southeast of NGC 205 at the position angle PA$= 133°$ (Figure 2.4). The dwarf galaxy is located very close to M31 in projection (8 kpc away at the distance of M31), and most probably is $\sim 30 - 100$ kpc behind the spiral galaxy along the line of sight (Saha, Hoessel, & Krist 1992; Mateo 1998;

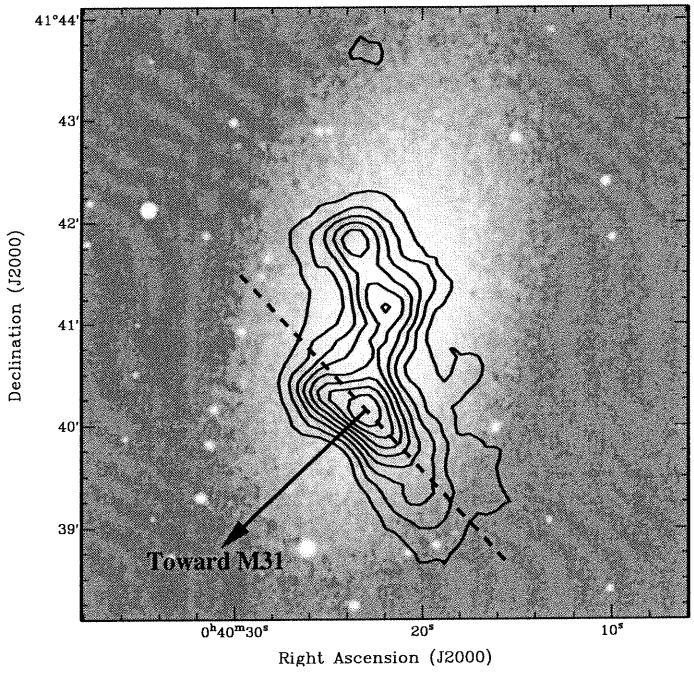

FIGURE 2.4 – HI flux contours of NGC 205 from Young & Lo (1997a), superposed on a DSS image (only the central brightest part of the optical disk is shown). The arrow shows the direction toward the M31 center at PA = 133°. The dashed line is perpendicular to the arrow.

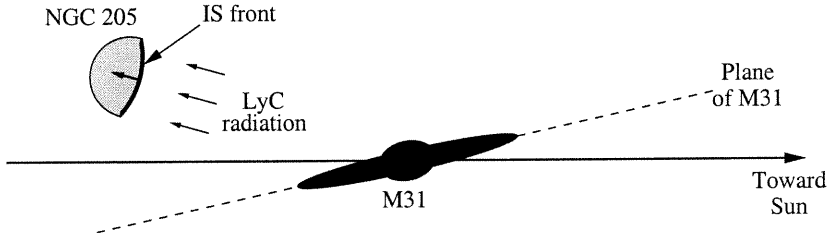

FIGURE 2.5 – Scheme showing a probable position of NGC 205 relative to M31 and the observer. In this configuration the IS front in the ISM of NGC 205 would be seen by the observer red-shifted relative to the stars of the dwarf galaxy.

Bond & Alves 2001). This places NGC 205 relatively close to the plane of the spiral galaxy, with the local galactic latitude $b_{loc} \sim 20°$. The morphology and kinematics of the disturbed gas is then consistent with an ionization-shock (IS) front driven by the LyC radiation from M31 toward the center of NGC 205 with a velocity ~ 25 km s^{-1} (Figure 2.5). The fact that the compressed part of the ISM shows the highest HI column density in NGC 205 and contains significant amounts of H_2 kinematically coupled to HI (Young 2000) supports this picture of a relatively strong shock. From Figure 2.4 we estimate that the shock front has already traveled ~ 300 pc inside the dwarf, indicating that the process started very recently: ~ 10 Myr ago (kinematic age).

Another important piece of evidence comes from the SFH of the dwarf galaxy. The central part of NGC 205 has experienced two recent star bursts — $20 - 80$ and ~ 500 Myr ago, with a puzzling gap in between (Lee 1996).

We propose the following scenario which explains both the ISM and recent SFH peculiarities of NGC 205. We argue that the dwarf galaxy experienced the two most recent star bursts during its passages through the plane of M31. The star formation $20-80$ Myr ago, the dwarf's present location close to the plane of the spiral, and the short time scale ~ 10 Myr for the observed IS front all suggest that NGC 205 has recently crossed the plane of M31. Associating the second to last star burst ~ 500 Myr ago with the previous crossing of the plane gives an estimate of the orbital period of the dwarf: $P \simeq 1$ Gyr. If we assume that the dwarf is on a circular orbit around M31 with orbital velocity $V_c = 220$ km s^{-1}, then the radius of the orbit is 36 kpc. At such a small distance, the LyC and FUV fluxes from M31 should be significant for most of the lifetime of NGC 205, with only short periods every 500 Myr with much lower levels of radiation during the passages through the plane of the host spiral galaxy.

The fact that the shock front velocity $V_s \sim 25$ km s^{-1} is larger than the sound speed in the HII gas ~ 10 km s^{-1} suggests that the ISM of the dwarf is in the initial phase of the IS front cloud implosion (Bertoldi 1989). The velocity of the IS front at this stage is given by (Bertoldi 1989, for $T_{\rm HII} = 10^4$ K)

$$V_s \simeq 0.0151 \sqrt{\frac{F}{n_0}} \text{ km s}^{-1}, \tag{2.9}$$

where F is the incident ionizing flux, and n_0 is the initial number density of the gas. The HI mass of 4.3×10^5 M$_\odot$ averaged over the volume of the ISM with the size 900×300 pc (Young & Lo 1997a) gives an estimate of the hydrogen number density $n_0 \simeq 0.41$ cm^{-3}. We take the lower value $n_0 \sim 0.2$ cm^{-3} to account for the fact that the shocked gas is located on the outskirts of the dwarf galaxy where the density of the gas should be lower than the averaged value. From equation (2.9) we derive the required LyC flux value $F \simeq 5.5 \times 10^5$ cm^{-2} s^{-1}.

2.3.4 Carina dSph Versus Ursa Minor dSph

The Carina and Ursa Minor dwarf spheroidals belong to the class of the lowest luminosity dSph galaxies. They have comparable luminosity ($L_V \sim [3-4] \times 10^5$ $L_\odot$), core radius ($r_c \sim$ 200 pc), central mass-to-light ratio ($m/L_V \sim 30-60$), and distance from the Milky Way galaxy ($R \sim 70-100$ kpc) (Mateo 1998). It is very surprising then that they exhibit two opposite SFH extremes: Carina has formed stars for most of its lifetime in three discrete bursts 3, 7, and 15 Gyr ago (Hurley-Keller, Mateo, & Nemec 1998), whereas Ursa Minor was formed in a single star burst $\gtrsim$ 14 Gyr ago (Olszewski & Aaronson 1985; Hernandez, Gilmore, & Valls-Gabaud 2000).

We note that Carina has the smallest absolute value of galactic latitude $\|b\| \simeq 22°$ among all the Milky Way satellite galaxies (excluding the special case of the Sagittarius dSph). This is consistent with Carina having relatively small angle between its orbit and the plane of the Galaxy — probably as small as 22°. If this is the case, the dwarf has spent a significant part of its lifetime hiding from the ionizing and FUV radiation from the Milky Way near the plane of the Galaxy, keeping its ISM neutral and episodically forming stars.

The opposite example is that of Ursa Minor. Both the proper motion measurements (Schweitzer, Cudworth, & Majewski 1997) and the relatively high location above the Galactic plane ($\|b\| \simeq 45°$) suggest that the dwarf is on close to polar orbit around the Milky Way galaxy. Galaxies less massive than $\sim 10^8$ $M_\odot$ should gradually lose their ISM when the gas is fully photoionized. We argue that the relatively small distance from the Galaxy and the almost polar orbit caused Ursa Minor to lose its ISM on a short time scale, leading to sharply declining SFR.

2.4 Discussion and Conclusions

Theoretical description of the formation and evolution of dIrr galaxies is a complex problem, which is far from being fully resolved. Nevertheless, recent semi-analytical models (Spaans & Norman 1997; Ferrara & Tolstoy 2000) appear to converge in that the isolated gas-rich dwarfs should have been forming stars with almost constant low efficiency for most of their lifetimes, with a possible exception of the early epoch ($z \gtrsim 1$) with increased SFR. The emerging consensus is that soon after the initial star burst, star formation becomes self-regulated through the feedback from massive stars (impact on the ISM of stellar winds, ionizing and FUV radiation, and supernovae). This is in accord with the findings of van Zee (2001), who showed that observed optical colors of a large sample of isolated dIrr galaxies are consistent with approximately constant SFR for at least 10 Gyr.

The situation with the early-type dwarfs (dSph and dE) is even more complicated. There are at least three observational facts that any successful dwarf evolution theory should explain:

1. *Impact of environment.* All Local Group dwarfs with $M_V > -15^m$ located within 250 kpc

from the Milky Way and M31 are early-type systems. The observed morphology-density relation for dwarf galaxies (Binggeli, Tarenghi, & Sandage 1990) appears to extend this trend beyond the Local Group.

2. *Absence of neutral gas.* With a few exceptions, the Local Group early-type dwarfs appear to be devoid of HI and H_2 — despite showing in many cases evidence for recent star formation. For example, Fornax has the very low HI mass upper limit of $5,000$ $M_\odot$ (Mateo 1998), but formed stars as recently as 200 Myr ago (Saviane, Held, & Bertelli 2000).

3. *Episodic SFH.* Some Local Group dSph/dE galaxies have puzzling gaps of $1-5$ Gyr in their SFHs. These time intervals are much longer than the $10^7 - 10^8$ yr timescales of internal mechanisms which could effect the star formation, — with a possible exception of the SNe Ia heating mechanism (Burkert & Ruiz-Lapuente 1997).

In this paper we showed that all the above observational facts can be explained by the impact of the ultraviolet radiation from the host spiral galaxy on the ISM of dwarf satellites. We gave evidence in support of the following key ingredients of our model:

1. FUV and LyC fluxes from giant spiral galaxies are sufficiently large to alter the state of the ISM in nearby dwarf galaxies such that star formation becomes unlikely. The LyC radiation can ionize the ISM through the process of photoevaporation, making it very hard to detect.

2. The UV radiation from the spiral galaxies like the Milky Way and M31 dominates over the metagalactic background radiation within a large sphere of radius $\gtrsim 200$ kpc.

3. The ultraviolet radiation field of a spiral galaxy is strongly anisotropic, with the flux dropping almost to zero in the narrow zone near the plane of the galaxy.

4. Many Local Group dSph galaxies have masses $\gtrsim 10^8$ $M_\odot$, and are able to keep the photoionized 10^4 K gas gravitationally bound for prolonged periods of time.

In our scenario, low mass galaxies orbiting around large spirals spend most of their lifetimes exposed to the ultraviolet radiation from their host galaxies, which keeps their ISM in a warm ($\sim 10^4$ K) and ionized state. Twice per orbital period, each satellite crosses a narrow "shadow" zone near the plane of the host galaxy, where the ultraviolet flux is dramatically reduced by absorption in the HI disk of the spiral. During such "eclipses", the ISM of the dwarf galaxy recombines, cools down, and collapses toward the center of the dwarf on timescales ~ 100 Myr. We expect the cold dense gas at the center of the dwarf to become self-gravitating, and under favorable conditions to start forming stars. For a short time, such early-type dwarfs can turn into a dIrr galaxy, with two-phase ISM structure, and low-efficiency star formation self-regulated through feedback mechanisms. Approaching the edge of the shadow zone, the dwarf galaxy experiences an increase in the external FUV flux, which can warm up the ISM and

quench the star formation. Finally, the increased LyC flux can photoionize the warm ISM through the process of photoevaporation.

One of predictions of our model which can be tested observationally is that at least some early-type dwarf satellites of the Milky Way and M31 should possess extended ionized ISM, with the temperature $T \sim 10^4$ K, and low number density. The total mass of the gas can be comparable to the mass of the stars. The sound speed in the photoionized gas (~ 10 km s^{-1}) is close to the stellar velocity dispersion in dSphs, hence both gas and stars are expected to have a comparable extent. The most promising candidates are the dwarfs with the complex and relatively recent star formation, located $\lesssim 100$ kpc away from the host galaxy: NGC 147, Fornax, and Carina. The extended HII atmospheres are also expected to surround the dwarfs whose ISM we believe is being currently photoionized by the LyC radiation from the host spiral galaxy: NGC 205 and Sculptor.

There are two possible ways to detect such tenuous ionized gas: either in absorption, by obtaining FUV spectra of QSOs and AGNs located behind the dwarf, or through its emission (e.g., in H_α line).

The absorption method was used by Bowen et al. (1997), who put an upper limit on the column density of the ionized gas around Leo I. They probed with HST three sight lines toward QSOs passing $\geq 34'$ from the center of the dwarf, and did not detect any absorption in C IV, Si II, or Si IV spectral lines at the velocity of Leo I. The photoionized gas in this dwarf (if present) is not expected to extend beyond its stellar tidal radius, which is equal to $12'.6$ (Mateo 1998), so the results of Bowen et al. (1997) cannot be used to test our model. Bowen et al. also showed, that with present day technology only the brightest quasars, with $m_V \lesssim 16^m$, can be used to search for the presence of the tenuous ionized gas in dSphs. To the best of our knowledge, there are no known QSO/AGN, brighter than $m_V \sim 17^m$, located in projection within the stellar extent of the Local Group early-type dwarfs (Tinney, Da Costa, & Zinnecker 1997; Tinney 1999; Schneider et al. 2002).

We believe that the ionized ISM detection in the H_α emission line is a more feasible approach. The expected H_α surface brightness is < 100 mR, so the required sensitivity of the observations should be at least 10 mR. The angular resolution should be at least $\sim 10'$ for the Milky Way satellites, and $\sim 1'$ for the M31 companions. The Galactic foreground radiation is expected to dominate over the radiation coming from the dwarfs (with the typical integral flux values of ~ 1 R for the high Galactic latitude dwarfs, and reaching ~ 20 R for Carina), so the observations should be carried out within a narrow, $20 - 40$ km s^{-1}, interval of the radial velocities centered at the optical velocity of the dwarf. Three available wide-field H_α surveys do not meet the above requirements: two complementing surveys, VTSS[1] (Virginia Tech Spectral-Line Survey, covering the northern hemisphere, Dennison, Simonetti, & Topasna 1998), and SHASSA[2] (Southern H-Alpha Sky Survey Atlas, Gaustad et al. 2001) lack

[1] http://www.phys.vt.edu/~halpha
[2] http://amundsen.swarthmore.edu/SHASSA

sensitivity (500 mR) and velocity information, whereas WHAM[3] (Wisconsin H-Alpha Mapper, northern hemisphere, Reynolds et al. 1998) having reasonably good sensitivity (50 mR) and spectral resolution (~ 10 km s^{-1}), does not qualify because of insufficient angular resolution (1°) and too narrow velocity coverage: $V_{\rm LSR} = -100 \ldots 100$ km s^{-1}. Targeted H_α emission observations can do a much better job: observations with sensitivity ~ 10 mR, angular and velocity resolutions $\sim 5'$ and ~ 10 km s^{-1}, are almost routine nowadays (Weiner et al. 2001; Weymann et al. 2001; B. J. Weiner 2001, private communication). With new differential techniques, even lower emission levels of $1-2$ mR might be reached (Bland-Hawthorn & Maloney 2001).

It is interesting to note that at least one of the dwarf galaxies in question, NGC 205, has a tentative extended H_α emission detection in VTSS[4] (field And07). The central part of the dwarf has a surface brightness of ~ 5 R, and the fainter emission with the brightness of $1-2$ R appears to fill out all the stellar extent of the galaxy. These large values of the H_α flux, if confirmed, could be explained by the phosphorescence of the recombining gas after the recent death of an O-star, by the combined contribution from some 30 known planetary nebulae in NGC 205 (Ciardullo et al. 1989), and/or by assuming that the dwarf is located very close to M31: $R \lesssim 20$ kpc. Future targeted H_α emission observations of NGC 205 are required to resolve the issue.

We are grateful to Frank Bertoldi, Andrea Ferrara, and Sergey Silich for insightful discussions and numerous helpful suggestions. We also thank Lisa Young for providing the HI data for NGC 205, and Ben Weiner for sharing the details of the H_α emission detection in Sculptor. C. C. acknowledges support from NSERC (Canada) and FCAR (Québec).

[3]http://www.astro.wisc.edu/wham

[4]The Virginia Tech Spectral-Line Survey (VTSS) is supported by the National Science Foundation.

References

Aparicio, A., Carrera, R., & Martínez-Delgado, D. 2001, AJ, 122, 2524

Barnes, D. G. & de Blok, W. J. G. 2001, AJ, 122, 825

Bell, E. F. & Kennicutt, R. C. 2001, ApJ, 548, 681

Bertoldi, F. 1989, ApJ, 346, 735

Bertoldi, F. & McKee, C. F. 1990, ApJ, 354, 529

Binggeli, B., Tarenghi, M., & Sandage, A. 1990, A&A, 228, 42

Bland-Hawthorn, J. & Maloney, P. R. 2001, preprint (astro-ph/0110044)

Bland-Hawthorn, J. & Putman, M. E. 2001, in ASP Conf. Ser. 240, Gas and Galaxy Evolution, ed. J. E. Hibbard, M. P. Rupen & J. H. van Gorkom (San Fransisco: ASP), 369

Blitz, L. & Robishaw, T. 2000, ApJ, 541, 675

Bond, H. E. & Alves, D. R. 2001, in Astrophysics and Space Science Library Vol. 265, Post-AGB Objects as a Phase of Stellar Evolution, ed. R. Szczerba & S. K. Gorny (Boston/Dordrecht/London: Kluwer Academic Publishers), 77

Bowen, D. V., Tolstoy, E., Ferrara, A., Blades, J. C., & Brinks, E. 1997, ApJ, 478, 530

Burkert, A. & Ruiz-Lapuente, P. 1997, ApJ, 480, 297

Cappellaro, E., Evans, R., & Turatto, M. 1999, A&A, 351, 459

Carignan, C., Beaulieu, S., Côté, S., Demers, S., & Mateo, M. 1998, AJ, 116, 1690

Chen, L.-W., Fabian, A. C., & Gendreau, K. C. 1997, MNRAS, 285, 449

Chiosi, C., Bressan, A., Portinari, L., & Tantalo, R. 1998, A&A, 339, 355

Ciardullo, R., Jacoby, G. H., Ford, H. C., & Neill, J. D. 1989, ApJ, 339, 53

de Vaucouleurs, G. 1958, ApJ, 128, 465

Dennison, B., Simonetti, J. H., & Topasna, G. A. 1998, Publications of the Astronomical Society of Australia, 15, 147

Devereux, N. A., Price, R., Wells, L. A., & Duric, N. 1994, AJ, 108, 1667

Dove, J. B., Shull, J. M., & Ferrara, A. 2000, ApJ, 531, 846

Draine, B. T. 1978, ApJS, 36, 595

Durrell, P. R., Harris, W. E., & Pritchet, C. J. 2001, AJ, 121, 2557

Efremov, Y. N. & Elmegreen, B. G. 1998, MNRAS, 299, 643

Ferrara, A. & Tolstoy, E. 2000, MNRAS, 313, 291

Gallart, C., Martínez-Delgado, D., Gómez-Flechoso, M. A., & Mateo, M. 2001, AJ, 121, 2572

Gaustad, J. E., McCullough, P. R., Rosing, W., & Van Buren, D. 2001, PASP, 113, 1326

Grebel, E. K. 1997, Reviews of Modern Astronomy, 10, 29

Haardt, F. & Madau, P. 1996, ApJ, 461, 20

Han, M., Hoessel, J. G., Gallagher, J. S., Holtsman, J., & Stetson, P. B. 1997, AJ, 113, 1001

Hernandez, X., Gilmore, G., & Valls-Gabaud, D. 2000, MNRAS, 317, 831

Holland, S. 1998, AJ, 115, 1916

Hurley-Keller, D., Mateo, M., & Nemec, J. 1998, AJ, 115, 1840

Kaplan, S. A. & Pikelner, S. B. 1970, The Interstellar Medium (Cambridge: Harvard University Press)

Kleyna, J. T., Wilkinson, M. I., Evans, N. W., & Gilmore, G. 2001, ApJ, 563, L115

Lee, M. G., Freedman, W. L., & Madore, B. F. 1993a, AJ, 106, 964

Lee, M. G., Freedman, W. L., & Madore, B. F. 1993b, ApJ, 417, 553

Lee, M. G. 1996, AJ, 112, 1438

Ma, J., Peng, Q., & Gu, Q. 1997, ApJ, 490, L51

Mac Low, M. & Ferrara, A. 1999, ApJ, 513, 142

Mac Low, M., McCray, R., & Norman, M. L. 1989, ApJ, 337, 141

Madsen, G. J., Reynolds, R. J., Haffner, L. M., Tufte, S. L., & Maloney, P. R. 2001, ApJ, 560, L135

Maloney, P. 1993, ApJ, 414, 41

Martínez-Delgado, D. & Aparicio, A. 1998, AJ, 115, 1462

Martínez-Delgado, D., Gallart, C., & Aparicio, A. 1999, AJ, 118, 862

Mashchenko, S. Y. & Silich, S. A. 1994, Astronomy Reports, 38, 207

Mateo, M. L. 1998, ARA&A, 36, 435

Mayer, L., Governato, F., Colpi, M., Moore, B., Quinn, T., Wadsley, J., Stadel, J., & Lake, G. 2001, ApJ, 559, 754

Miller, B. W., Dolphin, A. E., Lee, M. G., Kim, S. C., & Hodge, P. 2001, ApJ, 562, 713

Mould, J. R., Kristian, J., & Da Costa, G. S. 1983, ApJ, 270, 471

Murali, C. 2000, ApJ, 529, L81

Murthy, J., Hall, D., Earl, M., Henry, R. C., & Holberg, J. B. 1999, ApJ, 522, 904

Odenkirchen, M. et al. 2001, AJ, 122, 2538

Olszewski, E. W. & Aaronson, M. 1985, AJ, 90, 2221

Piatek, S., Pryor, C., Armandroff, T. E., & Olszewski, E. W. 2001, AJ, 121, 841

Piersimoni, A. M., Bono, G., Castellani, M., Marconi, G., Cassisi, S., Buonanno, R., & Nonino, M. 1999, A&A, 352, L63

Quilis, V. & Moore, B. 2001, ApJ, 555, L95

Read, A. M. & Ponman, T. J. 2001, MNRAS, 328, 127

Reynolds, R. J. 1991, ApJ, 372, L17

Reynolds, R. J., Tufte, S. L., Haffner, L. M., Jaehnig, K., & Percival, J. W. 1998, Publications of the Astronomical Society of Australia, 15, 14

Sage, L. J., Welch, G. A., & Mitchell, G. F. 1998, ApJ, 507, 726

Saha, A., Hoessel, J. G., & Krist, J. 1992, AJ, 103, 84

Sasseen, T. P., Lampton, M., Bowyer, S., & Wu, X. 1995, ApJ, 447, 630

Saviane, I., Held, E. V., & Bertelli, G. 2000, A&A, 355, 56

Schneider, D. P. et al. 2002, AJ, 123, 567

Schweitzer, A. E., Cudworth, K. M., & Majewski, S. R. 1997, in ASP Conf. Ser. 127, Proper Motions and Galactic Astronomy, ed. R. M. Humphreys (San Fransisco: ASP), 103

Shull, J. M., Roberts, D., Giroux, M. L., Penton, S. V., & Fardal, M. A. 1999, AJ, 118, 1450

Silich, S. A., Mashchenko, S. Y., Tenorio-Tagle, G., & Franco, J. 1996, MNRAS, 280, 711

Silk, J., Wyse, R. F. G., & Shields, G. A. 1987, ApJ, 322, L59

Spaans, M. & Norman, C. A. 1997, ApJ, 483, 87

Spitzer, L., Jr. 1978, Physical Processes in the Interstellar Medium (New York: A Wiley-Interscience Publication)

St-Germain, J., Carignan, C., Côte, S., & Oosterloo, T. 1999, AJ, 118, 1235

Stanek, K. Z. & Garnavich, P. M. 1998, ApJ, 503, L131

Stecher, T. P. et al. 1997, PASP, 109, 584

Stetson, P. B. et al. 1998, ApJ, 508, 491

Supper, R., Hasinger, G., Lewin, W. H. G., Magnier, E. A., van Paradijs, J., Pietsch, W., Read, A. M., & Trümper, J. 2001, A&A, 373, 63

Takeda, H., Nulsen, P. E. J., & Fabian, A. C. 1984, MNRAS, 208, 261

Tenorio-Tagle, G., Silich, S. A., Kunth, D., Terlevich, E., & Terlevich, R. 1999, MNRAS, 309, 332

Thornton, K., Gaudlitz, M., Janka, H.-T., & Steinmetz, M. 1998, ApJ, 500, 95

Tinney, C. G., Da Costa, G. S., & Zinnecker, H. 1997, MNRAS, 285, 111

Tinney, C. G. 1999, MNRAS, 303, 565

Tumlinson, J., Giroux, M. L., Shull, J. M., & Stocke, J. T. 1999, AJ, 118, 2148

van den Bergh, S. 1999, AJ, 117, 2211

van Zee, L. 2001, AJ, 121, 2003

Walterbos, R. A. M. & Braun, R. 1994, ApJ, 431, 156

Walterbos, R. A. M. & Kennicutt, R. C. 1988, A&A, 198, 61

Weiner, B. J., Vogel, S. N., & Williams, T. B. 2001, preprint (astro-ph/0109055)

Welch, G. A., Mitchell, G. F., & Yi, S. 1996, ApJ, 470, 781

Weymann, R. J., Vogel, S. N., Veilleux, S., & Epps, H. W. 2001, ApJ, 561, 559

Wolfire, M. G., Hollenbach, D., McKee, C. F., Tielens, A. G. G. M., & Bakes, E. L. O. 1995, ApJ, 443, 152

Yamaguchi, R., Mizuno, N., Onishi, T., Mizuno, A., & Fukui, Y. 2001, PASJ, 53, 959

Young, L. M. & Lo, K. Y. 1996, ApJ, 462, 203

Young, L. M. & Lo, K. Y. 1997a, ApJ, 476, 127

Young, L. M. & Lo, K. Y. 1997b, ApJ, 490, 710

Young, L. M. 2000, AJ, 120, 2460

Young, L. M. 2001, AJ, 122, 1747

Chapitre 3

Des nuages d'hydrogène neutre près des dSph et des dIrr/dSph du Groupe Local

Ce chapitre présente une partie importante du travail que j'ai accompli sur les galaxies naines. Il explique en détail le problème du manque de matière interstellaire dans les naines et montre les résulats des observations faites en Australie lors de mon stage à l'Australia Telescope National Facility sous la direction de Lister Staveley-Smith.

J'ai eu moi-même la chance de conduire les observations ici présentées, de traiter les données, de les analyser et d'écrire l'article qui tient ici lieu de chapitre. Lister Staveley-Smith et Claude Carignan m'ont été d'une grande aide dans le processus. Ils m'ont fourni le support dont j'ai eu besoin à chacune des étapes de la recherche et de la rédaction, que ce soit lors de la mise en forme des idées d'observations ou de la correction de mon anglais parfois boiteux.

HI Clouds near dSph and dIrr/dSph Galaxies of the Local Group

Antoine Bouchard
Département de physique and Observatoire du mont Mégantic, Université de Montréal, C.P. 6128, Succ. Centre-ville, Montréal, Québec, Canada H3C 3J7, and
Australia Telescope National Facility, PO Box 76, Epping, NSW 1710, Australia
e–mail: [redacted]

Claude Carignan
Département de physique and Observatoire du mont Mégantic, Université de Montréal, C.P. 6128, Succ. Centre-ville, Montréal, Québec, Canada H3C 3J7
e–mail: [redacted]

and

Lister Staveley–Smith
Australia Telescope National Facility, PO Box 76, Epping, NSW 1710, Australia
e–mail: [redacted]

To be submitted to Astronomical Journal

New HI observations of the surroundings of 9 dSph and dIrr/dSph galaxies of the Local Group from the Parkes radiotelescope are presented. This updates the previous study by Blitz and Robishaw (2000) and again, it is shown that the observed dwarfs are often associated with large off-centered hydrogen clouds. The possible physical association of the clouds with the dwarf galaxies and the mechanisms by which the gas could be expelled are discussed. We favor the explanation by which the ionizing radiation escaping the Milky Way can render the hydrogen content of dwarf galaxies undetectable. We also investigate the link between High Velocity Clouds and dwarf galaxies. The dwarf galaxies of our sample are (all but one) situated in regions where the HVC density well above the average HVC density as computed from the HVC catalog by Putman et al. (2002).

3.1 Introduction

Dwarf spheroidal galaxies (dSph) and mixed type dwarf irregulars/dwarf spheroidals (dIrr/dSph) of the Local Group (LG) are torn apart by the presence of all the other members of the group. Their shallow potential well makes them good targets for many kinds of disruption, from tidal forces to ram pressure due to the intergalactic medium (IGM). In fact, most of the dSph are found near larger galaxies (Mateo 1998). In the LG, the Milky Way has 7 dSph closer than 200 kpc, which is the size of its extended dark matter halo (Zaritsky 1999), where one could think that disruption processes are important.

Recently Blitz & Robishaw (2000, hereafter BR) compiled evidence that 10 of the 21 dSph and dIrr/dSph galaxies of the LG contain large amounts of HI situated in reservoirs that can be as far as 10 kpc away from the optical core of the galaxy. The offset is mainly attributed

to ram pressure but the authors also consider a tidal stripping mechanism. This followed the dicovery of HI clouds near Sculptor (Carignan et al. 1998), Phoenix (St-Germain et al. 1999) and other dwarfs like SagDIG (Young & Lo 1997a), where we can see a ring of HI surrounding the galaxy.

This recent evidence has many implications on the formation and evolution of the LG. BR argued that most likely "all of the LG dwarf galaxies have had loosely bound HI envelopes" and that some stripping mechanism removed the gas for galaxies closer than 250 kpc from the Milky Way (MW) or M31, consequently stopping any ongoing star formation (see Grebel 1998). This scenario is consistent with numerical simulations of galactic formation in a cold dark matter cosmogony that predict many more galactic halos than what is currently observed (Navarro, Frenk, & White 1996). A large number of substructures may also reside in the halo of the MW but most of them must have failed to form stars thus avoiding detection (Moore et al. 1999). According to BR, these halo substructures may harbor the HI clouds known as High Velocity Clouds (HVCs).

Murali (2000) noted that ram pressure stripping might not be as important as what one might think. The author revised the density of the gas present in the galactic halo to a value of $n_h < 10^{-5}$ cm^{-3} at a distance of 50 kpc, a factor of 10 lower than previously estimated. This led to the conclusion that tidal forces dominate over ram pressure, at least in the case of the Magellanic Stream. Though the implication for dwarf spheroidals is not that clear, the same kind of influence could be present.

Recent simulations showed that the gas removal occuring in a Blue Compact Dwarf galaxy by its starburst phase — resulting in a galactic wind — may also not be as devastating as previously thought (D'Ercole & Brighenti 1999). It is known that the winds from massive stars, combined with the effects of type II supernovae (SNe) release an energy in the interstellar medium (ISM) that is greater than the binding energy of the gas to the galaxy and could therefore remove a large quantity of it (Larson 1974). But the simulations showed that, after a time of about 100 Myr after the starburst, a large fraction of the ISM falls back on the galaxy. Of course, these simulations consider a single isolated galaxy, free of tidal interactions with its neighbours. In the case of dSph those tidal forces could hold the gas and prevent it from falling back towards the galaxy.

Other recent evidence showed that the star formation history (SFH) of some dSph in the LG is more complicated than what was supposed earlier (Hurley-Keller, Mateo, & Grebel 1999; Martínez-Delgado, Gallart, & Aparicio 1999; Grebel 1998). Since there is some star formation going on in these galaxies and since star formation does not efficiently destroy the ISM (Matzner & McKee 2000) it is therefore possible that clouds of hydrogen are still present in the vicinity of dwarfs.

Theoretical and SFH studies, as well as stellar velocity dispersions show that the total mass of these galaxies must be higher than what their luminosity reveals, giving them very high mass to luminosity ratios (Armandroff, Olszewski, & Pryor 1995). This would make the

potential well of the galaxies much deeper and therefore capable of retaining a large quantity of their ISM. Observational evidence does not yet support that claim.

A new mechanism has been proposed by Mashchenko et al. (2002) solving this problem. The ionizing flux escaping from the Milky Way and other large spiral galaxies might prevent hydrogen from being detected in dSph. This flux would keep hydrogen in its ionized state, which is barely detectable at the distances of dSph's — the only known detection in H_α is in Sculptor (Weiner, Vogel, & Williams 2001). But still HI should be found in low mass galaxies but, due to photoionisation, it can be shifted spatially or kinematically from the optical center of the dwarf.

In section 2, HI observations of several dSph and mixed type dIrr/dSph in the LG are presented. Results and comments on each detection are presented in section 3. Finally, a general discussion about HI gas removal can be found in section 4, along with comments on High Velocity Clouds.

3.2 Observations

3.2.1 The Sample

The main goal of this paper is to look for HI clouds in or near dSph and dIrr/dSph galaxies in the LG. BR have already begun this work, suggesting that many of these galaxies should now be considered as gas-rich systems. They found HI clouds, using the Leiden-Dwingeloo HI survey (LDS) near And III, And V, Leo I and Sextans and they confirmed the HI detections of DDO210 and Pegasus (Lo et al. 1993), LGS3 (Hulsbosch & Wakker 1988), Phoenix (Carignan, Demers, & Cote 1991), Sculptor (Carignan et al. 1998) and Tucana (Oosterloo, Da Costa, & Staveley-Smith 1996).

The LDS covers the whole northern sky and reachs a declination of -30°. This makes a perfect complement to the HI Parkes All Sky Survey (HIPASS) which covers all the southern sky up to a declination of +25°[1]. The list of the observed galaxies can be found in Table 3.1.

3.2.2 HIPASS

The HI Parkes All-Sky Survey (HIPASS) is a large blind HI survey covering the whole southern sky with a beam of 15.5′ (Barnes et al. 2001) and a velocity coverage of -1200 to +12700 km s^{-1} in 1024 channels, each 13.2 km s^{-1} wide (Staveley-Smith & et al. 2000). This was done with the Parkes radiotelescope, a 64 m antenna, equiped with a 13-beam receiver. Observation are obtained by scanning regions of 8° along the sky at a rate of 1°/min. Each point in the sky was observed 5 times for a total integration time of 460 s $beam^{-1}$. This gives an rms noise of about 13 mJy $beam^{-1}$.

[1]With the northern extension.

TABLE 3.1 – dSph and transitionnal dIrr/dSph galaxies of the local group. (Mateo 1998, and reference therein)

Name	α_{2000}	δ_{2000}	l	b	Type	Distance (kpc)	$V_{\odot}^{opt}$ (km s^{-1})	$V_{\odot}^{radio}$ (km s^{-1})
Current sample								
Cetus[a]	00 26 11	-11 02.6	101.5	-72.9	dSph	775±50	-	-
Sculptor	01 00 09	-33 42.5	287.5	-83.2	dSph	79±4	108±3	104±1[b]
LGS 3	01 03 53	+21 53.1	126.8	-40.9	dIrr/dSph	810±60	-282±4	-272±6
Phoenix	01 51 06	-44 26.7	272.2	-68.9	dIrr/dSph	445±30	-52±6[c]	-23±2
Fornax	02 39 59	-34 27.0	237.1	-65.7	dSph	138±8	53±3	-
Carina	06 41 37	-50 58.0	260.1	-22.2	dSph	101±5	224±3	-
Antlia	10 04 04	-27 19.8	263.1	+22.3	dIrr/dSph	1235±65	351±15[d]	361±2
Leo I	10 08 27	+12 18.5	226.0	+49.1	dSph	250±30	286±2	-
Sextans	10 13 03	-01 36.9	243.5	+42.3	dSph	86±4	227±3	-
Aquarius[e]	20 46 46	-12 51.0	34.0	-31.3	dIrr/dSph	800±250	-	-137±3
Tucana	22 41 50	-64 25.2	322.9	-47.4	dSph	880±40	-	-
Pegasus	23 28 34	+14 44.8	94.8	-43.5	dIrr/dSph	955±50	-	-182±2
Unobserved objects								
And III	00 35 17	+36 30.5	119.3	-26.2	dSph	760±40	-351±9[f]	-341±6[g]
NGC 185	00 38 58	+48 20.2	120.8	-14.5	dSph/dE3p	620±25	-210±7	-204±4
NGC 205	00 40 22	+41 41.4	120.7	-21.1	E5p/dSph-N	815±35	-242±3	-229±5
And I	00 45 43	+38 00.4	121.7	-24.9	dSph	805±40	-	-
And II	01 16 27	+33 25.7	128.9	-29.2	dSph	525±110	-	-
Leo II	11 12 29	+22 09.2	220.2	+67.2	dSph	205±12	76±2	-
Ursa Minor	15 09 11	+67 12.9	105.0	+44.8	dSph	66±3	-248±2	-
Draco	17 20 19	+57 54.8	86.4	+34.7	dSph	82±6	-293±2	-
Sagittarius	18 55 03	-30 28.7	5.6	-14.1	dSph-N	24±2	140±5	-

[a]See Whiting et al. (1999)
[b]Given in Bouchard et al. (2002, see Chapter 4)
[c]Given in Gallart et al. (2001)
[d]Given in Tolstoy & Irwin (2000)
[e]Also called DDO210
[f]Given in Côté et al. (2000)
[g]Given in Blitz & Robishaw (2000)

3.2.3 Parkes Narrowband System

The Parkes narrowband system is a high spectral-resolution alternative to the normal multibeam setting, used in HIPASS observations. It has a total bandwidth of 8 MHz splitted in 2048 channels and to 2 orthogonal linear polarisations (XX and YY).

The data have been reduced with the Livedata reduction package distributed with the AIPS++ software. The cube was formed using $4' \times 4' \times 0.82$ km s^{-1} pixels. Frequency switching mode and heliocentric velocity frame were used. The data have a resolution (FWHM) of $15.5'$ spatially and 1.12 km s^{-1} on the spectral axis. The RMS noise is 20 mJy.

The data were affected by parasite radiation which resulted in low-level ripples with a period of a few MHz. These were removed using two methods. Firstly, nearby regions with no HI emission were identified. Spectra from these regions were used as a template baseline for regions with HI emission. Secondly, parabolic baselines were fit to the residual data.

3.3 Results

We now present the results of our systematic HI search around dSph and dIrr/dSph galaxies. These results are presented in Figure 3.1 where the HI distribution maps and the spectra for clouds found are shown. In Table 3.2 is compiled quantitative information about the clouds that were analysed.

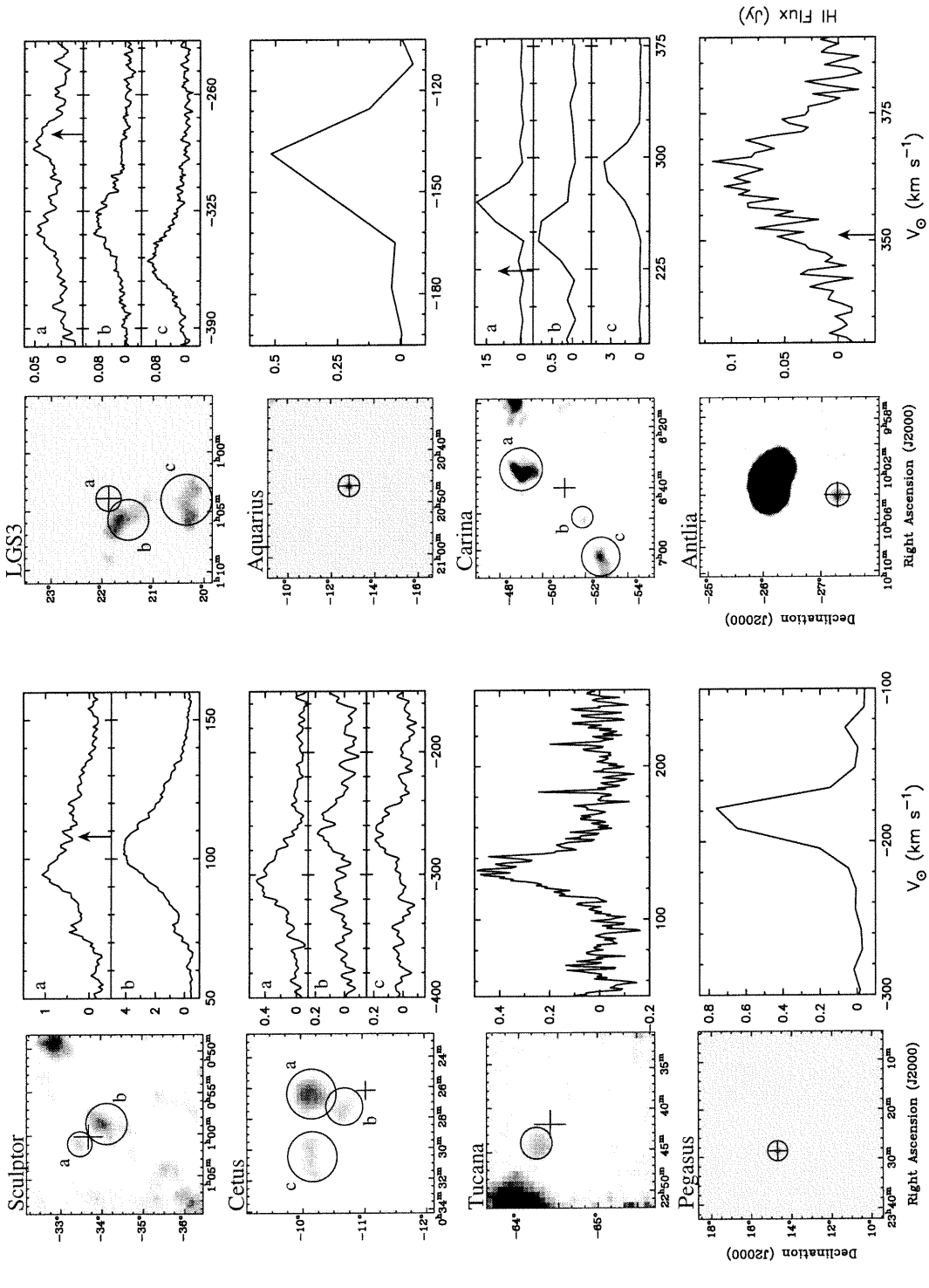

FIGURE 3.1 – Velocity-integrated maps for a large region surrounding dSph and dIrr/dSph galaxies. The crosses mark the position of the optical center of the dwarfs and each investigated cloud has been circled. If more than one cloud can be found near the center of the galaxy, a letter is given for easy reference. On the side of each moment map, the integrated spectra of circled clouds are shown. An arrow marks the position of the optical velocity in the spectra when it is known.

3.3.1 Sculptor

Two clouds of HI were previously detected in the field of Sculptor and are believed to be bound to the galaxy (Carignan et al. 1998). Newly acquired observations presented here and in Bouchard et al. (2002, in prep.) showed that 88% of the HI is contained inside the optical radius of the galaxy. The very close agreement between the optical and the HI radial velocity fields also supports the hypothesis that the clouds are physicaly linked to the dwarf.

The Magellanic Stream lies in the same general direction as Sculptor but has a radial velocity of ~ -60 km s^{-1} (Mathewson & Ford 1984a). It is therefore highly improbable that the Sculptor clouds belong to that structure. The other most plausible alternative to physical association — the clouds beeing HVCs — will be discussed in section 4.3.

3.3.2 Cetus

Recently discovered (Whiting, Hau, & Irwin 1999), the Cetus dwarf is the latest addition to the LG. It is classified as a dSph system because of its similarities to all the other known dSph, Tucana in particular. The 2 galaxies have roughly the same absolute magnitude and they are, strangely for dSph, isolated systems.

The star-formation history analysis reveals no obvious recent star formation in this galaxy (Sarajedini et al. 2002). But as for the other dSphs of the LG, one can assume that it is not a single, short burst that shaped the galaxy. Cetus is affected by the second-parameter effect, probably linked with age, and makes Cetus younger than what was expected. It was noted by Whiting et al. (1999) that because this galaxy does not seem to have any ongoing star formation, one would unlikely find HI within the galaxy. They have also reported a tidal radius of $\sim 5'$ and the clouds are situated well outside of it. The three clouds are situated less than 1.5° (a projected distance of 20 kpc) away from the dwarf and cloud b) seems to be ejected from the center. This recalls the case of Sculptor Cloud b) that also seemed to be ejected with a trailing arm that points toward the center of the galaxy (Bouchard et al. 2002, in prep.). This situation could be a sign of tidal or ram pressure stripping.

Alone, this is not sufficient evidence to prove beyond any doubt that the clouds belong to the Cetus system. No definite statement can and should be made before optical velocities are obtained for the stars in Cetus. But, assuming that the HI clouds do belong to the galaxy and if we look at the velocities of the clouds (-311, -262 and -268 km s^{-1}), the optical velocity of Cetus must be in the range of -280 ± 40 km s^{-1}. This velocity would be very similar to that of the two closest LG members WLM and IC1613.

3.3.3 Tucana

Oosterloo et al. (1996) were the first to report a reservoir of $1.5\times\ 10^6$ M$_\odot$ of HI near Tucana but they beleived it to be associated with the Magellanic Stream. They used the Australia Telescope Compact Array (ATCA) and, as would have been the case with any other aperture

synthesis array, the HI mass of this large structure was underestimated. Our observation of the Tucana dwarf, using a single dish telescope, is therefore much more precise and gives a mass of $M_{HI} = 1.79 \pm 0.15 \times 10^6$ $M_\odot$. We can conclude that 20% of the HI resides in structure inaccessible to the array.

3.3.4 LGS 3

Some previous HI observations had already shown that LGS 3 is a gas rich galaxy (Lo et al. 1993). We comfirm that there is an HI cloud at the same position and velocity as the optical galaxy. Figure 3.1 shows 2 other clouds that might be associated with LGS 3. These clouds were not discussed by Lo et al. (1993) and do not appear in their spectra but were presented earlier by Hulsbosch & Wakker (1988). They are spatially close to the galaxy but at sightly different velocities. The cloud centered on LGS 3 (Cloud a) shows a blueshifted feature that is probably an overlap from Cloud b.

A careful analysis of the HI distribution map shows that Clouds b and c are related to each other by some faint link. The shape of the clouds also suggests that they are in physical association with the galaxy. According to the theory proposed by Mashchenko et al. (2002), the case of LGS 3 might be very interesting. The angle to M31 is 12° from the vertical at a distance of approximately 275 kpc. This places Clouds b and c on the opposite side of the dwarf, as would be expected if the ionising flux from M31 affected the ISM of LGS 3.

3.3.5 Carina

Despite previous attempts (e.g. Mould et al. 1990), no HI has ever been reported in the vicinity of Carina. We used the HIPASS survey to search for HI near the dwarf. Higher resolution data is not available for this galaxy. Nevertheless, we found 3 clouds in the vicinity of Carina but they are situated far from the optical center of the dwarf.

Majewski et al. (2000) have observed the Carina dwarf in search of a tidal break in the distribution of the stars. They found a departure from a King profile at a radial distance of $20'$ but the stellar density profile continues to fall off more gradually up to a radius of $80'$. According to the model by Johnston et al. (1999), objects beyond this break are unbound to the galaxy and should be considered as extratidal. Unfortunately, they were unable to complete the spectroscopic study needed to determine any rotation-like motion that would be expected from extratidal debris.

But even if one considers that Carina has an optical radius of $80'$, no HI can be found within the boundaries of the galaxy. The three clouds circled in figure 3.1 are the three closest candidates for HI being related to the dSph. Two of them (Clouds a and b) are situated right at the edge of the $80'$ border and have velocities very close (especially for Cloud b) to the optical velocity of Carina.

3.3.6 Phoenix

The Phoenix galaxy was previously reported as having HI associated with it by St-Germain et al. (1999). At the time, the detection was still hypothetical but recent stellar spectroscopy (Gallart et al. 2001) confirmed the HI detection at -23 km s^{-1}.

We did not try to confirm the detection of HI in Phoenix with HIPASS because the survey has a velocity resolution of 13.2 km s^{-1}, which would have made it very difficult to separate local HI from HI associated with Phoenix.

3.3.7 Pegasus, Aquarius and Antlia

dIrr/dSph galaxies have generaly been named as such because of the presence of HI centered on the optical disks of the galaxies. For that reason these 3 galaxies do not hold many surprises as for the topic of this paper. HI in the three galaxies was previously reported by Lo et al. (1993, for Pegasus and Aquarius) and Barnes et al. (2001, for Antlia). High resolution spectroscopy was not necessary for these objects since the HIPASS detections were very clear and reliable.

However, Parkes narrowband observations have already been conducted on Antlia and NGC 3109 by Barnes & de Blok (2001). This galaxy is probably the most interesting one of the 3 because of its proximity to NGC 3109. Ionising flux coming from the larger companion may have disturbed the ISM of Antlia. Unfortunately, the poor angular resolution and the lack of known optical velocity for Antlia, make it very difficult to draw any conclusion on this phenomenon apart from the fact that the HI mass might be lower than what is expected for that kind of galaxy.

3.3.8 Fornax

The Fornax galaxy is probably one of the most problematic in the LG, at least for HI studies. It has an optical systemic velocity of $V_{\odot} = 53 \pm 3$ km s^{-1}. As can be seen in Figure 3.2, the Milky Way's HI in that general direction is not centered at zero velocity. The shape of the spectrum makes it quite difficult to analyse anything in that region, still having some emission in the range of velocities where Fornax's HI could be found. We are searching for a faint HI feature, not necessarily centered on the dwarf, on top of a very bright background.

We have performed a blind spectral inspection of the data. The cube was split in six equal sections, marked on Figure 3.3, and a spectrum was extracted for each of them. Each spectrum were subtracted from each other and the result is plotted in Figure 3.4.

There is an abrupt change in all the spectra at a velocity of +22 km s^{-1}. This can be attributed to the HI structure of the Milky Way. Only a slight change in that structure is needed to produce a large difference in the spectrum, due to the proximity of this gas. On the other hand, the rest of the spectrum seems to behave in a much smoother way. In all cases, the spectra become flat after $\sim$50 km s^{-1}, a sign that only background HI remains.

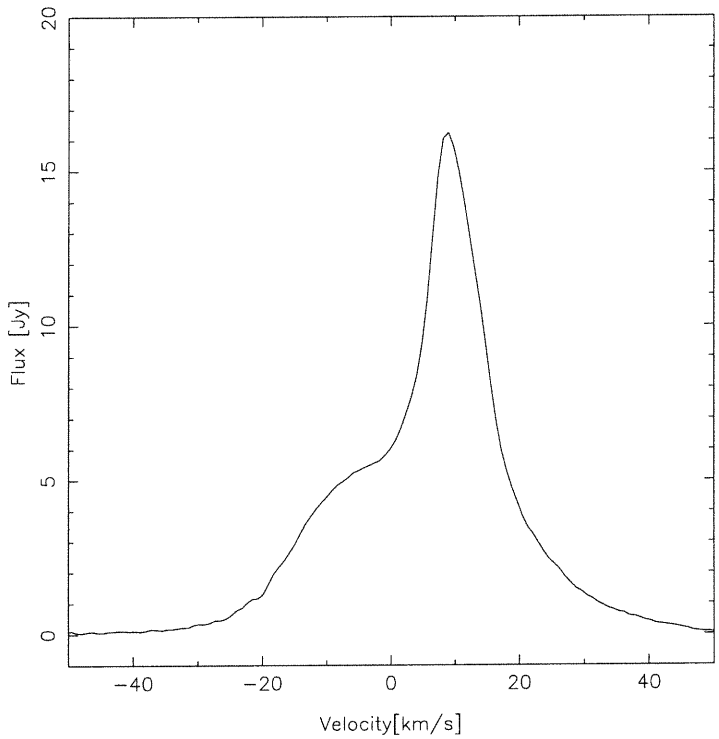

FIGURE 3.2 – The Milky Way's spectrum in the direction of Fornax. It can be seen that the main emission is slightly shifted towards positive velocities which makes it difficult to analyse the Fornax region.

We concluded that there is a distinct cloud superposed on the Milky Way's HI that is kinematically separated from it. This cloud has an HI mass of 1.5×10^5 $M_\odot$ if it is situated at the distance of Fornax. This should be regarded as a lower limit because part of the mass resides below the 22 km s^{-1}mark and is therefore not included in the mass estimate. This mass is very similar to what is found in other dwarf galaxies like Sculptor, Phoenix and LGS3.

3.3.9 Sextans and Leo I

Sextans and Leo I were both reported as having gas associated with them by BR. They argued that the velocity agreement and spatial overlap of the clouds with the galaxies were sufficient evidence to prove that they were associated. The chance of random agreement is around 1.5×10^{-3}. But carefull inspection of the HIPASS cube of the same regions reveals no trace of those clouds.

According to BR, the Leiden-Dwingeloo survey with which the detections were made has a sensitivity of 70 mK. The HIPASS survey is therefore much more sensitive with an rms noise of 10 mK. The initial Sextans detection was of very low significance and it is highly probable that the features reported were artefacts in BR's data.

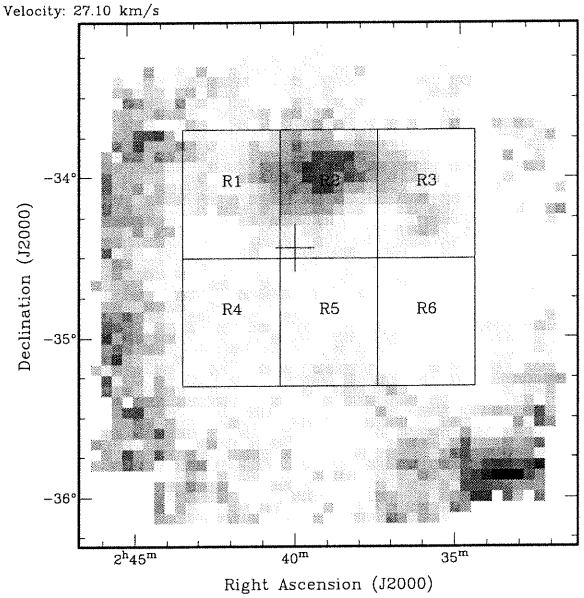

FIGURE 3.3 – One frame of the cube centered on Fornax, taken at a velocity of 27.1 km s^{-1}. The cross marks the position of the dwarf. The boxes show the regions where the spectra were taken (see text for details).

3.4 Analysis

3.4.1 HI Content of dSph and dIrr/dSph Galaxies

HI clouds are found near many dwarfs galaxies in the LG. Although it is not clear whether or not the clouds near dSph are really associated with the dSph's, many of them have been found in their vicinity. The mixed dIrr/dSph type is a little easier. The HI is found closer to their optical centers. The presence (or lack of) HI within a system is the main criteria used to differentiate between these two types of dwarfs. Since many of these galaxies show recent SF (Grebel 1998), it should not be surprising to find substantial amounts of HI close to them.

BR had several non-detections. Among those, only one, Antlia, was on our target list. It is now clear that Antlia has HI associated with it. So the list of non-detections in the LG, after being augmented by the two false detections made by BR (i.e. Sextans and Leo I), consists of 9 galaxies. And I, And II, And VII, Leo I, Leo II, Ursa Minor, Draco, Sagittarius and Sextans are now the only members of the LG where no HI has been found near their optical centers. Among those, Leo I and Leo II are very interesting cases. Despite the fact that they are quite far from the Milky Way, (e.g. further away than Sculptor), no HI is found in their vicinity. They are at comparable distances but have different masses and luminosities. Whatever phenomenon was involved in the ISM removal, it is likely to be linked mainly with enviromental factors that would be the same in both cases. For And I, And II and And VII, the proximity to Andromeda is probably the major factor influencing the absence of HI .

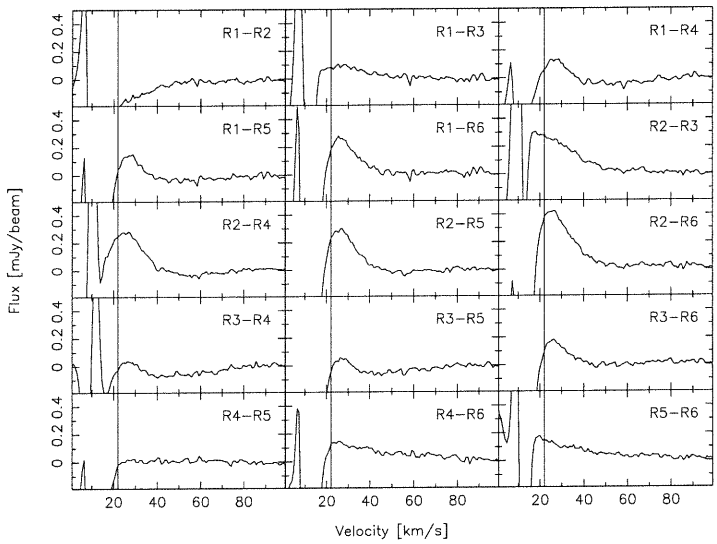

FIGURE 3.4 – Spectra taken from the Fornax region. See text for details.

Similarly, Ursa Minor, Draco and Sextans are all at less than 100 kpc from the Milky Way. Finally, the case of Sagittarius is quite different, being in direct interaction with the Galaxy.

3.4.2 Tidal Interaction, Ram Pressure and Ionizing Flux

Different mechanisms have been proposed to remove gas from dSph galaxies. The most often mentionned are tidal interactions with the more massive members of the LG and ram pressure from the IGM. From their locations, dSph's are often inside the gravitational field of a larger companion that can produce tidal features. It is well known that stars inside small galaxies or globular clusters are affected by such mechanisms (e.g. Mateo et al. 1998). Sculptor shows an interesting shape. Having one cloud on one side and the other cloud on the other side, while both of them are aligned with the proper motion, the shape could be attributed to tidal stretching. But the optical photometry and star counts show that the galaxy is aligned in the opposite way, which makes this explanation unlikely. Other dwarfs do not show any elongated shape which might be the sign of tidal stripping. We therefore believe that this phenomenon does not play a significant role in the gas removal from dSph galaxies.

Ram pressure could in principle be very devastating for any dSph in the vicinity of a large spiral. If its orbit leads it deep into the halo (or even the disk) such that the low density ISM of the halo comes in contact with the ISM of the dwarf, this could remove the gas from the low mass galaxy. The shape of Cetus, Tucana and LGS 3 is what could be associated with ram pressure but because we have no idea of the direction and magnitude of the proper motion, we cannot say if ram pressure actually plays an important role or not. Strangely, these 3 galaxies are 3 of the most isolated galaxies of our sample and the most distant from MW where HI was found to be off-centered with respect to their optical cores. This is exactly the situation

TABLE 3.2 – HI Clouds information

Cloud	L_V ($\times 10^6$ $L_\odot$)	Distance (kpc)	M_{HI} ($\times 10^6$ $M_\odot$)	$V_\odot^{HI}$ (km s^{-1})	$P_{association}$ [a] %	HVC density (deg^2 km s^{-1})$^{-1}$
Sculptor a	2.15	79±4	0.041±0.002	100±1	0.3	0.0022
Sculptor b	2.15	79±4	0.193±0.003	105.1±0.3	0.3	0.0022
Cetus a	0.84	775±50	2.7±0.1	−311±3	† 27.9	0.0018
Cetus b	0.84	775±50	0.74±0.08	−262±9	† 9.0	0.0018
Cetus c	0.84	775±50	0.95±0.07	−268±5	† 55.5	0.0018
Phoenix	0.90	445±30	0.19±0.01	−23±1	...	0.0004
Fornax	15.5	138±8	0.146±0.004	29±1	† 12.3	0.0015
Tucana	0.55	880±40	1.8±0.1	132±5	† 1.3	0.0009
Pegasus	12.0	955±50	5.4±0.2	−186±2	...	...
LGS3 a	1.33	810±60	0.16±0.01	−288±5	...	...
LGS3 b	1.33	810±60	0.50±0.02	−334±1	0.9 [b]	...
LGS3 c	1.33	810±60	0.53±0.02	−361±2	13.6 [b]	...
Aquarius	0.81	800±250	1.8±0.2	−144±3	...	0.0018
Carina a	0.43	101±5	1.04±0.09	265±6	68.5	0.0030
Carina b	0.43	101±5	0.09±0.02	256±15	44.9	0.0030
Carina c	0.43	101±5	0.36±0.02	287±4	99.4	0.0030
Antlia	1.73	1235±65	0.62±0.03	362±1	...	0.00005
Sextans	0.50	86±4	...	...	...	0.0007
LeoI	4.79	250±30	...	...	...	...

[a]When values are noted with a dagger (†) in front, the optical velocity information is either not available or simply not processed, in the case of Fornax. See text for details.

[b]Instead of using a local probability as in the other cases, we used the mean probability over the total extent of the HVC catalog because LGS3 is situated outside of it.

where ram pressure should normally be minimised. In principle these galaxies should be very close to the apastron of their orbits and their spatial motion should therefore be minimal. In addition the IGM density is also very low in those regions.

Sculptor is the only dSph from our sample with a known proper motion (Schweitzer et al. 1995) (others are Ursa Minor: Schweitzer & Cudworth 1996; Ursa Major: Schweitzer, Cudworth, & Majewski 1997; and Draco: Stetson 1980). Ram pressure is unlikely to have a major contribution in the ISM removal because we can see cloud *a* in front of the galaxy, a situation that is hard to explain only with this phenomenon.

According to Mashchenko et al. (2002), ionising flux from the Milky Way can affect the ISM of dwarf galaxies and make the hydrogen undetectable. The radiation escaping the Milky Way scales down by the square of the distance and can be shielded by the disk of dust around the spiral. Figure 3.5 shows a correlation between the hydrogen mass to light ratio and a quantity that is vaguely inversely proportional to the escaping flux from the Milky Way. At low galactic latitude and large distances, we should have a large probability of finding HI in the vicinity. This for now is the most promising theory to explain our results.

We believe Cetus and Tucana to be key galaxies in this debate. As was mentioned by

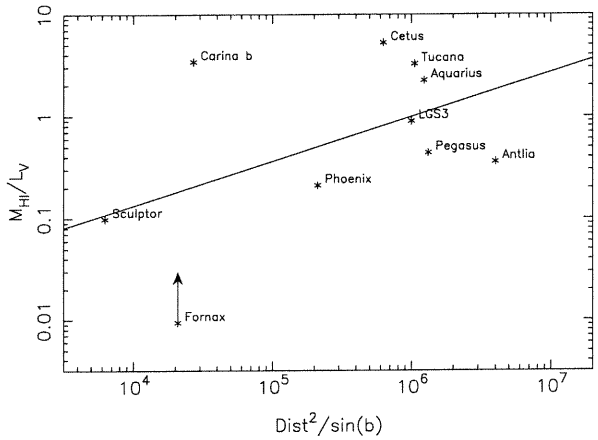

FIGURE 3.5 – The Mass to light ratio as a function of distance above the plane to MW. The value computed is inversely proportional to the quantity of ionising flux from the spiral. The line is a fit through the data.

Whiting et al. (1999), Cetus is a dSph with no apparent ongoing SF. For this reason they did not believe HI would be found within the optical boundary of the system. We found 3 clouds near Cetus in a pattern that is repeated in other dwarfs. Cetus and Tucana are the most isolated dSph of the LG. Thus, ram pressure, tidal forces and ionising flux are all minimised. Yet, as predicted, no HI is found at their center. Galactic wind can remove HI which could fall back after some time when the phenomenon scales down. We can see, from Figure 3.5 that both galaxies are those with the most HI associated with them with respect to their luminosity even if the gas is off-centered.

Finally, the case of Carina again requires our attention. All three clouds are situated outside the tidal radius of 80′. We believe that cloud *c* is not associated with Carina. It must be a member of the HI complex that can be partly seen in the HI distribution map because it is at a very large distance from the galaxy and has a radial velocity more than 60 km s^{-1} larger than that of Carina. Cloud *a* could also be ruled out even if it is directly at the edge of the tidal break radius. If we believe the ionising flux scenario, it is much too massive for a galaxy situated at the position of Carina.

3.4.3 HVCs

Some of the clouds presented in this paper are also listed in the High Velocity Cloud (HVC) catalog of Putman et al. (2002). The origin of HVCs is not known yet but many speculate on their galactic origin. The HVC catalog lists 1997 HI clouds that do not fit simple galactic rotation models. Among these objects, 8 of our 12 clouds that could have been found by this survey (-500 km s^{-1} < V_{LSR} < +500 km s^{-1}, $|V_{LSR}|$ > 90 km s^{-1} and $\delta < +2°$) are actually listed. It is interesting to note that the dIrr/dSph type galaxies Pegasus and Antlia are not listed in the catalog among the 40 galaxies that have an entry (both Sculptor clouds

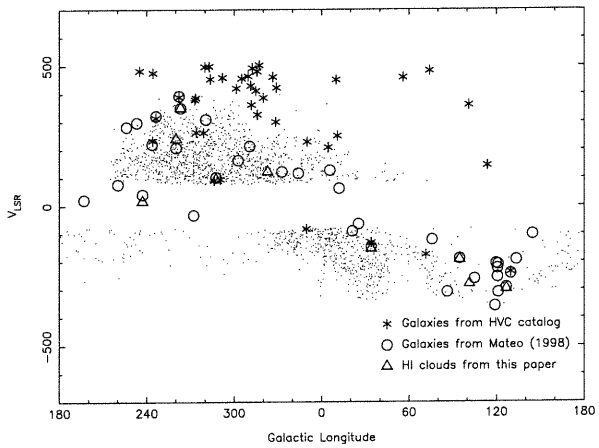

FIGURE 3.6 – The distribution of velocities of LG objects as a function of Milky Way galactic longitude. The dots represents the HVCs from the HVC catalog by Putman et al. (2002). The star symbols are the galaxies listed in the same catalog. Circles are LG galaxies (Mateo 1998) and triangles are the galaxies listed in this paper.

are marked as belonging to the Sculptor dSph galaxy).

The HVCs cover about 19% of the southern sky and can be found in the same range of velocities as the dwarf galaxies in the LG. Figure 3.6 shows the kinematic distribution of HVCs across the sky. The sinusoidal shape of the diagram is caused by galactic rotation and the gap near $V_{LSR} = 0$ km s^{-1} comes from the limits imposed on the catalog. In the figure, the stars represent galaxies that were listed in the HVC catalog. They have a distribution that is systematicaly redshifted. Inspection of the catalog reveals that most of them do not belong to the LG. The circles represents all the LG galaxies (Mateo 1998). They have a different distribution from that of HVC/galaxies but very similar to HVCs (dots) or our sample (triangles).

For each galaxy we observed, we scanned the HVC catalog for clouds near (spatially and kinematicaly) the target galaxies ($R < 10°$ and V inside $V_{gal} \pm 100$ km s^{-1}, or up to the limits of the catalog). We used these entries to compute a local probability that at least one of these N randomly distributed HVCs be situated at the position or closer (both spectroscopically and kinematically) than the clouds we assume associated with the dwarfs. This assumes that the HVCs are uncorrelated and distributed uniformly within the limits of our search. It is also based on angular distance rather than on actual distance, the latter being unknown, so we have to be carefull in the interpretation of these results. The probability is given by:

$$P = 1 - \left[1 - \left(\frac{R_1}{R_0}\right)^2 \frac{2\,\Delta V_1}{\Delta V_0}\right]^N . \tag{3.1}$$

The results are given in Table 3.2. When the optical velocity of the dwarf is unavailable, the value of $\frac{2\,\Delta V_1}{\Delta V_0}$ is considered equal to 1 and no constraints on velocity are applied when counting

the clouds near the galaxy. No values are listed for HI clouds that are directly superposed on the galaxies as this number would not be of any relevance.

The galaxies where HI clouds have been found *near* them but not *in* them are: Sculptor, Cetus, Fornax, Tucana, LGS 3, and Carina. The probability of having an HVC at the position or closer for Sculptor and Tucana is very low. For Sculptor, the probability can still be lowered if we consider the fact that 2 clouds are present near the galaxy. For Tucana, the probability does not take into account the optical velocity information because it is at this time unavailable. Despite this fact, the probability is very low and velocity information — if relatively close to that of the cloud — would not drastically alter the probability. We are therefore very confident that these clouds are associated with the corresponding dSph.

LGS 3 is situated outside of the boundaries of the catalog so the value listed in Table 3.2 is based on an average probability. For LGS3 b, the probability of a random association with an HVC is lower than 1%, meaning that this association as a good chance of being genuine. As we noted previously, the 2 clouds (LGS3 *b* and *c*) seem to be related to each other. LGS3 c as a probability of random association of 13.6%; even if this value is high, it should be regarded in relation to the other cloud. Equation 4.1 assumes that all clouds are uncorrelated and this is exactly a situation where the premises are false.

For Fornax, the velocity information was not processed because the optical velocity of the galaxy places it almost at the center of the velocity gap of the catalog and the HVC counts would therefore be unreliable. But even without velocity information, the chance of random association is still quite low (12.3%) but not low enough to rule out the HVC hypothesis.

Cetus is one of the weak cases. Except for cloud *b*, the evidences are that these clouds do not belong to the galaxy. Cloud *b* has a probability of random association of 9% but seems to be ejected out of the dwarf in the direction of cloud *c*. However, these probablities have been computed without any knowledge of radial velocity. If, as was stated in section 3.2, the optical velocity of Cetus happens to be -280 ± 40 km s^{-1} the probabilities for all clouds could go down to below 10%. But, even if the optical velocity does fall inside this range, further knowledge of the gas removal mechanism will probably be required in order to comfirm the cloud association beyond doubt.

The weakest case is that of Carina. Random HVC association will appear in more than 40% of the cases for any clouds. Chances are good that Carina is completely devoid of HI . This has major consequences on the ability we have to explain its SFH. Hurley-Keller, Mateo, & Nemec (1998) reported 3 distinct episodes of star formation with a quiescent period of $\sim$4 Gyr. The last of these episodes was around 2.5 to 3.5 Gyr ago. Yet there seems to be no gas which could have fueled this SFH. The mechanisms by which the gas could be removed must take these greatly disturbing facts into account. HI in Carina can disappear for a long period of time and then reappear to trigger SF. Carina b, if at the distance of Carina, would have a mass in the range expected for dSph's but is situated far from it (1.8°, projected distance of 3.2 kpc). Although it is not clear how this gas could fall back on the galaxy, it is quite easy

to figure out how it could have been expelled to that distance.

Simple kinematical studies cannot fully differentiate between the distribution of galaxies and that of HVCs inside the LG. We therefore think that kinematical arguments should be used with caution when discussing dSph and HI cloud associations because of the systematic confusion that will emerge from such correlations. It appears that dwarf galaxies from our sample are all situated in regions where the HVC density is much higher (sometimes up to a factor of 30) than that of the average density of the HVC distribution ($\sim$0.0001 (deg^2 km s^{-1})$^{-1}$). The only exception is Antlia, that is a fairly isolated system. The only conclusion that can be drawn from Figure 3.6 and Table 3.2 is that our cloud distribution is not different from that of LG galaxies and therefore is not outside the LG or taking part in galactic rotation.

It is our belief that the problem of cloud association and SFH cannot be resolved with these kinds of kinematical studies without further knowledge of the galactic formation mechanisms. Although velocity information can give many constraints on the probability of random association between HVCs and dSph galaxies, this probability remains to high in too many cases.

3.5 Conclusion

The Parkes single-dish radiotelescope was used to conduct a survey of the dSph and dIrr/dSph galaxies of the LG. HIPASS and follow-up narrowband observations enabled us to arrive at the following conclusions:

1. Most of the dSph and dIrr/dSph galaxies of the LG contain large amounts of HI , often off-centered with respect to the optical center of the galaxy.
2. There are several mechanisms to remove the gas from the center of the dwarf. The most often discussed are tidal forces applied by near spirals and ram pressure due to IGM. Both have been discarded has they seem unlikely when considering the total knowledge we have of these systems. A third mechanism, ionising flux escaping neighouring galaxies, is more promising. It helps to solve the problem of episodic SF because it does not have to remove the hydrogen from within the boundaries of the dwarfs but rather keeps it in an ionized and undetectable state. The gas can therefore be de-ionized and can collapse to trigger new episodes of SF.
3. A probability analysis has been conducted on whether or not the clouds could have randomly been situated at the position of the clouds we found, based on the local density of HVCs. The results range from 0.3% for Sculptor to over 99% for Carina. This means that the Sculptor clouds are, in all probability, part of the Sculptor system, while others are less certain. In any case, 11 out of the 16 investigated clouds have a probability of being a randomly distributed HVC that is below 15%.

4. All LG dSph and dIrr/dSph galaxies of the southern hemisphere (except Antlia) are situated in regions where the HVC density is above average.

We are grateful to the HIPASS team for giving us access to the survey data files and to David Barnes for providing high resolution data on the Antlia dwarf galaxy. AB would also like to thank Mark Calabretta for the much appreciated help during data reduction.

References

Armandroff, T. E., Olszewski, E. W., & Pryor, C. 1995, AJ, 110, 2131

Barnes, D. G. & de Blok, W. J. G. 2001, AJ, 122, 825

Barnes, D. G., Staveley-Smnith, L., de Blok, W. J. G., Oosterloo, T., Stewart, I. M., Wright, A. E., Banks, G. D., Bhathal, R., Boyce, P. J., Calabretta, M. R., Disney, M. J., Drinkwater, M. J., Ekers, R. D., Freeman, K. C., Gibson, B. K., Green, A. J., Haynes, R. F., te Lintel Hekkert, P., Henning, P. A., Jerjen, H., Juraszek, S., Kesteven, M. J., Kilborn, V. A., Knezek, P. M., Koribalski, B., Kraan-Korteweg, R. C., Malin, D. F., Marquarding, M., Minchin, R. F., Mould, J. R., Price, R. M., Putman, M. E., Ryder, S. D., Sadler, E. M., Schröder, A., Stootman, F., Webster, R. L., Wilson, W. E., & Ye, T. 2001, MNRAS, 322, 486

Blitz, L. & Robishaw, T. 2000, ApJ, 541, 675

Bouchard, A., Carignan, C., & Mashchenko, S. 2002 Submitted to AJ

Côté, P., Mateo, M., Sargent, W. L. W., & Olszewski, E. W. 2000, ApJ, 537, L91

Carignan, C., Beaulieu, S., Côté, S. ., Demers, S., & Mateo, M. 1998, AJ, 116, 1690

Carignan, C., Demers, S., & Cote, S. 1991, ApJ, 381, L13

D'Ercole, A. & Brighenti, F. 1999, MNRAS, 309, 941

Gallart, C., Martínez-Delgado, D., Gómez-Flechoso, M. A., & Mateo, M. 2001, AJ, 121, 2572

Grebel, E. K. 1998, Highlights in Astronomy, 11, 125

Hulsbosch, A. N. M. & Wakker, B. P. 1988, A&AS, 75, 191

Hurley-Keller, D., Mateo, M., & Grebel, E. K. 1999, ApJ, 523, L25

Hurley-Keller, D., Mateo, M., & Nemec, J. 1998, AJ, 115, 1840

Johnston, K. V., Sigurdsson, S., & Hernquist, L. 1999, MNRAS, 302, 771

Larson, R. B. 1974, MNRAS, 169, 229

Lo, K. Y., Sargent, W. L. W., & Young, K. 1993, AJ, 106, 507

Majewski, S. R., Ostheimer, J. C., Patterson, R. J., Kunkel, W. E., Johnston, K. V., & Geisler, D. 2000, AJ, 119, 760

Martínez-Delgado, D., Gallart, C., & Aparicio, A. 1999, AJ, 118, 862

Mashchenko, S., Carignan, C., & Bouchard, A. 2002, preprint (astro-ph/0203317)

Mateo, M., Olszewski, E. W., & Morrison, H. L. 1998, ApJ, 508, L55

Mateo, M. L. 1998, ARA&A, 36, 435

Mathewson, D. S. & Ford, V. L. 1984, in IAU Symp. 108: Structure and Evolution of the Magellanic Clouds, Vol. 108, 125–136

Matzner, C. D. & McKee, C. F. 2000, ApJ, 545, 364

Moore, B., Ghigna, S., Governato, F., Lake, G., Quinn, T., Stadel, J., & Tozzi, P. 1999, ApJ, 524, L19

Mould, J. R., Bothun, G. D., Hall, P. J., Staveley-Smith, L., & Wright, A. E. 1990, ApJ, 362, L55

Murali, C. 2000, ApJ, 529, L81

Navarro, J. F., Frenk, C. S., & White, S. D. M. 1996, ApJ, 462, 563

Oosterloo, T., Da Costa, G. S., & Staveley-Smith, L. 1996, AJ, 112, 1969

Putman, M. E., de Heij, V., Staveley-Smith, L., Braun, R., Freeman, K. C., Gibson, B. K., Burton, W. B., Barnes, D. G., Banks, G. D., Bhathal, R., de Blok, W. J. G., Boyce, P. J., Disney, M. J., Drinkwater, M. J., Ekers, R. D., Henning, P. A., Jerjen, H., Kilborn, V. A., Knezek, P. M., Koribalski, B., Malin, D. F., Marquarding, M., Minchin, R. F., Mould, J. R., Oosterloo, T., Price, R. M., Ryder, S. D., Sadler, E. M., Stewart, I., Stootman, F., Webster, R. L., & Wright, A. E. 2002, AJ, 123, 873

Sarajedini, A., Grebel, E. K., Dolphin, A. E., Seitzer, P., Geisler, D., Guhathakurta, P., Hodge, P. W., Karachentsev, I. D., Karachentseva, V. E., & Sharina, M. E. 2002, ApJ, 567, 915

Schweitzer, A. E. & Cudworth, K. M. 1996, in American Astronomical Society Meeting, Vol. 188, 0901

Schweitzer, A. E., Cudworth, K. M., & Majewski, S. R. 1997, in ASP Conf. Ser. 127: Proper Motions and Galactic Astronomy, 103

Schweitzer, A. E., Cudworth, K. M., Majewski, S. R., & Suntzeff, N. B. 1995, AJ, 110, 2747

St-Germain, J., Carignan, C., Côte, S. ., & Oosterloo, T. 1999, AJ, 118, 1235

Staveley-Smith, L. & et al. 2000, in ASP Conf. Ser. 217: Imaging at Radio through Submillimeter Wavelengths, 50

Stetson, P. B. 1980, AJ, 85, 387

Tolstoy, E. & Irwin, M. 2000, MNRAS, 318, 1241

Weiner, B. J., Vogel, S. N., & Williams, T. B. 2001, preprint (astro-ph/0109055)

Whiting, A. B., Hau, G. K. T., & Irwin, M. 1999, AJ, 118, 2767

Young, L. M. & Lo, K. Y. 1997, ApJ, 476, 127

Zaritsky, D. 1999, in ASP Conf. Ser. 165: The Third Stromlo Symposium: The Galactic Halo, 34

Chapitre 4

L'environnement HI de la naine sphéroïdale Sculptor

Cet article présente, chronologiquement, les premières données que j'ai eu à traiter durant ma maîtrise. Claude Carignan s'était rendu en Australie pour la première série d'observations de cette recherche. Il s'agit des données qui ont été récoltées au Australia Telescope Compact Array. Je les ai ensuite réduites et analysées. Nous nous sommes rapidement rendus compte que puisque ces données provenaient d'un interféromètre, les estimés de masses seraient probablement moins précis que si les données avaient été prises sur un télescope à simple antenne. Je me suis alors rendu en Australie pour la deuxième série d'observations. Ces dernières ayant leurs propres défauts, les deux séries sont donc présentées.

Sergey Mashchenko m'a beaucoup aidé pour cet article. Il est l'auteur d'une partie de l'introduction et de la partie qui traite de l'ionisation du milieu interstellaire de Sculptor par la radiation s'échappant de la Voie Lactée. C'est également lui qui a rédigé la conclusion et le sommaire de l'article.

The HI environment of the Sculptor dwarf spheroidal galaxy

Antoine Bouchard
Département de physique and Observatoire du mont Mégantic, Université de Montréal, C.P. 6128, Succ. Centre-ville, Montréal, Québec, Canada H3C 3J7, and
Australia Telescope National Facility, PO Box 76, Epping, NSW 1710, Australia
e–mail: [redacted]

Claude Carignan
Département de physique and Observatoire du mont Mégantic, Université de Montréal, C.P. 6128, Succ. Centre-ville, Montréal, Québec, Canada H3C 3J7
e–mail: [redacted]

and

Sergey Mashchenko
Département de physique and Observatoire du mont Mégantic, Université de Montréal, C.P. 6128, Succ. Centre-ville, Montréal, Québec, Canada H3C 3J7
e–mail: [redacted]

Submitted to Astronomical Journal, September 11, 2002.

New observations of the neutral hydrogen (HI) in the vicinity of the Sculptor dwarf are presented. The data obtained with the single-dish Parkes telescope cover a large area of $7^\circ \times 7^\circ$ around the dwarf, and have a resolution of $15\farcm5 \times 1.12$ km s^{-1}. The Australia Telescope Compact Array was used to map a smaller area of $2\fdg2 \times 2\fdg2$ centered on the dwarf with a higher resolution ($350'' \times 140'' \times 1.65$ km s^{-1}). Some 10 HI structures having velocities outside the range of the normal Galactic disk velocities were detected, including the two Sculptor clouds (northeast and southwest) of Carignan et al. (1998). The present study shows the total extent of the Sculptor clouds. Based on the Parkes data, the mass and the radial velocity of the SW cloud was found to be $(1.93 \pm 0.02) \times 10^5$ M$_\odot$ and 105.1 ± 0.3 km s^{-1}, respectively. The corresponding values for the NE cloud are $(0.41 \pm 0.02) \times 10^5$ M$_\odot$ and 100.2 ± 0.9 km s^{-1}. The total mass for the both clouds is $(2.34 \pm 0.03) \times 10^5$ M$_\odot$, and the velocity is 104.1 ± 0.4 km s^{-1}. (The masses are estimated for the assumed distance of 79 kpc.) Three different hypotheses concerning the association of the Sculptor clouds were considered. The case for the clouds belonging to the Sculptor group of galaxies is found to be inconsistent with the observational data. The probability of the Sculptor clouds to be Galactic HVCs superimposed by chance on Sculptor is estimated to be less than 2%. The third hypothesis assumes that the clouds are physically associated with Sculptor, and is supported by the following evidence: (a) the radial velocities for both clouds are very close to that of Sculptor ($\Delta V = 4 \pm 3$ km s^{-1}), (b) 88% of the total HI flux is contained within the optical disk of the dwarf galaxy, and (c) the clouds are located symmetrically relative to the center of Sculptor. Arguments are presented that the Sculptor clouds are still gravitationally bound to the dwarf galaxy, and are part of its interstellar medium.

4.1 Introduction

Dwarf galaxies are the most numerous type of galaxies in the Universe. Recently, the interest for the lowest luminosity dwarfs has been renewed, both on the observational and on the theoretical sides, in part because these stellar systems have the spatial scale at which the predictions of the presently favored ΛCDM cosmology have the largest discrepancies with observations. Most notably, ΛCDM simulations overpredict the number of low mass galaxies in the Milky Way and M31 halos (Moore et al. 1999). Another difficulty is the cuspy density profile of simulated halos, which is at odds with the almost flat cores observed in the inner few kiloparsecs of disk galaxies (e.g. de Blok et al. 2001).

Low luminosity dwarfs in the Local Group are classified as dwarf irregulars (dIrr), dwarf spheroidals (dSph), or intermediate type dwarfs (dIrr/dSph) (Mateo 1998). dIrr galaxies are gas rich and the HI is often seen in rings surrounding the optical center (SagDIG, Young & Lo 1997b) or bubble like structures (LeoA, Young & Lo 1996) and their complex Star Formation History (SFH) can easily be explained. For dSph galaxies, the data are harder to explain. The ISM is required to support the complex SFH (Grebel 1998) of these objects and until now, very few of them are actualy known to contain HI . This is what led Blitz & Robishaw (2000) to believe "that all of the LG dwarf galaxies have had loosely bound HI envelopes" thus implicitly making a link between High Velocity Clouds, dSph, and dIrr.

In the Local Group, all dwarf galaxies less luminous than $M_V \simeq -15^m$ and located within 250 kpc from a giant spiral (Milky Way or M31) are dSphs. All dIrr galaxies in the same luminosity range are isolated systems. This segregation of the dwarfs into dSphs and dIrrs according to their distance from giant spirals suggests that some (or many) environmental factors are at work. The most popular mechanisms discussed in the literature are total removal of the ISM by either tidal or ram pressure stripping (e.g. Blitz & Robishaw 2000). However, the total ISM removal cannot explain the puzzling situation with many dSphs, which have formed stars in the last 1-2 Gyrs, but have no HI gas around them which could have fueled the star formation.

Mashchenko, Carignan, & Bouchard (2002, hereafter MCB) proposed a possible solution for this puzzle. They showed that far ultraviolet (FUV) flux from spirals like the Milky Way and M31 can be strong enough to keep the ISM of satellite dSphs in a fully photoionized state for prolonged periods of time, and by assuming that many dSphs are massive enough (with the virial temperature $T_{\rm vir} \gtrsim 10^4$ K) to keep the photoionized gas gravitationally bound. Only during relatively short intervals of time, when the dSph moving along its orbit around the host galaxy is crossing the shadow produced by the HI disk of the host, can the ISM recombine and potentially form stars.

Any evidence for a physical association of HI gas with a low luminosity dSph galaxy would be crucial for understanding the factors governing the evolution of these systems. One of the most promising objects in this regard is the Sculptor dSph. Carignan et al. (1998,

TABLE 4.1 – Sculptor dSph physical parameters

Parameter	Value
RA (J2000)	$1^h00^m09\overset{s}{.}4$
DEC (J2000)	$-33°42'33''$
Galactic longitude, l	$287\overset{\circ}{.}53$
Galactic latitude, b	$-83\overset{\circ}{.}16$
Heliocentric distance[a]	79 ± 4 kpc
Isophotal major axis[b], D_{25}	$40'$
Core radius[c], r_c	$5\overset{'}{.}8 \pm 1\overset{'}{.}6$
Tidal radius[c], r_t	$76\overset{'}{.}5 \pm 5\overset{'}{.}0$
Major-axis position angle[c]	$99° \pm 1°$
Optical radial velocity[a], $V_\odot^{opt}$	108 ± 3 km s^{-1}
Proper motion velocity[d], V_{prop}	210 ± 125 km s^{-1}
Proper motion position angle[d]	$40° \pm 24°$

[a]Mateo 1998
[b]de Vaucouleurs et al. 1991
[c]Irwin & Hatzidimitriou 1995
[d]Schweitzer et al. 1995

hereafter C98) detected two HI clouds in the vicinity of the dwarf, which had virtually the same radial velocity as Sculptor. Their observations with a $\sim 0\overset{\circ}{.}5$ beam (FWHM) covered only a small portion of the stellar body of the dwarf with the major axis size of $\sim 2\overset{\circ}{.}5$ (Irwin & Hatzidimitriou 1995), which prevented the authors from giving a conclusive evidence for a physical association of the gas with the dwarf galaxy. New HI observations with a much larger spatial coverage were required to see the full extent of the clouds, and to make sure that these clouds were not Galactic HVCs.

Here we present new observations made with the Australia Telescope Compact Array (ATCA) and the Parkes single-dish telescope covering a large area of $7° \times 7°$ around the Sculptor dwarf. We analyze all HI structures detected in this area, and argue that the new data strengthen the case for the physical association of the Sculptor clouds with the dSph. By combining our new HI data with the data of Weiner, Vogel, & Williams (2001) on H_α emission from the Sculptor clouds, we give evidence in support of the radiation harassment scenario of MCB.

4.2 Observations of HI in the Sculptor dSph

4.2.1 Previous Observations

C98 made two sets of observations. First, they used the Parkes single dish radio-telescope and pointed it directly at the center of the galaxy. They used the PKS1934-638 source as a flux calibrator and they had a velocity resolution of 1.65 km s^{-1}. Their 100 minutes integration on

source resulted in a detection limit of 100 $M_\odot$. The spectrum they obtained revealed $\sim 10^4$ $M_\odot$ of HI, at a velocity of $V_\odot = 112$ km s^{-1}. But the 15′ beam did not cover all the optical extent of Sculptor (which has a tidal radius of $\sim 1.^\circ 3$, see Table 4.1) and it was not large enough to get a complete sampling of what was believed to be the gas associated with the dwarf.

Their second set of observations was done with the ATCA using the array configuration 375 which resulted in a spatial resolution of 240″ and a velocity resolution of 1.65 km s^{-1}. This yielded an HI mass of 3.0×10^4 $M_\odot$, at a velocity of 102 ± 5 km s^{-1}. But inevitable short spacing effects appeared in the data which made the authors believe that they missed a non-negligible fraction of the HI . Moreover a large fraction of the detected HI lay close to the half-power beam width (FWHM= 33′).

4.2.2 New Parkes Data

The 64 m Parkes radio-telescope was used, equipped with a 21 cm multibeam receiver in a narrowband mode. The total bandwidth of 8 MHz was divided in 2048 channels, resulting in a velocity increment of 0.82 km s^{-1} between each channel of the cube. A region of $7^\circ \times 7^\circ$ was mapped around Sculptor at a beam resolution of 15.5′ and a velocity resolution of 1.12 km s^{-1}, using frequency switching observations.

The reduction pipeline provided with the AIPS++ package was used to calibrate the data (task "Livedata") and to grid and form the cube (task "Gridzilla"). Both tasks are part of the standard HIPASS data acquisition system (Barnes et al. 2001). For the bandpass calibration, the data were Hanning smoothed and the median value of the baseline was subtracted.

4.2.3 New ATCA Data

The ATCA is located in Narrabri, Australia. It consists of six 22 meter antennae on an East-West track. This aperture synthesis array was used in the 375 configuration, with baselines ranging from 31 to 459 meters, giving the maximum possible weight to large structures.

The data cube is a 64 pointing mosaic with a resolution of $350'' \times 140'' \times 1.65$ km s^{-1}. The source PKS1934-638 was used as a flux calibrator while PKS0008-421 was the phase calibrator. The Miriad package was used to edit and calibrate the data.

4.2.4 Data Analysis

Figure 4.1 shows a wide field image taken with the Parkes radiotelescope equiped with the narrowband multibeam receiver. The region surrounding Sculptor appears to be heavily populated with HI features. Aside from the Sculptor (NE and SW) clouds, only one HI structure from Figure 4.1 has been previously associated with an optical object — the spiral galaxy NGC 300 from the Sculptor group. Many other features are catalogued as HVCs by Putman et al. (2002). The radial velocities for each feature marked in Figure 4.1 are listed in Table 4.2.

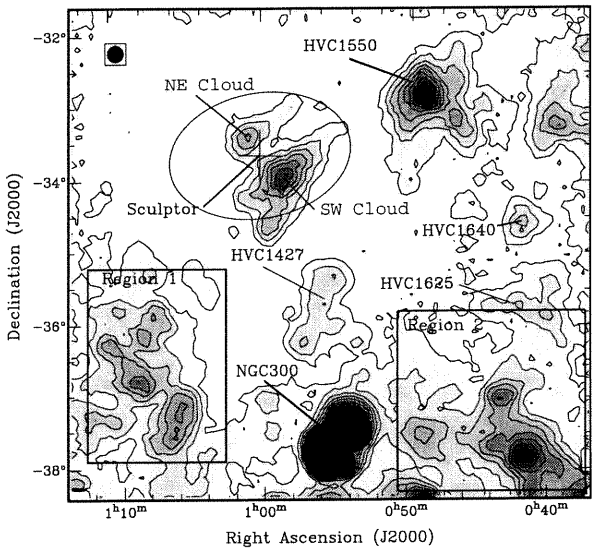

FIGURE 4.1 – Parkes narrowband integrated HI map. The contour levels are (1, 5, 10, 15, ..., 40)$\times 10^{18}$ cm^{-2}. We show the locations of the HVCs from the catalog of Putman et al. (2002), and define two regions of comparable velocities — Region 1 and Region 2. The ellipse shows the optical extent of the Sculptor dSph (Irwin & Hatzidimitriou 1995). The cross marks the location of the optical center of Sculptor.

This study will concentrate on the two HI features closest to the optical center of Sculptor — the NE and SW clouds (see Figure 4.1). A close-up view of the Sculptor clouds is shown in Figure 4.2. This is a higher spatial resolution image taken with the ATCA interferometer. The integrated spectra for the clouds are shown in Figure 4.3. The velocity information extracted from the spectra is summarized in Table 4.3. The table also contains HI mass estimates, based on the assumption that the clouds are located at the distance of Sculptor (79 kpc, see Table 4.1)

Parts of the Sculptor clouds were observed by C98. In our present study, we can see the full extent of the clouds. They have larger sizes and masses (Table 4.3) than those reported by C98, but appear to be almost completely contained within the optical extent of Sculptor (88% of the total flux). The existence of the third (central) cloud of C98 with low detection significance is not confirmed with our new data, which is evident from the spectrum of the central $15' \times 15'$ area shown in Figure 4.3d and the corresponding parameters given in Table 4.3. This central region has a slightly negative integral flux (resulted in a negative mass in Table 4.3). This is caused by an imperfect continuum subtraction performed on the image. The signal does not significantly come out of the noise (Figure 4.3d).

The lack of short spacings in the ATCA data is most obvious in panels b) and c) of Figure 4.3. The 375 configuration of the array used for the observations is not sensitive to scales larger than $\sim 30'$, resulting in the mass of the SW cloud being significantly underestimated

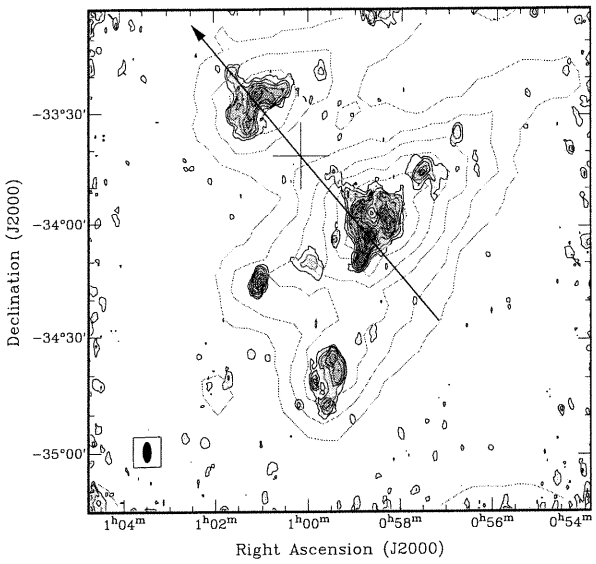

FIGURE 4.2 – ATCA integrated HI (grey-scale image and black contours) overlayed with the Parkes data from Figure 4.1 (grey contours). The contours for the ATCA data have levels (5, 10, 15, ..., 40)$\times 10^{18}$ cm^{-2}. The arrow shows the direction of the proper motion of Sculptor from Schweitzer et al. (1995).

(Table 4.3). The NE cloud with a size $\sim 22'$ has suffered less from this effect.

Figure 4.4 shows a slice along the velocity axis through both the ATCA and the Parkes data sets. The slice passes through the center of Sculptor along the proper motion direction (arrow in Figure 4.2). We clearly see the NE cloud (on the left side) and the SW cloud (on the right side). The cross marks the position of the galactic center and the velocity of the dwarf. It is clear from this figure that both clouds are distributed symmetrically relative to the dwarf's center and have similar velocities, though the velocity of the NE cloud tends to be slightly less than that of the SW cloud.

Velocity information can also be found in Figure 4.5. This velocity map from the Parkes data shows the two main Sculptor clouds and a third one (HVC 1550) close to the dwarf. Figure 4.6 shows the dispersion of the HI gas of the Sculptor surroundings. The maximum dispersion values of every feature identified in Figure 4.1 are listed in Table 4.2.

4.3 Discussion

4.3.1 Physical Association of the Sculptor Clouds

The quality of our present data on the HI distribution near Sculptor gives us an opportunity to address the issue of the physical association of HI gas with a dSph in a more conclusive manner than any previous study. In the past, the attempts to associate nearby HI

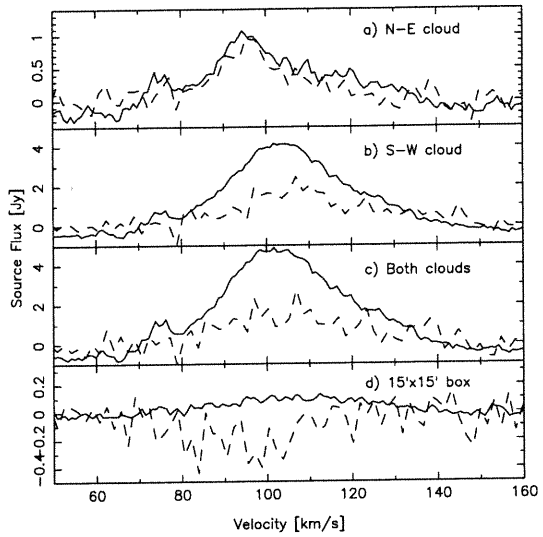

FIGURE 4.3 – Four spectra, taken both from the Parkes (solid line) and ATCA (dashed line) data sets. Panels a) and b) show the spectra integrated over the North-East and South-West clouds, respectively, panel c) shows the total spectrum, and panel d) shows the spectrum for a 15′ by 15′ box centered on the dwarf. The vertical dashed line corresponds to the optical radial velocity of Sculptor.

gas with dSph galaxies have been hampered by some of the following factors: lack of spatial coverage (C98), low angular and velocity resolution (Blitz & Robishaw 2000), and lack of stellar radial velocity information (Oosterloo, Da Costa, & Staveley-Smith 1996). In this study, we achieve both sufficiently large spatial coverage (7° × 7°, with the area covered being 14 times larger than the area of the Sculptor stellar body) and high angular/velocity resolution (5′.8 × 2′.3×1.65 km s^{-1}) by combining the single-dish Parkes with intereferometric ATCA observations. In addition, the stellar radial velocity of Sculptor is known to a high accuracy (Table 4.1).

The location and radial velocity of the NE and SW clouds leave us with only two possible alternatives in regards to the physical association with Sculptor: the case of a larger distance (the clouds belong to the Sculptor group of galaxies), and the case of a smaller distance (the clouds are Galactic HVCs). We will consider both possibilities in turn.

At the distances of the Sculptor group members (1.7 – 4.4 Mpc, Jerjen et al. 1998) the clouds would have very large size ($\sim 25 - 60$ kpc) and total mass ($[1 - 5] \times 10^8$ $M_\odot$). Isolated intergalactic HI clouds of this size are not known. Moreover, the H_α flux of 0.22 R, detected in the densest part of the SW cloud (see Section 4.3.2), is too large to be caused by the metagalactic ionizing radiation background, and is most naturally explained by the impact of the LyC radiation from the Milky Way, implying a small distance to the clouds of $\lesssim 100$ kpc. The clouds also cannot belong to a galaxy located at the distance of the Sculptor group: a gas-rich galaxy of this size would be a disk galaxy, which is at odds with both the irregular shape of the clouds and the absence of a clear rotation signature. We conclude that the Sculptor

TABLE 4.2 – Properties of the HI features around Sculptor

	$V_\odot$ (km s^{-1})	σ_{max} (km s^{-1})
NE cloud (HVC 1321)	100	6.0
SW cloud (HVC 1353)	105	9.9
NGC 300	145	37.6
HVC 1427	135	7.9
HVC 1550	117	11.0
HVC 1625	169	21.5
HVC 1640	175	13.4
Region 1 (broad region)	121	9.0
Region 1 (artifact)	121	21.0
Region 2	40	4.4

TABLE 4.3 – Data on the Sculptor HI clouds

	Parkes		ATCA	
	Velocity (km s^{-1})	HI mass ($\times 10^4 M_\odot$)	Velocity (km s^{-1})	HI mass ($\times 10^4 M_\odot$)
North East	100.2±0.9	4.07±0.18	99.7±1.7	2.84±0.23
South West	105.1±0.3	19.33±0.24	110.2±1.6	8.67±0.68
Central $15' \times 15'$	106.3±0.7	0.61±0.02	...	(-1.13±0.27)[a]
Total	104.1±0.4	23.35±0.32	109.3±2.0	8.68±0.83

[a]See text for details

group hypothesis appears to be inconsistent with the available data.

The second alternative — the SW and NE clouds being HVCs — is more difficult to discard. HVCs are clouds that do not fit a simple galactic rotation model. These clouds are often associated in large HVC complexes that are believed to be of similar origin. One of these complexes, the Magellanic Stream, has many components near Sculptor, but its velocity in this direction, ~ -60 km s^{-1} (Mathewson & Ford 1984b), makes it a very unlikely association.

Not every HVC is part of an HVC complex. What is seen in Figure 4.1 could be independent HVCs which happened to project on Sculptor and have radial velocities very close to the radial velocity of the dwarf. We estimated the probability of such an event in the following manner. We counted the number N of HVCs from the catalog of Putman et al. (2002) located within $R_0 = 10°$ from Sculptor and having heliocentric radial velocities within the interval $V = +80 \cdots + 210$ km s^{-1}: $N = 28$ (excluding the Sculptor clouds). We considered the NE and SW clouds to be one cloud. The center of mass of this cloud is located at the distance $R_1 = 0.°318$ from the Sculptor center, and has a radial velocity of 104 km s^{-1}, resulting in the difference $\Delta V_1 = 4$ km s^{-1} between the stellar and HI velocities. Assuming that locations and radial velocities of the N HVCs are uncorrelated and distributed uniformly within the circle

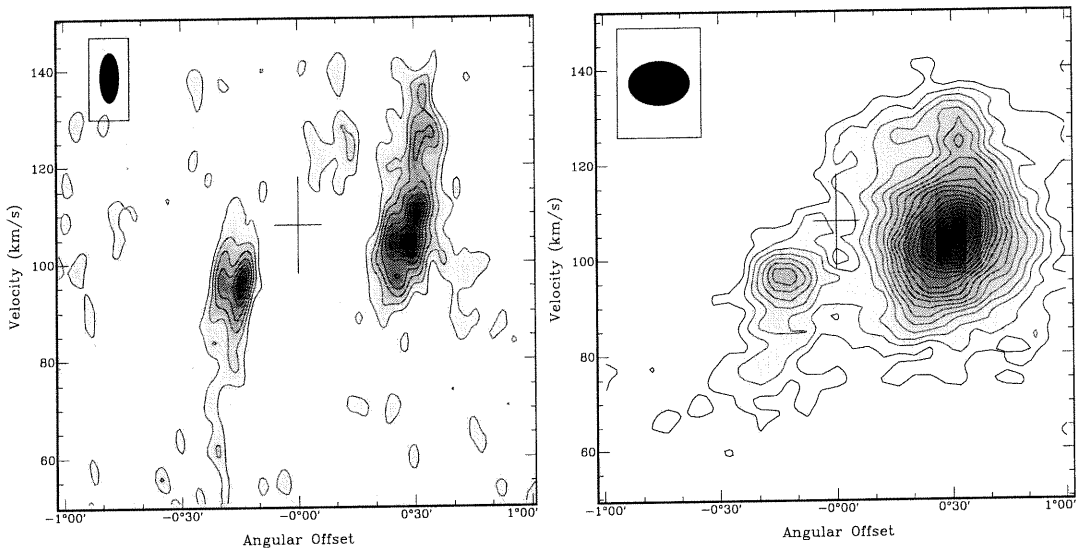

FIGURE 4.4 – A cut through the ATCA (left panel) and Parkes narrowband (right panel) data sets. The slice is 12′ wide in both cubes and is aligned with the galaxy's proper motion (position angle of 40°, see Figure 4.2). The ATCA data have been smoothed in velocity to 11.41 km s^{-1} and have contour levels from 10 to 70 mJy by steps of 10 mJy. The narrowband data are smoothed in velocity to 10.66 km s^{-1} and the levels are from 2.5 to 50 mJy by steps of 2.5 mJy.

with the angular radius R_0 and the velocity interval ΔV_0, the probability P to find *at least one* HVC projected within angular distance R_1 from the center of Sculptor and having radial velocity within ΔV_1 from the velocity of the dwarf galaxy is given by the following expression:

$$P = 1 - \left[1 - \left(\frac{R_1}{R_0}\right)^2 \frac{2\,\Delta V_1}{\Delta V_0}\right]^{N+1} . \tag{4.1}$$

(The exponent is $N+1$ because we also include the Sculptor cloud; the velocity interval ΔV_1 is multiplied by 2 because the difference in velocities can be both positive and negative.) In our case, $\Delta V_0 = 130$ km s^{-1}, and the probability that the Sculptor cloud is an HVC is $P = 0.18\%$. If we considered the Sculptor clouds to be two independent HVCs, the corresponding probability would be a few orders of magnitude lower. Of course, either one or both of our assumptions (absence of correlation, and uniform distribution) might prove to be wrong, so the probability $P \sim 0.2\%$ derived above should be treated with caution.

There is one fundamental flaw in the above probability derivations. To obtain equation (4.1), we implicitly assumed that our choice of a dSph galaxy (Sculptor) is an unbiased one. In reality, there are other Galactic dSphs, and the reason we are so interested in Sculptor is because it happened to have HI gas in its vicinity with similar radial velocity. The correct question to ask would be: "What is the probability that at least one of the Galactic dSphs has at least one HVC in its vicinity, which is located as close (or even closer) to the dwarf galaxy

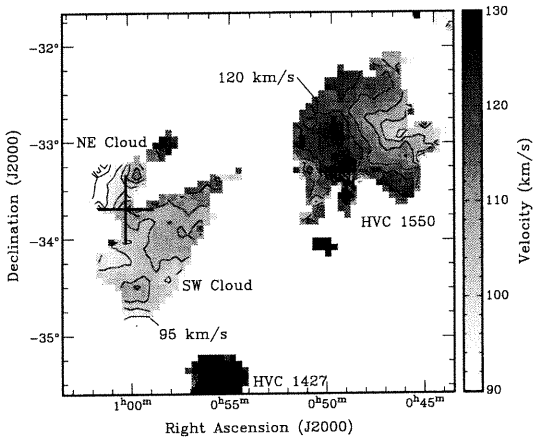

FIGURE 4.5 – The velocity map for the Parkes narrowband data. The contours are separated by 5 km s^{-1}, ranging from 90 to 130 km s^{-1}.

(both spatially, and in radial velocity) as the Sculptor cloud is?" To answer this question one would need to calculate corresponding individual probabilities P_i using equation (4.1) for the 8 known Galactic dSphs (we exclude Sagittarius as it appears to be in the process of being disrupted by the Galactic tidal field), and then to estimate the total probability as

$$P_{tot} = 1 - \prod_{i=1}^{8}(1 - P_i). \tag{4.2}$$

Assuming for simplicity that the individual probabilities P_i are the same for all Galactic dSphs, and are equal to the derived above probability for Sculptor ($P = 0.18\%$), the total probability is $P_{tot} = 1-(1-P)^8 \simeq 1.4\%$. Even in this more realistic approach, the probability of the Sculptor clouds being HVCs appears to be very low.

It is clear from Figure 4.6 and Table 4.2 that the Sculptor clouds are quite different from at least some of other nearby features. NGC 300 is a spiral galaxy; its HI cannot be confused with other structures in Figure 4.6. Region 2 can also be discarded quite easily, as it has a very low velocity and very low dispersion. A careful inspection of the dataset reveals that it is probably an extension of the Milky Way's HI to velocities higher than what would be normally expected in this direction. This cloud extends beyond the velocity range used for the dispersion map computations and therefore its velocity dispersion value is most probably underestimated. In any case, the difference in radial velocities alone makes any physical association of the Region 2 with the Sculptor clouds very unlikely.

HVC 1625 has two distinct components: a large (1°) filament with a low velocity dispersion and a compact (spatially unresolved) core with a higher dispersion. HVC 1640 is a compact

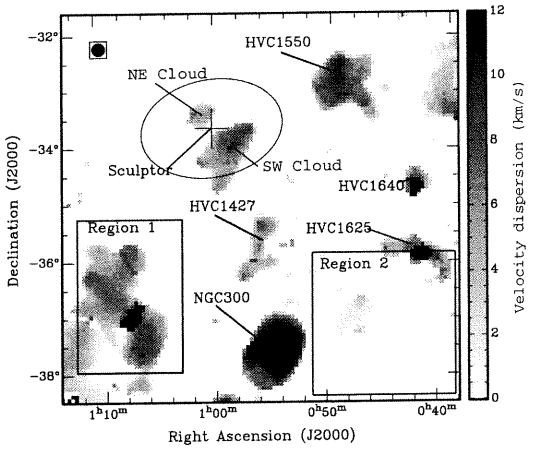

FIGURE 4.6 – Velocity dispersion from the Parkes dataset.

object having a high dispersion, similar to HVC 1625. These objects have velocity structures that are very different from the other clouds seen in Figure 4.6. Therefore they are probably of different origin.

Region 1 is composed of two types of structure: a broad region with a low dispersion and a very high dispersion compact core. This apparently high dispersion value is artificially inflated by the overlap of two clouds with different velocities and should be treated as an artifact. The compact cloud is probably an extension of the Galactic HI , similar to the case of the Region 2. The rest of the Region 1, HVC 1427, and HVC 1550 are all similar in size and kinematic structure to the Scl clouds. It is conceivable then that these clouds are part of a larger HI stream. The shape of the SW cloud also suggests that this link might be real. Analysis of the velocity field (Figure 4.5) suggests a velocity gradient between Scl SW and HVC 1550.

One of the most interesting results obtained in the present work is the almost perfect agreement between the HI velocity for the both Sculptor clouds (Table 4.3) and the optical velocity of the dwarf (Table 4.1). The difference in velocities for the Parkes data is $V_{\odot}^{opt} - V_{HI} = 4 \pm 3$ km s^{-1}. However, a kinematic agreement between HI clouds and dSph galaxies is to be regarded with caution. Alone, this should never be considered as an evidence for HI association.

In the case of Sculptor, the fact that almost all of the detected HI emission is contained within the optical disk of the dwarf galaxy (Figure 4.1), the symmetric location of the two clouds relative to the galactic center (Figure 4.2), the closeness of the radial velocities for the clouds and dwarf, the low inferred probability $P_{tot} \simeq 2\%$ for the clouds to be HVCs, and the presence of an arm coming out of the SW cloud and pointing in the direction of the Sculptor center (Figure 4.2), strongly favor the physical association of the clouds with the dwarf galaxy. In the absence of accurate distance measurements to the HI clouds, the HVC

hypothesis remains a possible (though unlikely) alternative.

4.3.2 Nature of the Sculptor Clouds

Having assumed that the NE and SW clouds are physically associated with Sculptor, the important question to answer is whether the clouds are still gravitationally bound to the dwarf galaxy, or if they have been removed by some mechanism — either internal (winds from red giants, supernovae type Ia), or external (ram pressure stripping by the Galactic hot halo gas, Galactic tidal field).

The symmetric location of the clouds relative to the center of Sculptor along its proper motion vector (see Figure 4.2) appears to be consistent with the tidal removal picture. However, the orientation of the stellar body of the dwarf which has a comparable angular extent to that of the HI gas (see Figure 4.1) indicates that the tidal forces have not played a major part in shaping the galaxy. The biggest obstacle for another external removal mechanism — ram pressure stripping — is the presence of the NE cloud ahead of the proper motion (Figure 4.2).

An important observational evidence for the clouds being gravitationally bound to the dwarf would be a rotation signature for the gas. C98 speculated on the possibility of rotation of the NE and SW clouds around the center of the Sculptor dwarf. It is clear from Figure 4.4 that there is a velocity gradient between the two clouds. The classical Newtonian formula gives a central mass of $\sim 6.7 \times 10^5$ $M_\odot$ when using the Parkes velocity information (rotation speed of 2.5 km s^{-1} at a distance of 20′, see Table 4.3 and Figure 4.4). The ATCA velocity information gives an enclosed mass of 2.7 $\times 10^6$ $M_\odot$ with the same conditions but a rotation speed of 5 km s^{-1}. These estimates assume edge-on circular motion, no projection effect on the distance of the clouds and that the gas is neither infalling nor expanding. Mateo (1998) gives a total mass of 6.4 $\times 10^6$ $M_\odot$ for Sculptor. The inferred rotation speed values are comparable to or less than the internal velocity dispersion in the clouds (see Table 4.2). In this respect, Sculptor would be similar to low luminosity dIrr and dIrr/dSph galaxies, such as GR 8, Leo A, SagDIG, and LGS 3.

Our main argument against any HI removal scenario (either internal or external) is that the gas removal would not solve the ISM crisis in dSph galaxies (Mateo 1998). The alternative is that the NE and SW clouds are gravitationally bound to Sculptor, and are part of its ISM.

MCB proposed a scenario which can explain the statistical differences between the low luminosity dwarf galaxies in the Local Group. They showed that the FUV radiation escaping from spiral galaxies can warm up and photoionize the ISM of their dSph satellites, quenching star formation and making the ISM virtually unobservable. Only during relatively short duration passages through the plane of the host galaxy does the FUV radiation flux become small enough to allow the ISM to recombine and potentially form stars. An important requirement of the model is that many dSph galaxies should possess extended and very massive dark matter halos (with virial temperature $\gtrsim 10^4$ K), allowing them to keep the warm photo-

ionized ISM with temperature $T \sim 10^4$ K gravitationally bound. There is a growing amount of evidence supporting the idea of the dSph galaxies being more massive than the predictions of the mass-follows-light King model (Odenkirchen et al. 2001; Kleyna et al. 2001; Hayashi et al. 2002).

Sculptor is located relatively close to the Milky Way (80 kpc away), and is close to the southern Galactic pole. According to the photoevaporation model of MCB, it is expected that the ionizing radiation escaping from the Galactic disk should affect significantly the Sculptor HI clouds. Because the Sun is located much closer to the Galactic center than to the Sculptor dSph, the photoionized regions of the clouds would be seen approximately face-on. In the photoevaporation scenario, the photoionized gas expands with a speed comparable to its sound speed ($\sim$ 10 km s^{-1}). First it moves normally to the HI cloud surface. If the HII gas stays gravitationally bound to the galaxy, it will soon deviate from the normal direction. As a result, the H_α spectral line from the photoionized gas is expected to be blue-shifted by $\sim 5 - 10$ km s^{-1} relative to the 21 cm spectral line from the neutral cloud.

Weiner et al. (2001) detected H_α emission from the SW cloud with a flux of 220 ± 23 mR. The heliocentric radial velocity of the ionized gas is $V_{HII} = 97 \pm 3 \pm 5$ km s^{-1} (formal / systematic errors) (B. J. Weiner 2001, private communication). Figure 4.7 shows both the H_α detection and the HI spectral line integrated over the same area. The HI line has a peak at $V_{HI} \simeq 109$ km s^{-1} (which is virtually identical to the stellar radial velocity). The HII gas appears to be blue-shifted by $V_{HI} - V_{HII} = 12 \pm 8$ km s^{-1} relative to the HI cloud, which is consistent with the prediction of the photoevaporation model of MCB. More accurate measurements of the radial velocity of the H_α emitting gas are required to confirm this result with higher confidence.

Another interesting feature of Figure 4.7 is the presence of a red-shifted tail in the HI spectral line. Both analytical (Bertoldi & McKee 1990) and numerical (Lefloch & Lazareff 1994) calculations showed that under a wide range of initial conditions photoevaporating interstellar clouds tend to a quasi-equilibrium cometary state. The cometary tail in these models consists of the neutral gas accelerated away from the cloud. The gas in the tail is neutral because it is shielded from the ionizing radiation by the bulk of the cloud. The red-shifted HI gas in Figure 4.7 could be a cometary tail of the photoevaporating cloud.

4.4 Conclusions

New observations of the HI gas in the large area of $7^\circ \times 7^\circ$ around the Sculptor dSph are presented. Combination of the single-dish (Parkes) and interferometric (ATCA) observations allowed us to achieve both large angular coverage and high angular resolution. Our principal results are:

1. The existence of the two HI clouds in the vicinity of Sculptor discovered by C98 is confirmed. The present study shows the full extent of the clouds. The size of the clouds

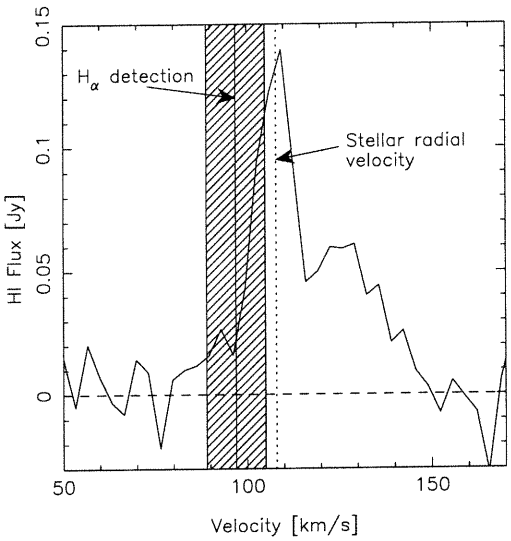

FIGURE 4.7 – H_α detection from the Sculptor dSph (Weiner et al. 2001; B. J. Weiner 2001, private communication). Vertical filled stripe corresponds to the radial velocity of the H_α emission from the southwest HI cloud inside a circle with a radius $5'$ centered at $\alpha_{2000} = 0^h58^m22^s$, $\delta_{2000} = -34°00'$. The width of the stripe reflects both formal and systematic errors. We also show the HI spectral line from the ATCA data integrated within the same circle area (solid line) and the stellar radial velocity of Sculptor (vertical dashed line).

is found to be much larger than the largest angular scale ($\sim 22'$) the C98 observations were sensitive for.

2. The single-dish Parkes observations give the total HI mass of the Sculptor clouds of 2.3×10^5 $M_\odot$ (at the assumed distance of 79 kpc). The heliocentric radial velocity of the gas is 104 km s^{-1}.

3. The arguments that the Sculptor clouds are physically associated with the dwarf are presented, the most important ones being the closeness of the radial velocity for the HI gas and stars ($\Delta V = 4 \pm 3$ km s^{-1} based on the Parkes data), and the location of almost all of the HI emission (88% of the total flux) within the stellar body of the dwarf (in projection). The unlikely possibility of the clouds being Galactic HVCs cannot be ruled out on the basis of the available data.

4. The combination of the present HI observations with the H_α emission line detection from the southwest cloud (Weiner et al. 2001) gives support to the FUV radiation harassment model of MCB. The difference in radial velocities between the neutral and ionized gas is found to be 12 ± 8 km s^{-1}, which is consistent with the Sculptor clouds being photoevaporated by the Galactic LyC radiation.

We are grateful to Lister Staveley-Smith for helpfull discussions.

References

Andersen, R.-P. & Burkert, A. 2000, ApJ, 531, 296

Barnes, D. G. et al. 2001, MNRAS, 322, 486

Bertoldi, F. & McKee, C. F. 1990, ApJ, 354, 529

Blitz, L. & Robishaw, T. 2000, ApJ, 541, 675

Burkert, A. & Ruiz-Lapuente, P. 1997, ApJ, 480, 297

Carignan, C., Beaulieu, S., Côté, S., Demers, S., & Mateo, M. 1998, AJ, 116, 1690 (C98)

de Blok, W. J. G., McGaugh, S. S., Bosma, A., & Rubin, V. C. 2001, ApJ, 552, L23

de Vaucouleurs, G., de Vaucouleurs, A., Corwin, H. G., Jr., Buta, R. J., Paturel, G., & Fouque, P. 1991, Third Reference Catalogue of Bright Galaxies (New York: Springer-Verlag)

Ferrara, A. & Tolstoy, E. 2000, MNRAS, 313, 291

Grebel, E. K. 1997, Reviews of Modern Astronomy, 10, 29

Grebel, E. K. 1998, Highlights in Astronomy, 11, 125

Hayashi, E., Navarro, J. F., Taylor, J. E., Stadel, J., & Quinn, T. 2002, ApJ, submitted (astro-ph/0203004)

Irwin, M. & Hatzidimitriou, D. 1995, MNRAS, 277, 1354

Jerjen, H., Freeman, K. C., & Binggeli, B. 1998, AJ, 116, 2873

Kleyna, J. T., Wilkinson, M. I., Evans, N. W., & Gilmore, G. 2001, ApJ, 563, L115

Lefloch, B. & Lazareff, B. 1994, A&A, 289, 559

Mac Low, M. & Ferrara, A. 1999, ApJ, 513, 142

Mashchenko, S., Carignan, C., & Bouchard, A. 2002, ApJ, submitted (astro-ph/0203317) (MCB)

Mateo, M. L. 1998, ARA&A, 36, 435

Mathewson, D. S. & Ford, V. L. 1984, in IAU Symp. 108: Structure and Evolution of the Magellanic Clouds, 125

Moore, B., Ghigna, S., Governato, F., Lake, G., Quinn, T., Stadel, J., & Tozzi, P. 1999, ApJ, 524, L19

Odenkirchen, M. et al. 2001, AJ, 122, 2538

Oosterloo, T., Da Costa, G. S., & Staveley-Smith, L. 1996, AJ, 112, 1969

Putman, M. E. et al. 2002, AJ, 123, 873

Schweitzer, A. E., Cudworth, K. M., Majewski, S. R., & Suntzeff, N. B. 1995, AJ, 110, 2747

Spaans, M. & Norman, C. A. 1997, ApJ, 483, 87

van Zee, L. 2001, AJ, 121, 2003

Weiner, B. J., Vogel, S. N., & Williams, T. B. 2001, preprint (astro-ph/0109055)

Young, L. M. & Lo, K. Y. 1996, ApJ, 462, 203

—. 1997, ApJ, 490, 710

Chapitre 5

Conclusion

Dans les précédents chapitres j'ai démontré que les galaxies naines du Groupe Local et en particulier les naines sphéroïdales ne sont pas aussi dépourvues de gaz que ce qu'on croyait auparavant.

5.1 Flux ionisant provenant de la Voie Lactée

Précédemment, l'historique de formation stellaire des naines était extrêmement difficile à expliquer. Grâce aux nouvelles données, il est maintenant possible de mieux comprendre ces astres. En effet, le chapitre 2 explique comment le flux de radiation ionisante s'échappant de la Voie Lactée peut ioniser le gaz qui se trouve dans les naines. Ce gaz peut donc devenir tout à fait indétectable avec les moyens dont nous disposons présentement. Ceci a plusieurs conséquences très intéressantes.

Premièrement, le fait que le gaz n'est pas obligatoirement expulsé de la naine implique donc qu'il peut en rester des réservoirs très importants au centre de ces astres. Ce gaz est nécessaire pour expliquer les divers épisodes de formation stellaire que l'on retrouve dans les naines. Ces épisodes sont souvent espacés de plusieurs millions ou parfois même milliards d'années. En effet, rien n'empêche le gaz de se désioniser une fois que le flux de radiation ionisante a cessé et ainsi les épisodes de formations stellaires peuvent recommencer.

Une autre des conclusions qui peut être tirée de ce chapitre et qui va dans le même sens que plusieurs autres études, est que les naines sont probablement beaucoup plus massives que ce qui était cru auparavant. Ceci aide grandement à comprendre pourquoi les nouvelles études sur l'étendue spatiale de ce type de galaxies arrivent souvent aux conclusions que les forces de marées ne sont pas aussi dévastatrices que ce qu'elles laissent croire. Les profils de luminosité de la forme de ceux de King, qui supposent que l'intensité de la radiation que l'on recoit d'une galaxie est un bon traceur de sa distribution de masse pourraient être lentement mis de côté pour d'autres modèles plus représentatifs.

5.2 Les naines sphéroïdales

Le chapitre 3 présentait des observations radio de 9 dSph et dIrr/dSph du Groupe Local. Malgré que les résultats de ces observations peuvent être sujets à plusieurs interprétations différentes, il est maintenant clair que la plupart de ces galaxies ont du gaz qui se situe proche d'elles. La question majeure qui est posée est à savoir si le gaz appartient ou non à ces systèmes.

Déjà le fait que l'on retrouve ces reservoirs près de ces galaxies est un signe encourageant. Ceci permet alors d'essayer de comprendre les méchanismes de formation de ces galaxies. Les épisodes de formation stellaires ont besoin de gaz et ceci peut être vu par certains comme une preuve suffisante de leur association.

En creusant plus loin, on remarque que les naines sont presque toutes situées dans des régions où l'on retrouve une concentration anormale de HVC. Ces nuages ont été identifiés à cause de leur vitesse qui ne correspond pas à une rotation galactique simple. Mais, le problème majeur est que personne ne connaît leurs distances. La majorité des théories placent les objets à de petites distances de la VL (de 1 à 5 kpc) donc beaucoup plus proche de nous que des galaxies naines. Par conséquent on peut très facilement confondre un HVC avec un nuage rattaché à une naine, si une telle chose existe.

Néanmoins, une étude statistique démontre que les nuages sont en fait très proches des naines. Ils sont en général beaucoup plus proches que ce qu'une distribution aléatoire des nuages autour de la galaxie ne le permettrait de façon générale.

5.3 Sculptor

Deux nuages de gaz ont été découverts près de Sculptor. Ces nuages sont en fait extrêmement proches du centre galactique et sont placés symétriquement par rapport à la galaxie. L'article du chapitre 4 suppose en partie que les nuages sont associés à Sculptor et en dérive les propriétés.

Un des faits saillants est qu'il existe une détection infrarouge d'un des deux nuages de Sculptor. Cette détection, lorsque bien analysée, illustre très bien la théorie expliquée au chapitre 2. Il est à noter que bien que nous soyons en présence d'un phénomène clair de photoionisation, ceci ne consiste en rien une preuve que les nuages soient associés à la galaxie. Un tel phénomène devrait également apparaître dans les HVC. Mais la démonstration étant plus ou moins faite au début de l'article, il s'agit d'une hypothèse de travail fort acceptable.

5.4 Des contraintes sur la formation du Groupe Local

Tout ce travail avait, entre autre, pour but de poser des contraintes sur les hypothèses de formation des groupes de galaxies. Quoique le travail effectué ne permet aucune conclusion

claire dans ce domaine, il permet tout de même de favoriser certaines approches plutôt que d'autres.

Les galaxies naines sont considérées depuis longtemps comme des éléments clefs pour comprendre la cosmogonie de l'univers. Elles représentent les plus petits objets du GL et par conséquent les plus fragiles. Ces objets peuvent porter les marques de l'évolution du groupe et d'en comprendre les propriétés permet de comprendre les origines de notre environnement.

Déjà, il était connu que les naines étaient de vieux objets qui se sont formés au premiers temps du GL. Mais il n'est pas encore clair s'ils sont en fait les progéniteurs des galaxies spirales ou encore les résidus de la formation de telles galaxies. Des simulations numériques utilisant des halos de matière sombre froide ont démontré que les naines devraient être près d'une centaine de fois plus nombreuse que ce qu'elles sont présentement.

Ce qu'on sait maintenant des naines nous permet de dire que ce sont des objets qui sont moins âgés, plus massifs et moins affectés par les phénomènes de force de marées et de pression de contact que ce que nous croyions précédemment. Ces caractéristiques laissent croire, qu'en effet, la matière sombre doit jouer un important rôle dans ces galaxies. Elle doit également régir en grande partie les étapes de formation du GL.

5.5 Les HVC et les galaxies naines

Plusieurs facteurs présentés dans ce mémoire laissent croire que les HVC et les naines ne sont pas des objets fondementalement différents. Ils ont en fait des distributions cinétiques et spatiales similaires. En fait, suite à une proposition de Blitz & Robishaw (2000), il se peut même que les naines et les HVC soient issus des mêmes structures. Les halos de matière sombre supposément en orbite autour de la VL pourraient être en fait remplis par ces objets. Ceci aurait pour effet que les naines ne serait plus les plus petits objets du GL mais seulement les premiers assez massifs pour générer des étoiles.

Si les HVC en venaient à être reconnus comme extra-galactique, la théorie cosmologique traitant de la formation des galaxies par effondrement de la matière sur un halo de matière sombre froide serait grandement favorisée vis-à-vis ces adversaires. Mais, de toute évidence, ce n'est pas le genre d'études effectuées pour ce mémoire qui règlera la question. Trop d'inconnus restent encore dans le débat et aucune des études présentées ici ne peut faire la différence entre les HVC et les nuages associés aux naines ou même démontrer qu'il s'agit d'objets similaires ou complètement différents.

Bibliographie

Abbott, D. C. & Conti, P. S. 1987, ARA&A, 25, 113

Armandroff, T. E. & Da Costa, G. S. 1986, AJ, 92, 777

Armandroff, T. E., Olszewski, E. W., & Pryor, C. 1995, AJ, 110, 2131

Arribas, S., Colina, L., & Borne, K. D. 2000, ApJ, 545, 228

Audouze, J., Dennefeld, M., & Kunth, D. 1980, The Messenger, 22, 1

Baade, W. & Gaposchkin, C. H. P. 1963, Evolution of Stars and Galaxies. (Cambridge, Harvard University Press, 1963.)

Barnes, D. G. & de Blok, W. J. G. 2001, AJ, 122, 825

Barnes, D. G., Staveley-Smnith, L., de Blok, W. J. G., Oosterloo, T., Stewart, I. M., Wright, A. E., Banks, G. D., Bhathal, R., Boyce, P. J., Calabretta, M. R., Disney, M. J., Drinkwater, M. J., Ekers, R. D., Freeman, K. C., Gibson, B. K., Green, A. J., Haynes, R. F., te Lintel Hekkert, P., Henning, P. A., Jerjen, H., Juraszek, S., Kesteven, M. J., Kilborn, V. A., Knezek, P. M., Koribalski, B., Kraan-Korteweg, R. C., Malin, D. F., Marquarding, M., Minchin, R. F., Mould, J. R., Price, R. M., Putman, M. E., Ryder, S. D., Sadler, E. M., Schröder, A., Stootman, F., Webster, R. L., Wilson, W. E., & Ye, T. 2001, MNRAS, 322, 486

Bertoldi, F. & McKee, C. F. 1990, ApJ, 354, 529

Binggeli, B. 1994, in Dwarf Galaxies, ed. G. Meylan & P. Prugniel, 13

Blais-Ouellette, S. ., Amram, P., & Carignan, C. 2001, AJ, 121, 1952

Blitz, L. & Robishaw, T. 2000, ApJ, 541, 675

Bouchard, A., Carignan, C., & Mashchenko, S. 2002, Submitted to AJ

Braine, J., Lisenfeld, U., Duc, P., & Leon, S. . 2000, Nature, 403, 867

Braun, R. & Burton, W. B. 1999, A&A, 341, 437

Bullock, J. S., Kravtsov, A. V., & Weinberg, D. H. 2001, ApJ, 548, 33

Côté, P., Mateo, M., Sargent, W. L. W., & Olszewski, E. W. 2000, ApJ, 537, L91

Carignan, C. 1999, Publications of the Astronomical Society of Australia, 16, 18

Carignan, C., Beaulieu, S., Côté, S. ., Demers, S., & Mateo, M. 1998, AJ, 116, 1690

Carignan, C., Demers, S., & Cote, S. 1991, ApJ, 381, L13

Carignan, C. & Purton, C. 1998, ApJ, 506, 125

Carroll, B. W. & Ostlie, D. A. 1996, "An Introduction to Modern Astrophysics" (Reading, Mass. : Addison-Wesley Pub., c1996.)

de Avillez, M. A. 2000, Ap&SS, 272, 23

de Blok, W. J. G. & Walter, F. 2000, ApJ, 537, L95

D'Ercole, A. & Brighenti, F. 1999, MNRAS, 309, 941

Dohm-Palmer, R. C., Helmi, A., Morrison, H., Mateo, M., Olszewski, E. W., Harding, P., Freeman, K. C., Norris, J., & Shectman, S. A. 2001, ApJ, 555, L37

Ferguson, H. C. & Binggeli, B. 1994, A&A Rev., 6, 67

Gallart, C., Freedman, W. L., Aparicio, A., Bertelli, G., & Chiosi, C. 1999, AJ, 118, 2245

Gallart, C., Martínez-Delgado, D., Gómez-Flechoso, M. A., & Mateo, M. 2001, AJ, 121, 2572

Gervais, S. & St-Louis, N. 1999, AJ, 118, 2394

Grebel, E. K. 1998, Highlights in Astronomy, 11, 125

Henning, P. A., Staveley-Smith, L., Kraan-Korteweg, R. C., & Sadler, E. M. 1999, Publications of the Astronomical Society of Australia, 16, 35

Hogg, D. E., Roberts, M. S., Schulman, E., & Knezek, P. M. 1998, AJ, 115, 502

Hubble, E. P. 1925, ApJ, 62, 409

Hulsbosch, A. N. M. & Wakker, B. P. 1988, A&AS, 75, 191

Hurley-Keller, D., Mateo, M., & Grebel, E. K. 1999, ApJ, 523, L25

Hurley-Keller, D., Mateo, M., & Nemec, J. 1998, AJ, 115, 1840

Ibata, R. A., Gilmore, G., & Irwin, M. J. 1994, Nature, 370, 194

Irwin, M. & Hatzidimitriou, D. 1995, MNRAS, 277, 1354

Jacobson, M. R., Kneale, R. C., Gillett, F. C., Raybould, K., Filhaber, J. M., Carniglia, C. K., Laird, R., Kitchens, D., Shimshock, R. P., & Booth, D. C. 1998, in Proc. SPIE Vol. 3352, p. 477-502, Advanced Technology Optical/IR Telescopes VI, Larry M. Stepp; Ed., Vol. 3352, 477–502

Jerjen, H., Freeman, K. C., & Binggeli, B. 1998, AJ, 116, 2873

Johnston, K. V., Sigurdsson, S., & Hernquist, L. 1999, MNRAS, 302, 771

Karachentsev, I. 1996, A&A, 305, 33

Karachentsev, I. D., Karachentseva, V. E., Dolphin, A. E., Geisler, D., Grebel, E. K., Guhathakurta, P., Hodge, P. W., Sarajedini, A., Seitzer, P., & Sharina, M. E. 2000, A&A, 363, 117

Kilborn, V. A., Staveley-Smith, L., Marquarding, M., Webster, R. L., Malin, D. F., Banks, G. D., Bhathal, R., de Blok, W. J. G., Boyce, P. J., Disney, M. J., Drinkwater, M. J., Ekers, R. D., Freeman, K. C., Gibson, B. K., Henning, P. A., Jerjen, H., Knezek, P. M., Koribalski, B., Minchin, R. F., Mould, J. R., Oosterloo, T., Price, R. M., Putman, M. E., Ryder, S. D., Sadler, E. M., Stewart, I., Stootman, F., & Wright, A. E. 2000, AJ, 120, 1342

Knapp, G. R., Kerr, F. J., & Bowers, P. F. 1978, AJ, 83, 360

Koribalski, B., Johnston, S., & Otrupcek, R. 1994, MNRAS, 270, L43

Krautter, J. 1980, A&A, 89, 74

Lamers, H. J. G. L. M. & Cassinelli, J. P., eds. 1999, Introduction to Stellar Winds (New York : Cambridge University Press, 1999)

Larson, R. B. 1974, MNRAS, 169, 229

Lefloch, B. & Lazareff, B. 1994, A&A, 289, 559

Little, B. & Tremaine, S. 1987, ApJ, 320, 493

Lo, K. Y., Sargent, W. L. W., & Young, K. 1993, AJ, 106, 507

Majewski, S. R., Ostheimer, J. C., Patterson, R. J., Kunkel, W. E., Johnston, K. V., & Geisler, D. 2000, AJ, 119, 760

Martin, C. L. 1998, ApJ, 506, 222

Martínez-Delgado, D., Gallart, C., & Aparicio, A. 1999, AJ, 118, 862

Marzke, R. O. & da Costa, L. N. 1997, AJ, 113, 185

Mashchenko, S., Carignan, C., & Bouchard, A. 2002, preprint (astro-ph/0203317)

Mateo, M., Olszewski, E. W., & Morrison, H. L. 1998, ApJ, 508, L55

Mateo, M. L. 1998, ARA&A, 36, 435

Mathewson, D. S. & Ford, V. L. 1984a, in IAU Symp. 108: Structure and Evolution of the Magellanic Clouds, Vol. 108, 125–136

Mathewson, D. S. & Ford, V. L. 1984b, in IAU Symp. 108: Structure and Evolution of the Magellanic Clouds, Vol. 108, 125–136

Matzner, C. D. & McKee, C. F. 2000, ApJ, 545, 364

Moore, B. 1996, ApJ, 461, L13

Moore, B., Ghigna, S., Governato, F., Lake, G., Quinn, T., Stadel, J., & Tozzi, P. 1999, ApJ, 524, L19

Mould, J. R., Bothun, G. D., Hall, P. J., Staveley-Smith, L., & Wright, A. E. 1990, ApJ, 362, L55

Murali, C. 2000, ApJ, 529, L81

Navarro, J. F., Frenk, C. S., & White, S. D. M. 1996, ApJ, 462, 563

Oh, K. S., Lin, D. N. C., & Aarseth, S. J. 1995, ApJ, 442, 142

Oosterloo, T., Da Costa, G. S., & Staveley-Smith, L. 1996, AJ, 112, 1969

Pearce, F. R., Jenkins, A., Frenk, C. S., Colberg, J. M., White, S. D. M., Thomas, P. A., Couchman, H. M. P., Peacock, J. A., Efstathiou, G., & The Virgo Consortium. 1999, ApJ, 521, L99

Prinja, R. K., Barlow, M. J., & Howarth, I. D. 1990, ApJ, 361, 607

Puche, D. & Westpfahl, D. 1994, in Dwarf Galaxies, ed. G. Meylan & P. Prugniel, 273

Putman, M. E., de Heij, V., Staveley-Smith, L., Braun, R., Freeman, K. C., Gibson, B. K., Burton, W. B., Barnes, D. G., Banks, G. D., Bhathal, R., de Blok, W. J. G., Boyce, P. J., Disney, M. J., Drinkwater, M. J., Ekers, R. D., Henning, P. A., Jerjen, H., Kilborn, V. A., Knezek, P. M., Koribalski, B., Malin, D. F., Marquarding, M., Minchin, R. F., Mould, J. R., Oosterloo, T., Price, R. M., Ryder, S. D., Sadler, E. M., Stewart, I., Stootman, F., Webster, R. L., & Wright, A. E. 2002, AJ, 123, 873

Putman, M. E. & Gibson, B. K. 1999, Publications of the Astronomical Society of Australia, 16, 70

Putman, M. E., Gibson, B. K., Staveley-Smith, L., Banks, G., Barnes, D. G., Bhatal, R., Disney, M. J., Ekers, R. D., Freeman, K. C., Haynes, R. F., Henning, P., Jerjen, H., Kilborn, V., Koribalski, B., Knezek, P., Malin, D. F., Mould, J. R., Oosterloo, T., Price, R. M., Ryder, S. D., Sadler, E. M., Stewart, I., Stootman, F., Vaile, R. A., Webster, R. L., & Wright, A. E. 1998, Nature, 394, 752

Rohlfs, K. & Wilson, T. L. 1996, Tools of Radio Astronomy (Tools of Radio Astronomy, XVI, 423 pp. 127 figs., 20 tabs.. Springer-Verlag Berlin Heidelberg New York. Also Astronomy and Astrophysics Library)

Sarajedini, A., Grebel, E. K., Dolphin, A. E., Seitzer, P., Geisler, D., Guhathakurta, P., Hodge, P. W., Karachentsev, I. D., Karachentseva, V. E., & Sharina, M. E. 2002, ApJ, 567, 915

Scheffler, H., Elsässer, H., & Armstrong, A. H. 1987, "Physics of the Galaxy and Interstellar Matter" (Physics of the Galaxy and Interstellar Matter, XI, 492 pp. 207 figs.. Springer-Verlag Berlin Heidelberg New York. Also Astronomy and Astrophysics Library)

Schwarz, U. J., Wakker, B. P., & van Woerden, H. 1995, A&A, 302, 364

Schweitzer, A. E. & Cudworth, K. M. 1996, in American Astronomical Society Meeting, Vol. 188, 0901

Schweitzer, A. E., Cudworth, K. M., & Majewski, S. R. 1997, in ASP Conf. Ser. 127: Proper Motions and Galactic Astronomy, 103

Schweitzer, A. E., Cudworth, K. M., Majewski, S. R., & Suntzeff, N. B. 1995, AJ, 110, 2747

Spitzer, L. J. & Baade, W. 1951, ApJ, 113, 413

St-Germain, J., Carignan, C., Côte, S. ., & Oosterloo, T. 1999, AJ, 118, 1235

Staveley-Smith, L. & et al. 2000, in ASP Conf. Ser. 217: Imaging at Radio through Submillimeter Wavelengths, 50

Stetson, P. B. 1980, AJ, 85, 387

Thuan, T. X. & Martin, G. E. 1979, ApJ, 232, L11

Tolstoy, E. & Irwin, M. 2000, MNRAS, 318, 1241

Tully, R. B. 1982, ApJ, 257, 389

Unavane, M., Wyse, R. F. G., & Gilmore, G. 1996, MNRAS, 278, 727

van den Bergh, S. 1993, AJ, 105, 971

van der Hulst, T. & Sancisi, R. 1988, AJ, 95, 1354

van Dokkum, P. G., Franx, M., Fabricant, D., Kelson, D. D., & Illingworth, G. D. 1999, ApJ, 520, L95

van Woerden, H., Peletier, R. F., Schwarz, U. J., Wakker, B. P., & Kalberla, P. M. W. 1999a, in ASP Conf. Ser. 166: Stromlo Workshop on High-Velocity Clouds, 1

van Woerden, H., Schwarz, U. J., Peletier, R. F., Wakker, B. P., & Kalberla, P. M. W. 1999b, in IAU Symp. 186: Galaxy Interactions at Low and High Redshift, Vol. 186, 58

Vollmer, B., Marcelin, M., Amram, P., Balkowski, C., Cayatte, V., & Garrido, O. 2000, A&A, 364, 532

Wahde, M. 1998, A&AS, 132, 417

Wakker, B. P. & van Woerden, H. 1997, ARA&A, 35, 217

Weiner, B. J., Vogel, S. N., & Williams, T. B. 2001, preprint (astro-ph/0109055)

Whiting, A. B., Hau, G. K. T., & Irwin, M. 1999, AJ, 118, 2767

Wilkinson, M. I. & Evans, N. W. 1999, MNRAS, 310, 645

Young, L. M. & Lo, K. Y. 1996, ApJ, 462, 203

—. 1997a, ApJ, 476, 127

—. 1997b, ApJ, 490, 710

Zaritsky, D. 1999, in ASP Conf. Ser. 165: The Third Stromlo Symposium: The Galactic Halo, 34

Annexe A

Les unités en radio-astronomie

Les radiotélescopes sont des instruments de mesure dont il est important de connaître le fonctionnement interne pour être capable de bien interpréter les données qui y sont récoltées. Ceci est particulièment vrai en ce qui a trait au traitement des unités. Le passage des unités observationnelles aux unités physiques peut être fastidieux si un soin particulier n'est pas porté aux tâches parfois trop automatiques qui constituent le pipeline standard.

Pour commencer, les données, une fois réduites, sont sous forme de cube. Un cube est composé de trois axes soit deux spatiaux (l'ascension droite et la déclinaison) qui donnent la position d'une source ou structure sur le plan du ciel et un spectral, qui contient l'information sur la vitesse des structures observées. Il s'agit en fait de plusieurs spectres collés les uns aux autres, espacés d'un intervalle régulier et placés à l'endroit exact sur le ciel où il aurait été pris si un seul spectre avait été desiré.

À chaque pixel dans le cube correspond une valeur de flux. Ce flux est généralement donné en $Jy/Beam$. Il arrive également, après avoir effectué une intégration de plusieurs plans spectraux (par exemple des cartes de moments compilés avec la tâche MOMNT de AIPS) que les unités soient converties en $Jy/Beam\ m/s$ ou encore en $Jy/Beam\ km/s$. Il est alors important de se rappeler que

$$1\ Jy/Beam\ km/s = 1\ \frac{Jy \times s}{Beam \times km} \tag{A.1}$$

ce qui définit la conversion à apporter lorsqu'il s'agit de passer de l'un à l'autre. Pour passer de $Jy/Beam\ m/s$ à des $Jy/Beam$, il faut multiplier la valeur par l'incrément de vitesse entre deux canaux, tel que défini sur l'axe spectral. La commande PRTHD dans MIRIAD ou IMHEAD dans AIPS permet de l'afficher à l'écran.

Pour ce qui est de la valeur du faisceau (*Beam* en anglais), il s'agit en fait d'un terme qui exprime intrinsèquement la résolution de l'antenne ou de l'ouverture de synthèse utilisée. Ce terme apparaît aussi sous le nom de «somme de l'*Antenna Pattern*» ou SAP.

$$SAP = 2\pi \left(\frac{B_{min}}{2,345 \times pix}\right) \times \left(\frac{B_{maj}}{2,345 \times pix}\right) \tag{A.2}$$

où B_{min} et B_{maj} sont respectivement les axes mineur et majeur du $Beam$ (la pleine largeur à mi-hauteur du patron de diffraction du télescope) et pix est la grosseur d'un pixel, le tout en arcseconde ou, du moins, dans les mêmes unités. Il est à noter que cette expression implique une approximation gaussienne du faisceau et qu'elle est valide uniquement dans les cas où le faisceau est réellement de forme gaussienne. Dans le cas où plusieurs observations en ouverture de synthèse avec différentes configurations ont été utilisées, il y a de bonnes chances que le faisceau n'ait pas du tout une allure simple et facilement approximable.

La SAP est en fait l'inverse du faisceau de telle sorte qu'il suffit de diviser les $Jy/Beam$ par la SAP pour obtenir des Jy. Et cette dernière unité est en fait

$$1\ Jy = 10^{-26}\ W\ m^{-2}\ Hz^{-1} \tag{A.3}$$

soit des unités de flux, indépendantes du télescope.

Ainsi, un flux total d'une galaxie est souvent donné en Jy ou encore, de façon plus évidente, directement en termes de la masse de la galaxie, avec la formule suivante

$$M = 2,356 \times 10^5\ \ D^2\ \varphi \tag{A.4}$$

où φ est le flux en Jy, D la distance en Mpc et M est la masse en $M_\odot$. Évidemment, ceci implique que la distance est déjà connue.

De façon plus générale, on peut dire que la masse totale d'une galaxie est égale à

$$M_{HI} = 2,356 \times 10^5\ D^2 \int_{v_{min}}^{v_{max}} \varphi_\nu dv \tag{A.5}$$

ou, en terme pratique, utilisé directement pour le traitement des cubes,

$$M_{HI} = 2,356 \times 10^5\ D^2 \Delta v \sum_{v_{min}}^{v_{max}} \varphi_\nu \tag{A.6}$$

où v_{min} et v_{max} sont des contraintes sur la vitesse de la galaxie. Ici, le flux φ_ν est directement celui que l'on retrouve à chacun des canaux du cube de données et l'intégrale (ou la somme) se fait sur les canaux du cube.

On peut également retrouver l'équivalent du flux (en $mJy/Beam$) en termes de température de brillance (T_B, en Kelvin).

$$T_B(1\ mJy/Beam) = \frac{687\ (1420.40575168460/\nu_0)^2}{SAP \times pix^2} \tag{A.7}$$

où ν_0 est la fréquence d'observation.

Mais les unités qui sont généralement les plus intéressantes sont celles qui évoquent intrinsèquement des quantités physiques simples telles que la densité. Pour les cartes de moment 0, i.e. une carte intégrée sur l'axe spectral qui donne la distribution spatiale du gaz, la *densité de colonne* en *atomes* (d'hydrogène) cm^{-2} est la plus souvent utilisée.

$$\mathcal{N}_H = 1.8224(3) \times 10^{18} \sum T_B \times \Delta v \tag{A.8}$$

donc

$$1\ mJy/Beam\ km/s = 1.823 \times 10^{18} \times T_B(1\ mJy/Beam)\ atomes/cm^2 \tag{A.9}$$

et

$$1 mJy/Beam = 1.823 \times 10^{18} \times \Delta v \times T_B(1\ mJy/Beam)\ atomes/cm^2 \tag{A.10}$$

où Δv est l'incrément de vitesse entre deux canaux du cube.

Finalement, $\mathcal{N}_H$ est relié à ρ_H, la *densité volumique* (en *atomes* cm^{-3}) par

$$\mathcal{N}_H = \int_0^\infty \rho_H(s)\mathrm{d}s \tag{A.11}$$

où s est la distance à la source. Ce dernier point est un des plus cruciaux. Il n'est pas possible de connaître directement la valeur de ρ_H puisque la seule quantité observable est $\mathcal{N}_H$ et il n'existe aucun moyen direct, du moins en imagerie radio, de connaître la distance d'un nuage d'hydrogène. Certaines personnes y sont quand même parvenues, en employant une technique qui est exposée à la section 1.1.4 sur les *HVC*.

Ces informations sont tirées de Rohlfs & Wilson (1996).